The Calcium-dependent Potassium Current in Olfactory Interneurons of the Cockroach *Periplaneta americana*

Inaugural-Dissertation

zur Erlangung des Doktorgrades

der Mathematisch-Naturwissenschaftlichen Fakultät

der Universität zu Köln

vorgelegt von

Sabine Schleicher

aus Schweinfurt

Zoologisches Institut

Universität zu Köln

2014

Berichterstatter: Prof. Dr. Peter Kloppenburg

Prof. Dr. Ansgar Büschges

Tag der mündlichen Prüfung: 23.06.2014

Contents

Abbreviations

4-AP 4-aminopyridine

$[Ca^{2+}]_i$ .... intracellular Ca^{2+} concentration

$[Ca^{2+}]_O$ .... extracellular Ca^{2+} concentration

I/V relation .... current-voltage relation

I_A .... voltage activated potassium current

I_{Ca} .... voltage activated calcium current

$I_{K(Ca)}$ .... Ca^{2+}-dependent potassium current

$I_{K(V)}$ .... delayed rectifying potassium current

I_{Na} .... voltage activated sodium current

AHP .... afterhyperpolarization

AL(s) .... antennal lobe(s)

AMPA-receptor .... α-amino-3-hyrdoxy-5-methyl-4-isoxazolepropionic acid receptor

AP(s) .... action potential(s)

BK channel(s) .... large conductance Ca^{2+}-activated potassium channel(s)

Ca_V channel(s) .... voltage-gated Ca^{2+} channel(s)

ChTX .... charybdotoxin

CNQX 6-cyano-7-nitroquinoxaline-2.3-dione

DL-AP5 .... DL-2amino-5-phosphonopentanoic acid

EGTA .... ethylene glycol bis(2-aminoethylether)-N,N,N′,N′-tetraacetic acid

GABA .... γ-aminobutyric acid

HEPES .... 4-(2-hydroxyethyl)-1-piperazineethanesulfonic acid

iACT .... inner antenno-cerebral tract

IbTX . . . . iberiotoxin

IK channel(s) . . . . intermediate conductance Ca^{2+}-activated potassium channel(s)

IUPHAR . . . . International Union of Basic and Clinical Pharmacology

K_{Ca} channel(s) . . . . Ca^{2+}-activated potassium channel(s)

LLP . . . . lateral lobe of the protocerebrum

LN(s) . . . . local interneuron(s)

MB . . . . mushroom body

NMDA-receptor . . . . N-methyl-D-aspartate receptor

OSN(s) . . . . olfactory sensory neuron(s)

PBS . . . . phosphate buffered saline

PTX . . . . picrotoxin

RT . . . . room temperature

SD . . . . standard deviation

SFA . . . . spike frequency adaptation

SK channel(s) . . . . small conductance Ca^{2+}-activated potassium channel(s)

TTX . . . . tetrodotoxin

uPN(s) . . . . uniglomerular projection neuron(s)

$V_{0.5(act)}$ . . . . voltage for half-maximal activation

VSG . . . . ventrolateral somata group

Zusammenfassung

Das olfaktorische System von Insekten hat sich seit langem bewährt um allgemeine Mechanismen der olfaktorischen Informationsverarbeitung zu untersuchen. Gerüche werden von olfaktorischen Rezeptorzellen detektiert, welche in spezifische Glomeruli des Antennallobus (AL) projizieren. Hier wird die olfaktorische Information von lokalen Interneuronen (LNs) prozessiert und von Projektionsneuronen (PNs) zu höheren Hirnregionen weitergeleitet. Die beteiligten Neurone lassen sich anhand von Transmittern und Ionenkanälen sowie ihrer elektrophysiologischen Eigenschaften unterscheiden, dennoch ist unbekannt wie die verschiedenen elektrophysiologischen Eigenschaften durch zelleigene Ionenkanäle generiert und moduliert werden. In dieser Studie wurden deshalb biophysikalische und pharmakologische Eigenschaften des kalziumabhängigen Kaliumstroms ($I_{K(Ca)}$) mit Hilfe der 'whole-cell patch-clamp' Technik untersucht und spezifischen Interneuronen des Antennallobus aus intakten Hirnpräparaten von adulten Schaben (*Periplaneta americana*) zugeordnet.

Steady-state Aktivierung mit definierten intrazellulären Kalziumkonzentrationen ($[Ca^{2+}]_i$) zeigte, dass der $I_{K(Ca)}$ von Typ I LNs die größte Sensitivität für Kalzium besitzt. In den übrigen AL Interneurontypen sind mehr als 10 mal höhere $[Ca^{2+}]_i$ notwendig um den $I_{K(Ca)}$ bei physiologischem Membranpotential zu aktivieren. In allen AL Interneuronen wies der $I_{K(Ca)}$ deutliche Kalzium- und Spannungabhängigkeit auf, jedoch zeigten die biophysikalischen Eigenschaften Unterschiede in der kalziumabhängigen Aktivierung. Während in Typ I LNs der $I_{K(Ca)}$ starr als Reaktion auf Ca^{2+} Einstrom aktiviert wird, weisen in uniglomerulären PNs (uPNs) und Typ II LNs die biophysikalischen Eigenschaften auf einen kooperativen Effekt zwischen I_{Ca} und $I_{K(Ca)}$ Aktivierung hin.

Steady-state Aktivierungen bei simultanem Ca^{2+} Einstrom zeigten, dass der $I_{K(Ca)}$ schon bei unterschwelligem Membranpotential aktivierbar ist und, dass sich in uPNs, Typ IIb LNs und den meisten Typ IIa LNs bei hohen $[Ca^{2+}]_O$ die $I_{K(Ca)}$ Aktivierung vom I_{Ca} emanzipiert. In uPNs wurde zudem eine außergewöhnlich hohe Stromdichte festgestellt, dagegen wurde in Typ I LNs der langsamste Verlauf der kalziumabhängigen Aktivierung gemessen. Der $I_{K(Ca)}$ ist in allen AL Interneuronen bereits bei unterschwelligem Membranpotential aktivierbar um erregenden Ca^{2+} Einstrom entgegen zu wirken. Dennoch wurde bei 'current-clamp' Experimenten kein Einfluss auf das Ruhemembranpotential von uPNs und Typ I LNs nachgewiesen. In Typ IIb LNs zeigte der $I_{K(Ca)}$ den schnellsten Verlauf von kalziumabhängiger Aktivierung und Inaktivierung. Während in der Population von Typ IIa LNs die breiteste Streuung der Messwerte festzustellen war. Dies könnte auf unterschiedliche Subtypen von IIa LNs zurückzuführen sein.

Trotz großer Unterschiede in der Kalziumsensitivität konnten diese keinen Kanal Subtypen zugeordnet werden. In allen AL Interneuronen war $I_{K(Ca)}$ unempfindlich gegenüber dem SK Kanal Imhibitor Apamin. Dagegen wurde bei allen AL Interneuronen mit Charybdotoxin eine vollständige Inhibition des $I_{K(Ca)}$ erreicht. In uPNs wurde ein EC_{50} Wert von 2 nM ermittelt, in allen Typen von LNs lag der EC_{50} Wert bei 4 nM. Iberiotoxin, ein BK Kanal Inhibitor mit hoher Spezifität, zeigte einen ähnlichen aber weniger wirksamen Effekt als ChTX. Selbst bei der höchsten verwendeten IbTX Konzentration wurde nur ein Teil des $I_{K(Ca)}$ gehemmt. Obwohl $I_{K(Ca)}$ aus verschiedenen AL Interneuronen Unterschiede in der Kalziumsensitivität, in der kalziumabhängigen sowie spannungsabhängigen Aktivierung aufweisen, scheint der $I_{K(Ca)}$ in allen AL Interneuronen durch BK Kanäle geleitet zu werden.

Abstract

The olfactory system of insects has already served as a suitable model to investigate mechanisms of general information processing. Thus, insect olfactory neurons were used to study physiology, transmitter content, from that evoked currents as well as sensory processing on a network level. As an important step towards understanding how distinct electrophysiological properties of neurons are generated by intrinsic currents, I used whole-cell patch-clamp recordings to analyze biophysical and pharmacological properties of $I_{K(Ca)}$ from unequivocally identified uniglomerular projection neurons (uPNs) and local interneurons (LNs) in the adult, intact brain of the cockroach *Periplaneta americana*.

Steady-state activation at defined $[Ca^{2+}]_i$ revealed highest Ca^{2+} sensitivity of $I_{K(Ca)}$ from type I LNs, $I_{K(Ca)}$ from other AL interneurons require at least 10 fold higher $[Ca^{2+}]_i$ to activate at physiological membrane potential. $I_{K(Ca)}$ from all AL interneurons was clearly dependent on voltage and calcium, while biophysical properties of $I_{K(Ca)}$ delineate distinct qualities in calcium dependent activation. While $I_{K(Ca)}$ from type I LNs is rigidly activated in response to Ca^{2+} influx, biophysical properties of $I_{K(Ca)}$ from uPNs and type II LNs suggest a beneficial effect by I_{Ca} activation.

Steady-state activation with simultaneous Ca^{2+} influx revealed that $I_{K(Ca)}$ is active at subthreshold potential and high $[Ca^{2+}]_O$ uncoupled $I_{K(Ca)}$ activation from I_{Ca} in uPNs, type IIb LNs, and the major part of type IIa LNs. A remarkable high current density of $I_{K(Ca)}$ was found in uPNs, whereas in type I LNs the slowest time course of Ca^{2+}-dependent activation was observed. Although $I_{K(Ca)}$ from all AL interneurons is actived at subthreshold potential, buffering the membrane

potential after excitatory Ca^{2+} influx, current-clamp recordings of spiking AL interneurons preclude an impact of $I_{K(Ca)}$ on membrane resting potential.

Within the population of type II LNs, the quality of biophysical properties varied within the range bounded by uPNs and type I LNs. Whereby $I_{K(Ca)}$ from type IIb LNs displayed fastest time course of Ca^{2+} dependent activation and inactivation. In type IIa LN population greatest variability of data was observed, which might arise from different subtypes of type IIa LNs.

However, differential Ca^{2+} sensitivity could not be assigned to K_{Ca} channel subtypes. $I_{K(Ca)}$ from all AL interneurons were insensitive to the SK channel blocker apamin, whereas charybdotoxin achieved complete inhibition of $I_{K(Ca)}$ yielding in EC_{50} of 2 nM for uPNs and 4 nM for both type I and type II LNs. Iberiotoxin, a BK channel specific inhibitor displayed similar but less potent effects than ChTX, suppressing only a fraction of $I_{K(Ca)}$ in all AL interneurons even at highest applied concentration. Biophysical properties of $I_{K(Ca)}$ delineate distinct qualities in calcium sensitivity and calcium dependent as well as voltage dependent activation, even though $I_{K(Ca)}$ seems to be mediated by BK channels in all types of AL interneurons.

1 Introduction

Odor detection and discrimination is a powerful evolutionary advantage, as it is essential for sensing dangers, food and fertile mates as well as it is a substantial part of social behavior and learning. As an example of convergent evolution the olfactory systems of vertebrates and invertebrates share striking similarities in physiology and neuronal organization, suggesting that olfactory information is processed through similar mechanisms in these unlike classes of animals (Eisthen, 2002; Hildebrand & Shepherd, 1997; Strausfeld & Hildebrand, 1999; Wilson & Mainen, 2006). Therefore the insect olfactory system has been studied in great detail as a model system to understand general principles of sensory processing on a network level (Distler *et al.*, 1998; Fiala, 2007; Galizia & Roessler, 2010; Laurent, 1999; Vosshall & Stocker, 2007). As an important step towards understanding how intrinsic electrophysiological properties of different circuit components are produced by the ion channels they endow, I analyzed biophysical properties of the calcium-dependent potassium current $I_{K(Ca)}$ in distinct antennal lobe (AL) interneurons of *Periplaneta americana*. Additionally, pharmacological properties of $I_{K(Ca)}$ were investigated, establishing concentration-response relations for K_{Ca} channel inhibitors with high specificity. On this basis exclusion experiments will be performed to elucidate the impact of $I_{K(Ca)}$ on firing properties of AL interneurons.

1.1 The insect olfactory system

When an insect perceives an odor, it is bound by odorant binding proteins located in the membrane of olfactory sensory neurons (OSNs). OSNs are housed in

olfactory sensilla located on the insects antennea. Generally, one OSN expresses a single functional receptor gene and its excitatory output terminates in a discrete spherical structure of the ipsilateral antennal lobe (AL) called glomerulus, which is the primary olfactory center and the first synaptic relay processing olfactory information. OSNs expressing the same receptor type converge into the same glomerulus and there they form synapses onto both local interneurons (LNs) and projection neurons (PNs).

PNs convey the integrated olfactory information from the AL to higher order brain centers where multimodal information processing associated to learning and memory formation occurs. Uniglomerular PNs (uPNs) branch in a single glomerulus within the AL and send their axons to the calyxes of the mushroom body (MB) and the lateral lobe of the protocerebrum (LLP) (Ernst & Boeckh, 1983; Malun, 1991a; Fusca *et al.*, 2013).

Within the AL LNs connect different glomeruli with each other, while their neurite branching pattern is limited to the AL (Ernst & Boeckh, 1983; Malun, 1991b; Distler & Boeckh, 1998). Based on early immunohistochemical (Hoskins *et al.*, 1986; Malun, 1991b; Distler *et al.*, 1998; Bicker, 1999) and electrophysiological work (Waldrop *et al.*, 1987; Christensen *et al.*, 1993), LNs have been regarded as mostly GABAergic and inhibitory. However, recent work showed that LNs are a more heterogeneous population of neurons with very different morphological and intrinsic electrophysiological properties (Seki & Kanzaki, 2008; Olsen & Wilson, 2008; Husch *et al.*, 2009b,a; Reisenman *et al.*, 2011; Fusca *et al.*, 2013). Hence, the composition and biophysical properties of ion currents from distinct interneuron types are likely to differ, too.

1.2 Olfactory processing within the AL

Hitherto it is clear that LNs can also contain neurotransmitters like acetylcholine (Shang *et al.*, 2007; Fusca *et al.*, 2013) or glutamate (Daniels *et al.*, 2008) additional to neuromodulators such as peptides and biogenic amines (Ignell, 2001; Homberg, 2002; Nässel & Homberg, 2006; Dacks *et al.*, 2010; Neupert *et al.*, 2012).

Up to date, two types of LNs can be distinguished by their transmitter content, as well as morphological and electropysiological properties (Husch *et al.*, 2009a,b; Fusca *et al.*, 2013). Type I LNs (LN I) display GABA-like immunoreactivity, and upon odor stimulation or depolarizing current injection they generate Na^+ driven action potentials (Husch *et al.*, 2009a). Type II LNs are nonspiking interneurons which accordingly do not possess voltage activated sodium channels and presumably accomplish graded transmitter release. Within the type II LN population at least two subtypes can be distinguished by their dinstinct morphological features and active membrane properties (Husch *et al.*, 2009b). Type IIb LNs respond to odorants with relatively uniform depolarization, whereas type IIa LNs generate more complex changes in membrane potential that include depolarizations, sometimes with Ca^{2+} driven spikelets or pure hyperpolarization. Both nonspiking LN subtypes exhibit large voltage activated Ca^{2+} currents (I_{Ca}), but type IIa LNs display a fast inactivating I_{Ca} component, while type IIb LNs show a more sustained current profile during voltage pulses (Husch *et al.*, 2009b). As a result, the interglomerular circuits provided by diverse LN types, mediate complex excitatory and inhibitory interactions to structure the olfactory representation within the AL and ultimately determine the tuning profile of uPNs (Bazhenov *et al.*, 2001; Stopfer, 2005; Olsen *et al.*, 2007; Shang *et al.*, 2007; Olsen & Wilson, 2008; Assisi *et al.*, 2012).

Without external stimulation uPNs are spontaneously active and respond to olfactory stimuli with sequences of depolarizing and hyperpolarzing epochs, each lasting hundreds of milliseconds (Christensen *et al.*, 1998; Bazhenov *et al.*, 2001). A single uPN responds to a broader range of odors than the matching presynaptic OSN, whereby one odor might elicit a temporally complex pattern with phases of excitation and inhibition, whereas another odor elicit a phasic excitation with no inhibition (Laurent *et al.*, 1996; Ito *et al.*, 2008; Lei *et al.*, 2011). Imaging studies have shown that different odors evoke temporally synchronized activity pattern in different glomeruli, leading to spatial maps finally encoding for odor identity (Galizia *et al.*, 1999; Silbering *et al.*, 2008; Watanabe *et al.*, 2012). Higher odor concentrations evoke broader glomerular activation patterns which results in greater

spatial overlap among different odor representations (Cleland & Linster, 2002; Sachse & Galizia, 2003).

Although network responses to odors and response profiles of participating neurons are well documented we have only limited information about intrinsic electrophysiological properties of participating neurons and how they are determined by cellular mechanisms. Husch *et al.* (2009a) already described distinct properties of I_{Ca} from AL interneurons which correlate with their electrophysiological properties (Husch *et al.*, 2009b). As the electrophysiological properties of a certain neuron are produced by the complement of intrinsic ion channels, investigation on $I_{K(Ca)}$ is the next step towards understanding how olfactory information is processed on the cellular level.

1.3 Calcium-dependent potassium channels

Since its first observation in red blood cells by Gardos (1958), $I_{K(Ca)}$ has been described in numerous cell types with diverse physiological roles. Beside i.e. it regulates secretion in endocrine and exocrine cells (Petersen & Maruyama, 1984), as well as myogenic tone and contraction of smooth muscle (Ghatta *et al.*, 2006). Calcium-dependent potassium channels (K_{Ca} channels) are activated by rises in cytosolic calcium concentration ($[Ca^{2+}]_i$) leading to a rapid potassium efflux, thereby coupling intracellular Ca^{2+} signalling to the membrane potential. In neurons K_{Ca} channels play a crucial role in controlling a variety of firing characteristics. They contribute to action potential repolarization, shaping the amplitude and width of action potentials (Shao *et al.*, 1999). They mediate fast (in the range of milliseconds) and slow (in the range of seconds) after hyperpolarization (AHP) following action potentials (Pineda *et al.*, 1992; Stocker *et al.*, 2004), control repetetive firing patterns, and mediate spike frequency adaptation (Gu *et al.*, 2007; Vandael *et al.*, 2012). Three families of K_{Ca} channels have been identified, which can be separated on biophysical, genetical and pharmacological grounds and have been named K_{Ca} channels of big, intermediate, and small conductance (BK, IK, and SK channels), respectively (Sah, 1996; Vergara *et al.*, 1998).

BK channels

Large conductance K_{Ca} channels (BK channels; also known as maxi-K or slo-channels) have a large unitary conductance of ~ 100 to 300 pS and are composed of four α subunits, where a single α subunit is encoded by the *slowpoke* gene (IUPHAR name $K_{Ca}1.1$) (Atkinson *et al.*, 1991; Adelman *et al.*, 1992). Functional diversity is achieved through alternative mRNA splicing and the use of tissue-specific transcriptional promoters (Atkinson *et al.*, 1998; Brenner *et al.*, 1996). The *slo* gene encodes a pore-forming α subunit that shares significant homology with pore regions of other potassium channels (Wei *et al.*, 1994). The resultant polypeptide comprises seven transmembrane domains (S0 – S6), a short extracellular amino-terminus and a large intracellular carboxyl-terminus. The intracellular domain contains four hydrophobic segments (S7 – S10), two domains that regulate the conductance of K^+ (RCK domains), and a stretch of aspartate residues responsible for Ca^{2+} binding (Meera *et al.*, 1997; Wang & Sigworth, 2009; Wu *et al.*, 2010).

BK channels activate in response to membrane depolarization and binding of intracellular Ca^{2+} (Marty, 1981; McManus, 1991). Interestingly, it appears that the effect of Ca^{2+} and membrane potential are allosterical processes, both of which enhance the open probability (Horrigan & Aldrich, 2002; Latorre *et al.*, 2010). Each α subunit can be modulated by an accessory β subunit, which increases the channel's Ca^{2+} sensitivity by stabilizing the voltage sensor activation (Bao & Cox, 2005). However, no β subunit has been found in insects yet (Littleton & Ganetzky, 2000; Orio *et al.*, 2002; Berkefeld *et al.*, 2010). The Ca^{2+} ions required for activation are mainly delivered by voltage-gated Ca^{2+} channels ($Ca_{(V)}$ channels) directly linked to BK channels (Robitaille *et al.*, 1993; Berkefeld *et al.*, 2006).

Several pharmacological blockers of BK channels have been described so far, including the two toxin peptides charybdotoxin (ChTX) and iberiotoxin (IbTX), which are derived from scorpion venom of *Leiurus quinquestriatus* var. *hebraeus* and *Buthus tamulus*, respectively (Miller *et al.*, 1985; Galvez *et al.*, 1990). Both polypeptides are comprised of 37 amino acids displaying 68% sequence homology and a solution structure of a α helix affixed by disulfide bonds to a three-

stranded β sheet (Galvez *et al.*, 1990; Miller, 1995). Mutational studies and radi-olabeling have provided molecular information of interaction between peptide toxin and BK channel, and the resolved ChTX-BK complex structure unveiled that the β sheet of ChTX is the main binding surface with Lys27 occluding the channel pore (Qiu *et al.*, 2009). Moreover, specific inhibition with ChTX and IbTX revealed the physiological role of BK channels, which mediate action potential (AP) repolarization and fast AHP in many neurons (Pineda *et al.*, 1992; Shao *et al.*, 1999; Gu *et al.*, 2007).

SK channels

Initially, small conductance Ca^{2+}-activated potassium channels (SK) were named according to their single-channel conductance, which ranges from 2 to 20 pS. Later, three genes *SK1*, *SK2* and *SK3* (IUPHAR names are $K_{Ca}2.1$, $K_{Ca}2.2$ and $K_{Ca}2.3$, respectively) sharing 60% sequence homology were identified and at-tributed to the SK channel family (Köhler *et al.*, 1996). Members display a tertiary structure consisting of six transmembrane domains with intracellular amino- and carboxyl-terminus. SK channels possess no voltage-sensing segment therefore lacking voltage dependence, instead they are activated by low Ca^{2+} concentra-tions (Hirschberg *et al.*, 1999). Calcium sensitivity is conferred by calmodulin, which is constitutively bound to the C-terminus of SK channels (Schumacher *et al.*, 2001). Binding of Ca^{2+} to calmodulin leads to a conformational change of the channel protein, opening the channel pore, and allowing potassium efflux (Xia *et al.*, 1998).

Specific inhibition of SK channels by apamin allowed for their initial characteri-zation and assigned their impact to slow AHP, spike frequency adaptation (SFA), and tonically firing pattern (Blatz & Magleby, 1986; Bennett *et al.*, 2000; Faber & Sah, 2003). Up to date several pharmacological agents are known which selec-tively inhibit SK channels, including D-tubocurarine (Ishii *et al.*, 1997a; D'hoedt *et al.*, 2004), bicuculine salts (Seutin & Johnson, 1999) and the scorpion toxin scyl-latoxin (Auguste *et al.*, 1990, 1992).

IK channels

The third type of K_{Ca} channels display an intermediate single-channel conductance of 20-100 pS and therefore have been named intermediate conductance channels (IK channels) (Ishii *et al.*, 1997b). Encoded by the *SK4* gene, this channels share structural features of SK channels, forming tetrameres from subunits consisting of six transmembrane segments with an intracellular amino- and carboxyl-terminus (Joiner *et al.*, 1997; Khanna *et al.*, 1999). But also formation of IK channels from interaction by *slo* and *slack* subunits has been reported (Joiner *et al.*, 1998). Nevertheless, they form a distinct group of K_{Ca} channels (IUPHAR name $K_{Ca}3.1$) which are not expressed in neuronal tissue and can clearly be seperated from BK and SK channels by their sensitivity to pharmacological agents (Wei *et al.*, 2005; Jensen *et al.*, 2002).

IK channels have been shown to be sensitive to clotrimazole and the peptide toxins charybdotoxin and margatoxin, whereas IbTX the structurally-related selective BK channel blocker, and the specific SK channel blocker apamin were without effects (Jensen *et al.*, 2001; Bychkov *et al.*, 2002).

Much of the knowledge about K_{Ca} channels, how they contribute to neuronal firing properties and their sensitivity to specific neurotoxins, arises from studies in vertebrate species. Although the *Drosophila* genome contains one *SK* and a *slowpoke* gene (Littleton & Ganetzky, 2000), studies from insect are rare but hint at differential pharmacological properties of invertebrate and vertebrate K_{Ca} channels. However, a depth knowledge of cell type specific firing properties and membrane conductances that mediate them, is an important prerequisite towards detailed understanding the cellular basis of olfactory information processing. Therefore, I analyzed the Ca^{2+}-dependent K^+ currents in uPNs and different types of LNs, as $I_{K(Ca)}$ plays a crucial role in controlling neuronal firing characteristics (Faber & Sah, 2003).

1.4 Objective of this thesis

Insect olfactory neurons have been used to study physiology, transmitter content, from that evoked currents as well as sensory processing on a network level. In this thesis, biophysical, and pharmacological properties of $I_{K(Ca)}$ were analyzed and assigned to unequivocally identified uPNs and three LN types. The specific objectives of this study were:

- First, to analyze $I_{K(Ca)}$ with particular regard to calcium sensitivity, voltage dependence, and calcium dependence. To analyze $I_{K(Ca)}$ activation associated to Ca^{2+} influx through voltage-gated Ca^{2+} channels. This part aimed to characterize the complex aspects of $I_{K(Ca)}$ activation and presents averaged data from a large number of experiments allowing comparison among AL interneurons.

- Second, to examine the sensitivity of $I_{K(Ca)}$ to highly specific K_{Ca} channel blocker as apamin, charybdotoxin, and iberiotoxin and establish concentration-response relations. This will set the stage for exclusion experiments which elucidate the electrophysiological role of $I_{K(Ca)}$ in spiking uPNs and type I LNs.

2 Materials and Methods

2.1 Animals & Materials

Periplaneta americana were reared in crowded colonies at 27 °C under a 12:12 light/dark photoperiod regimen and fed on a diet of dry rodent food, oatmeal and water. All experiments were performed *in situ* on brains from adult male animals.

All chemicals, unless stated otherwise, were obtained from AppliChem (Darmstadt, Germany) or Sigma-Aldrich (Taufkirchen, Germany) with a purity grade p.a. (per analysis).

2.2 Preparation

The intact brain preparation was based on an approach described previously (Demmer & Kloppenburg, 2009; Husch *et al.*, 2009a) in which the entire olfactory network is left intact. Before dissection animals were anesthetized by CO_2 for several minutes. The animal's legs were amputated distal of the coxa and the animals were placed in custom built holders. Heads and antennae were immobilized with adhesive tape (tesa ExtraPower Gewebeband, tesa AG, Hamburg Germany). The head capsule was opened by cutting a window between the two compound eyes at the bases of the antennae. The brain was dissected in extracellular saline (see below) and pinned in a Sylgard-coated (Dow Corning Corp., Midland, Michigan, USA) recording chamber. To gain access to the recording site and facilitate penetration of pharmacological agents into the tissue, parts of the AL were desheathed using fine forceps. The preparations were also enzymati-

cally treated with a mixture of papain (0.3 mg/ml) and L-cystein (1 mg/ml) dissolved in extracellular saline (~ 3 min, 37 °C). For electrophysiological recordings, the somata of the AL neurons were visualized with a fixed upright microscope (BX51WI, Olympus, Hamburg, Germany) using a 40× water-immersion objective (UMPLFL, 0.8 numerical aperture (NA), 3.3 mm working distance, Olympus).

2.3 Electrophysiological recordings

2.3.1 Whole-cell recordings

Whole-cell recordings were performed at room temperature (RT) following the methods described by Hamill *et al.* (1981). Electrodes with a tip resistance between 2.5 - 3.5 MΩ were fashioned from borosilicate glass (inner diameter (ID) 0.86 mm, outer diameter 1.5 mm, GB150-8P, Science Products, Hofheim, Germany) with a temperature-controlled pipette puller (PP-830, Narishige International, London, U.K.). For patch-clamp recordings the pipettes were filled with intracellular saline solution containing (in mM): 190 K-aspartate, 10 NaCl, 1 CaCl$_2$, 2 MgCl$_2$, 10 HEPES and 10 EGTA to pH 7.2 with KOH, resulting in an osmolarity of ~ 415 mOsm. During the experiments, if not stated otherwise, cells were superfused constantly with extracellular saline solution (in mM): 185 NaCl, 4 KCl, 1 CaCl$_2$, 2 MgCl$_2$, 10 HEPES and 35 D-glucose. The solution was adjusted to pH 7.2 with NaOH and to 430 mOsm with glucose. Whole-cell voltage and current-clamp recordings were made with an EPC9 patch-clamp amplifier (HEKA-Elektronik) that was controlled by the program Patch Master (version2.5, HEKA-Elektronik) running under Windows. The electrophysiological data were sampled at 20 kHz. Recordings were low pass filtered at 2 kHz with a 4-pole Bessel-Filter. Compensation of the offset potential and capacitive currents was performed using the 'automatic mode' of the EPC9 amplifier. Whole-cell capacitance was determined by using the capacitance compensation (C-slow) of the amplifier. The liquide junction potential between intracellular and extracellular solution of 15.6 mV was calculated with Patcher's-Power-Tools plug-in

(http://www3.mpibpc.mpg.de/groups/neher/index.php?page=software) for Igor Pro (Wavemetrics, Portland, Oregon) and was compensated. To remove uncompensated leakage and capacitive currents, a p/6 protocol was used. Voltage errors due to the series resistance (Rs) were minimized using the Rs-compensation of the EPC9. Rs was compensated between 50% and 90% with a time constant (τ) of 100 μs. For current clamp recordings the bridge-balance setting was set to 70% to compensate for the potential drop due to the pipette. To isolate the recorded cell from synaptic input 10 μM CNQX (6-cyano-7-nitroquinoxaline-2.3-dione, C127, Sigma Aldrich), 50 μM DL-AP5 (DL-2amino-5-phosphonopentanoic acid, BN0086, Biotrend), and 100 μM PTX (picrotoxin, P1675, Sigma Aldrich) were added to the extracellular saline during current clamp recordings. These chemicals block AMPA-, NMDA, $GABA_A$ and nicotinic acetylcholine receptors respectively. Stimulus protocols used for each set of experiments are given in the Results section.

2.3.2 Current isolation

$I_{K(Ca)}$ was isolated using a combination of pharmacological blockers, appropriate holding potential and digital current subtraction protocols, based on protocols that have been effective in insect preparations. Voltage activated Na^+ currents were blocked by tetrodotoxin (10^{-6} M, TTX, T-550, Alomone, Jerusalem, Israel). Ca^{+2} currents were blocked by $CdCl_2$ (5×10^{-4} M), whereby $I_{K(Ca)}$ was indirectly eliminated. The transient K^+ current (I_A) was blocked by 4-aminopyridine (10^{-2} M, 4-AP, A78403, Sigma-Aldrich). To compensate for changes in osmolarity, the glucose concentration was appropriately adjusted. Details of recording solutions and voltage protocols for each set of experiments are given in the Result section.

2.3.3 Data analysis

I used the software Igor Pro 6.0.1 (Wavemetrics, including the Patcher's Power Tools plug-in) for analysis of electrophysiological data. All calculated values are

expressed as mean ± standard deviation (SD), if not stated otherwise. To determine concentration-response relations, each concentration was applied at least two times. Current amplitudes were scaled as a fraction of maximal current and fit to a modified form of the Hill equation. The Hill equation (2.1) describes simultaneous and saturating binding of ligands activating a multi-subunit complex.

$$\frac{I}{I_{Max}} = \frac{K^{n_H} \cdot [S]^{n_H}}{1 + K^{n_H} \cdot [S]^{n_H}} \tag{2.1}$$

In case of complete inhibition, the formulation is transformed to following equation:

$$\frac{I}{I_{Max}} = \frac{1}{1 + 10^{([S]-K) \cdot n_H}} \tag{2.2}$$

I is the measured current amplitude at toxin concentration $[S]$, I_{Max} is the maximal current amplitude under control conditions, K is the association constant decribed by log of the concentration with half maximal effect, n_H is the Hill coefficient describing the slope of the curve. All calculated curves have a standard slope n_H equals -1.

Conductance (G) was calculated using the equation:

$$G = \frac{I}{V - V_{rev}} \tag{2.3}$$

Where I is the current density, V the test pulse potential and V_{rev} is the K$^+$ equilibrium potential. To convert current density to conductance, a K$^+$ equilibrium potential of -98.5 mV was calculated.

To determine voltages for half-maximal current activation, data of steady-state activation were fit using a first-order (n = 1) Boltzmann equation:

$$\frac{G}{G_{Max}} = \frac{1}{(1 + e^{(V_{0.5}-V)/s})^n} \tag{2.4}$$

Where G_{Max} is the maximal conductance, V equals test pulse potential, G is the conductance at voltage V, s is the slope factor and $V_{0.5}$ is the voltage at which half-maximal activation of current occurs.

2.4 Single cell labeling

To label individual cells, 1% (w/v) biocytin (B4261, Sigma) was added to the intracellular solution. After electrophysiological recordings, brains were fixed in Roti-Histofix (P0873, Carl Roth, Karlsruhe, Germany) for 2 - 3 h at RT. Subsequently the brains were rinsed in 0.1 M phosphate buffered saline (PBS, 3×20 min, RT). PBS contained (in mM): 72 $Na_2HPO_4 \cdot 2H_2O$ and 28 $NaH_2HPO_4 \cdot H_2O$, resulting in pH 7.2. All brains were processed as whole mounts. To facilitate streptavidin penetration, brains were treated with a commercially available collagenase/dispase mixture (1 mg/ml, 269638, Roche Diagnostics, Mannheim, Germany) and hyaluronidase (1 mg/ml, H3506, Sigma-Aldrich) disolved in PBS (20 min, 37 °C). Afterwards the brains were rinsed in PBS (3×10 min, 4 °C) and incubated in PBS containing 1% Triton X-100 (Serva, Heidelberg, Germany) to improve streptavidin penetration, and 10% normal goat serum (Vector Labs, Burlingame, CA, USA) to prevent unspecific interactions, for 40 min at RT. Subsequently the brains were rinsed in PBS (3×10 min, RT) and incubated in Alexa Fluor 633 (Alexa 633) conjugated streptavidin (S21375, Molecular Probes, Eugene, OR, USA) dissolved 1:400 in PBS containing 10% normal goat serum and 1% Triton X-100 for 1 - 2 days at 4 °C. Finally brains were rinsed in PBS (3×10 min, RT), dehydrated in Ethanol (50%, 70%, 90%, 100% and 100%, each concentration for 10 min), cleared and mounted in methylsalicylate (M6752, Sigma-Aldrich). The fluorescence images were captured with a confocal microscope (LSM 510, Carl Zeiss, Göttingen, Germany) equipped with PlanNeofluar 10× (0.3 NA) and Plan

Apochromat 20× (0.75 NA) objectives. Alexa 633 was excited with a He-Ne Laser at 633 nm and emission was collected through a 650 nm LP filter. For overview pictures overlapping image stacks were merged in Photoshop CS5 (Adobe Systems Incorporated, San Jose, Ca, USA).

Sectioning

After capturing fluorescence images of the whole mounts, brains were washed for 10 min in 100% ethanol and rehydrated in a descending ethanol series. Brains were stored in 70% ethanol and selected brains were further rehydrated, embedded in agarose (4% (w/v) Serva, Heidelberg, Germany) disolved in PBS and 100 µm thick ventrodorsal sections were cut with a vibration microtome (HM 650 V, Thermo Scientific, Walldorf, Germany). The slices were reincubated with streptavidin overnight at -4 °C, rinsed with PBS (3 × 10 min) and H_2O and dried on coated slices (HistoBond 0800001, Marienfeld-Superior, Lauda-Königshofen, Germany). After a dehydrating ethanol series (25%, 50%, 70%, 90% and 2 × 100%, 10 min each) the slices were treated with xylene for 10 min to remove lipids and mounted in Entellan (107961 Merck, Darmstad, Germany). Slices could be stored and were used to obtain high resolution detail images of the innervated brain areas with an 40× oil-immersion Plan-Neofluar (1.30 NA) objective.

3 Results

This study aimed to characterize the $I_{K(Ca)}$ in olfactory interneurons of the insect antennal lobe. Here, primary sensory input detected by olfactory sensory neurons is processed. Uniglomerular projection neurons (uPNs) relay the integrated olfactory information from this first order neuropile to higher order brain centers. Whereas local interneurons (LN) ramify only within the AL, to ultimately restructure and shape the output of uPNs. In most neurons Ca^{2+}-dependent K^+ outward currents are crucial to shape their intrinsic firing properties.

To reveal biophysical properties of $I_{K(Ca)}$ in AL interneurons, whole-cell voltage-clamp recordings were performed. The complex aspects of calcium and voltage interaction have been investigated in a large number of experiments, performed in collaboration with Dr. Cathleen Bradler and Andreas Klein, whose contribution is indicated in respective sections and figure legends. Sensitivity of $I_{K(Ca)}$ to peptide neurotoxins apamin, charybdotoxin, and iberiotoxin was investigated and concentration-response relations were established. On this basis exclusion experiments were performed, in which portions of $I_{K(Ca)}$ were pharmacologically blocked, to unveil the impact of $I_{K(Ca)}$ in shaping the intrinsic electrophysiological properties of spiking AL interneurons. This studies were done by Dr. Ben Warren, Viktor Bardos, Merit Klemann, and Sandra Wendler and are provided in an appendix section 5. All recordings were performed under visual control from cell bodies within the ventrolateral somata group (VSG) in an intact brain preparation of male *P. americana*.

3.1 Identification of AL interneurons

The cell bodies of uPNs are located in a homogeneous cluster at the ventral part of the VSG. Each of the recorded uPNs innervated a single glomerulus within the AL by surrounding it with thick neurite fibres that give rise to fine processes entering the dense neuropile and arborizing within the entire glomerulus (Malun, 1991a). Each uPN sends a single axon through the inner antenno-cerebral tract (iACT) to the mushroom body calyces and the lateral lobe of the protocerebrum (LLP) where it arborizes and terminates in boutons. Morphology and response properties of uPNs have been investigated extensively in *P. americana* and are well documented (Boeckh & Tolbert, 1993; Boeckh *et al.*, 1984; Distler *et al.*, 1998; Lemona & Getz, 1998; Malun, 1991a).

The somata of LNs are arranged dorsal to the uPN soma cluster. Type I LNs own long primary neurites that bifurcate and give rise to the Y-shaped tract (Distler, 1989). Within the AL, neurites arborize in thick branches innervating many, but not all glomeruli. The density of processes vary between glomeruli of a given neuron. Type I LNs are spiking interneurons that generate Na^+ driven action potentials (APs) (Husch *et al.*, 2009a). Further dorsally located somata belong mostly to non-spiking type II LNs, referred to as type IIa and type IIb LNs (Husch *et al.*, 2009a,b). Neurons of both LN II subtypes innervate all glomeruli of the AL, but subtypes could be distinguished by their branching pattern within the glomeruli. Type IIa LNs display uniform innervation of the whole glomerulus, whereas type IIb LNs innervate all glomeruli only partially. All neurons were labeled by dye injection via the recording pipette and were subsequently identified by their definite morphology.

Figure 3.1 *(following page).* **Morphological characteristics of LN types.** Morphology of recorded LNs was revealed by staining via the patch pipette. (A) Morphology of type I LN (310 μm image stack, left side). The neuron innervated many, but not all glomeruli of the AL. The density of neurites varied between glomeruli, shown in detail at the right side (20 μm image stack). (B) Type IIa LN (320 μm image stack, left side) displayed homogeneous innervation of all glomeruli (20 μm image stack, right side). (C) Type IIb LN (375 μm image stack, right side) innervated all glomeruli only partially (20 μm image stack, right side).
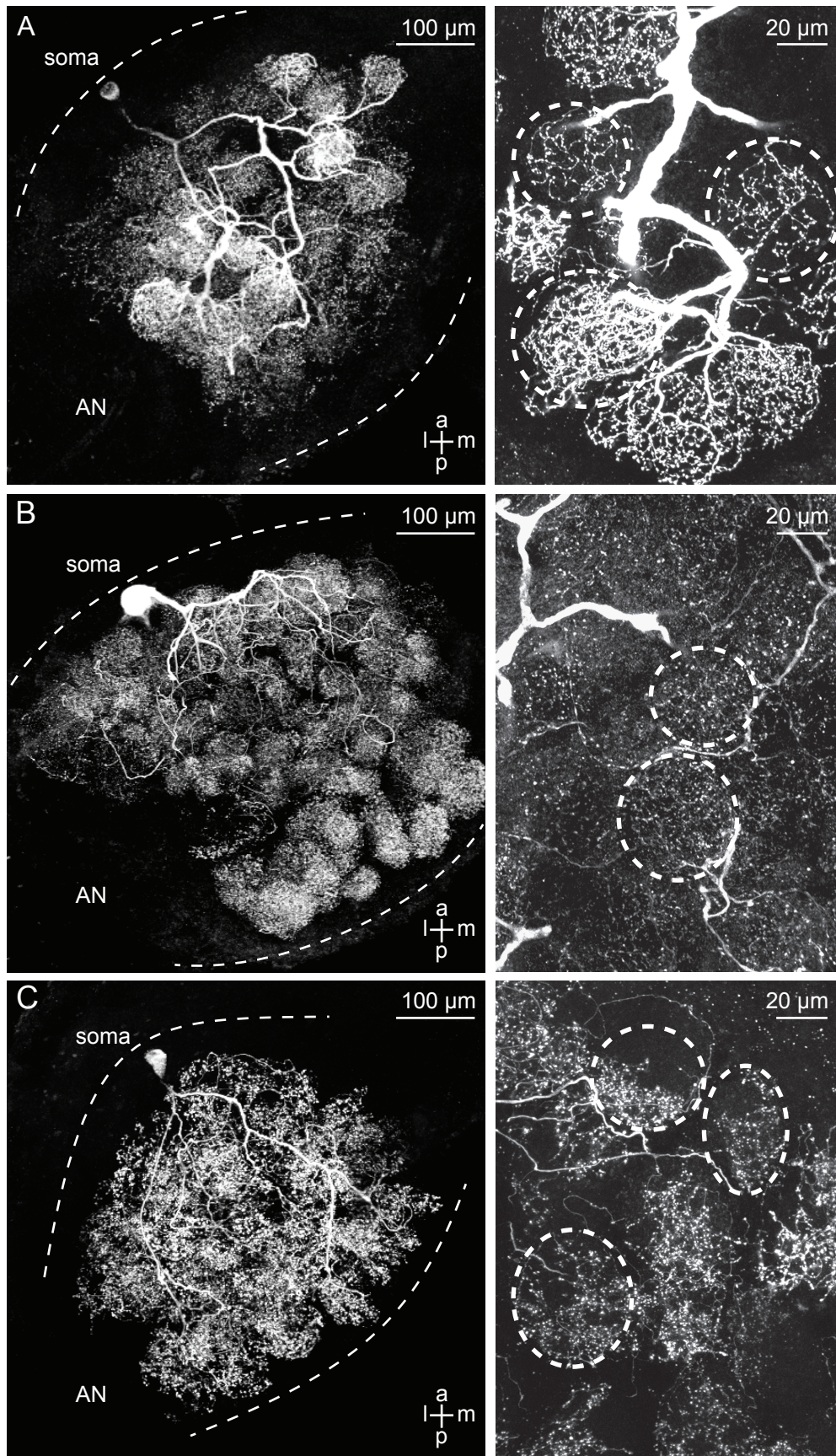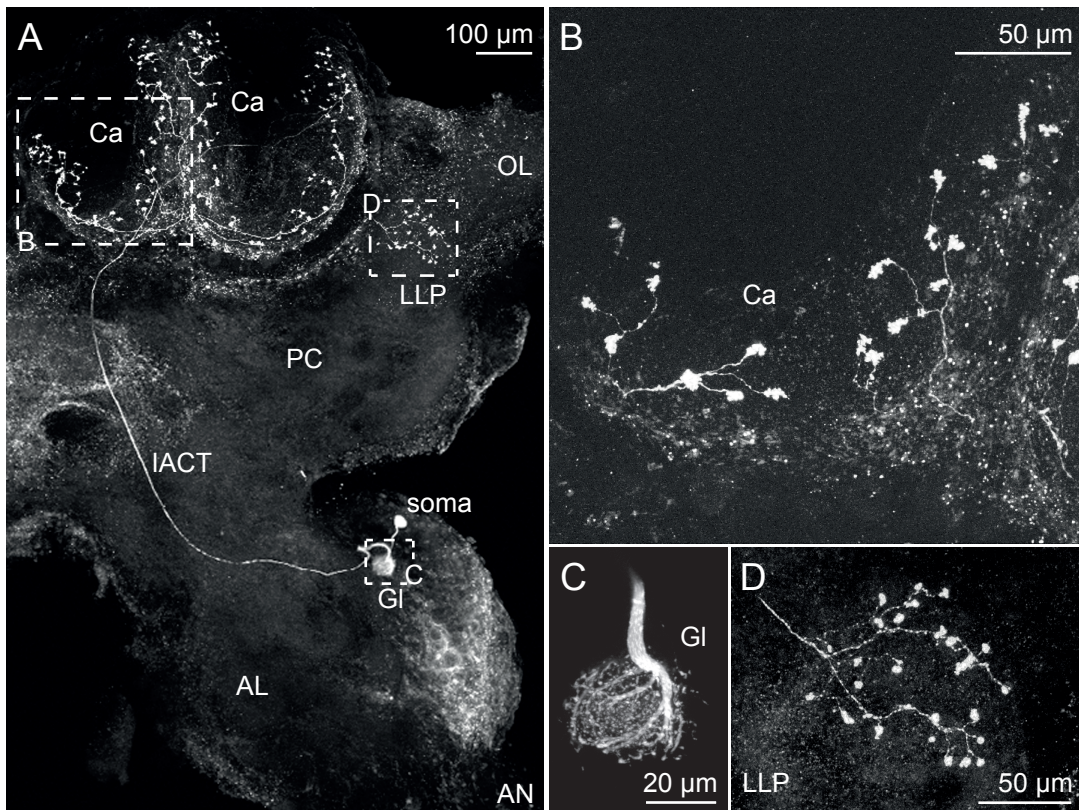
Figure 3.2. Morphological characteristics of an uPN. Morphology of a recorded uPN revealed by staining via the patch pipette. (A) 600 µm image stack of the right hemisphere. The uPN innervated a single glomerulus (Gl) within the antennal lobe (AL) and sent a single axon along the inner antenno-cerebral tract (iACT) to the mushroombody's calyces (Ca) and the lateral lobe of the protocerebrum (LLP). AN: antennal nerve, OP: optical lobe, PC: protocerebrum. (B – D) Higher magnification of the innervated glomerulus (C), a single calyx (B) and the LLP (D).

3.2 Steady-state activation of $I_{K(Ca)}$

Steady-state activation of $I_{K(Ca)}$ was investigated at defined intracellular Ca^{2+} concentration ($[Ca^{2+}]_i$) or by influx of 1 or 6 mM extracellulare Ca^{2+} concentration, respectively ($[Ca^{2+}]_O$). Thus, recording conditions were designed to activate $I_{K(Ca)}$ by either persistent Ca^{2+} concentration or by Ca^{2+} influx through simultaneously activated Ca_V channels. Currents were activated by 300 ms depolarizing voltage steps up from -60 mV, increased in 10 mV increments.

3.2.1 Steady-state activation at defined calcium concentrations

Defined $[Ca^{2+}]_i$ were applied via the recording pipette to evaluate calcium sensitivity, and voltage dependent activation of $I_{K(Ca)}$. Pipette solutions were prepared by using an EGTA-Ca^{2+} buffering system, resulting in $[Ca^{2+}]_i$ of 56, 143, 540, and 1800 μM. The preparation was superfused with saline containing 10^{-6} M TTX to block voltage activated Na^+ currents (I_{Na}), 10^{-2} M 4-AP to block transient potassium currents (I_A), and 5×10^{-4} M $CdCl_2$ to block voltage activated Ca^{2+} currents (I_{Ca}). Thus, $I_{K(Ca)}$ was activated by a series of depolarizing voltage pulses at defined $[Ca^{2+}]_i$. Recordings fom uPNs were perfomed by Dr. Cathleen Bradler and myself. Analysis and figures of uPNs were kindly provided by Dr. Cathleen Bradler.

During a sustained voltage pulse $I_{K(Ca)}$ displayed a sustained, noninactivating current profile (Fig. 3.3A and B). Moreover, $I_{K(Ca)}$ amplitudes increased with progressively depolarizing voltage pulses, showing clear voltage dependence of steady-state activation at all applied $[Ca^{2+}]_i$. Comparing the *G/V* relations from different $[Ca^{2+}]_i$ showed that increasing $[Ca^{2+}]_i$ lowered the voltage threshold for activation (Fig. 3.3C) and the voltage for half-maximal activation ($V_{0.5(act)}$) (Fig. 3.3D). At an $[Ca^{2+}]_i$ of 143 μM, $V_{0.5(act)}$ equals 100 mV in uPNs, 58 mV in type I LNs, 215 mV in type IIa LNs and 113 mV in type IIb LNs (Fig. 3.4B), ascribing highest calcium sensitivity to type I LNs. Nonspiking type II LNs required higher $[Ca^{2+}]_i$ to activate at 0 mV, compared to spiking uPNs and type I LNs. Higher $[Ca^{2+}]_i$ are required to activate $I_{K(Ca)}$ from non-spiking type II LNs. At a

Table 3.1. Steady-state activation of $I_{K(Ca)}$ at defined Ca^{2+} concentrations. Conductance was calculated using equation (2.3). To determine G$_{max}$, conductances were fit to a first-order Boltzmann equation (2.4) and calculated as a fraction of G$_{max}$. Normalized conductances were fit to a first-order Boltzmann equation (2.4) yielding in following voltages for half-maximal activation. All values are are expressed as mean ± SD.

	uPNs	type I LNs	type IIa LNs	type IIb LNs
$[Ca^{2+}]_i$ (µM)		V$_{0.5(act)}$ (mV)		
56	125 ± 9	–	–	–
143	100 ± 11	58 ± 2	215 ± 1	113 ± 3
540	69 ± 2	–	–	–
1800	50 ± 2	–	87 ± 1	62 ± 2

defined $[Ca^{2+}]_i$ of 1.8 mM, V$_{0.5(act)}$ equales 87 mV in type IIa LNs and 62 mV in type IIb LNs (Fig. 3.4A).

Elevation of $[Ca^{2+}]_i$ in this extent occure only in very local spatiotemporal domains close to a calcium source (Augustine *et al.*, 2003). The $[Ca^{2+}]_i$ is strictly controlled as calcium serves as second messenger signal with diverse effects on enzyme activity, gene expression, cell growth, and cell death via apoptosis. Since K$_{Ca}$ channels are activated by I_{Ca}, steady-state activation of $I_{K(Ca)}$ with calcium influx through Ca$_V$ channels should resemble more physiological conditions.
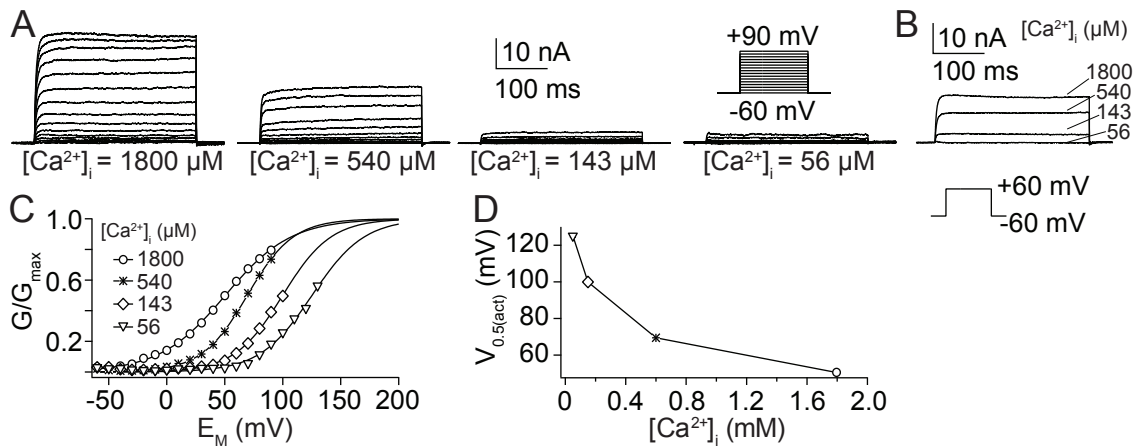
Figure 3.3. Voltage dependence of $I_{K(Ca)}$ from uPNs. (A) Current traces of steady-state activation from four uPNs with distinct $[Ca^{2+}]_i$ applied via the recording pipette. (B) Current traces elicited by a depolarizing voltage pulse to 60 mV with different $[Ca^{2+}]_i$. (C) *G/V* relations of steady-state activation with different $[Ca^{2+}]_i$. Conductances were calculated according to equation (2.3) and fit to a first-order Boltzmann equation (2.4). Conductances were calculated as a fraction of maximal conductance and again fit to a first-order Boltzmann equation to determine voltages for half-maximal activation ($V_{0.5(act)}$). (D) Voltage of half-maximal activation as a function of $[Ca^{2+}]_i$. This figure was kindly provided by Dr. Cathleen Bradler.
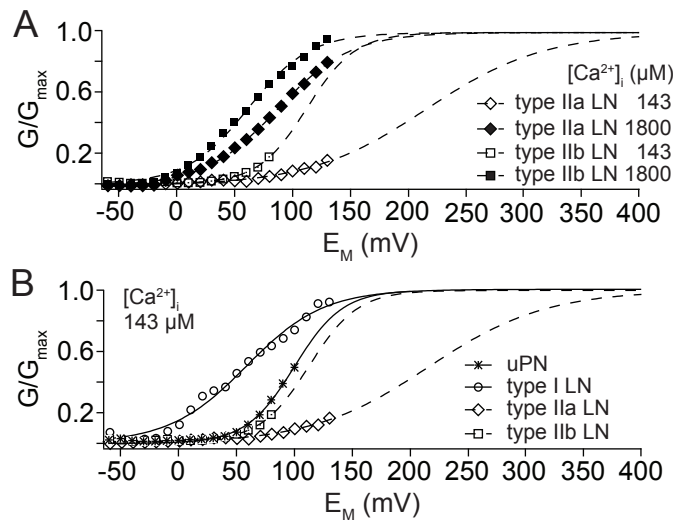
Figure 3.4. Voltage dependence of $I_{K(Ca)}$ from different AL interneurons. (A) *G/V* relation from steady-state activation of $I_{K(Ca)}$ from type IIa and b LNs with 1.8 mM or 143 µM $[Ca^{2+}]_i$. (B) Comparision of G/V relations for steady-state activation from different AL interneurons with 143 µM $[Ca^{2+}]_i$. Conductances were calculated according to equation (2.3) and fit to a first-order Boltzmann equation (2.4). Conductances were calculated as a fraction of maximal conductance and again fit to a first-order Boltzmann equation to determine voltages for half-maximal activation ($V_{0.5(act)}$).

3.2.2 Steady-state activation with calcium influx

$I_{K(Ca)}$ was isolated using a combination of pharmacological tools, appropriate holding potential and current subtraction protocols. The preparation was superfused with saline containing 10^{-6} M TTX and 10^{-2} M 4-AP to abolish voltage activated sodium (I_{Na}) and transient potassium currents (I_A). The $[Ca^{2+}]_O$ was adjusted to 6 mM or 1 mM, respectively. To determine current-voltage relations (*I/V* relations), series of 300 ms voltage pulses between -60 and +60 mV were applied in 10 mV increments, while neurons were held at -60 mV between voltage protocols. Afterwards, another series was recorded with saline containg 5×10^{-4} M $CdCl_2$ additionally, which completely abolished voltage activated Ca^{2+} currents (I_{Ca}). Accordingly, under Cd^{2+} treatment $I_{K(Ca)}$ was blocked too and only the delayed rectifying K^+ outward current ($I_{K(V)}$) was recorded. $I_{K(V)}$ was digitally subtracted from the 'untreated' series and the resulting current profile was defined as $I_{K(Ca)}$ (see Fig. 3.5 – 3.8A –E). The current profiles were dominated by $I_{K(Ca)}$ but contain underlying I_{Ca}. Experiments contributing to this section were performed by Dr. Cathleen Bradler, Andreas Klein, and myself. The results are summarized in table 3.2.

Uniglomerular Projection Neurons

During a 300 ms voltage pulse, $I_{K(Ca)}$ consisted of a sustained, noninactivating component and a transient component, inactivating at diverse time scales (Fig. 3.5D and E). Activated by influx of 6 mM $[Ca^{2+}]_O$, $I_{K(Ca)}$ amplitudes increased with progressively depolarizing voltage pulses (Fig. 3.5D) and reached a maximal current amplitude of 28 ± 18 nA at 60 mV. At 20 mV an average current amplitude of 18 ± 12 nA (Fig. 3.5F) was achieved. With 1 mM $[Ca^{2+}]_O$, peak currents were reached at 17 ± 11 mV and decreasing $I_{K(Ca)}$ amplitudes were observed with progressively depolarizing voltage pulses (Fig. 3.5E). This is reflected in an inverted U-shape of the *I/V* relation (Fig. 3.5G). An average maximal current amplitude of 18 ± 7 nA was reached at 10 mV.
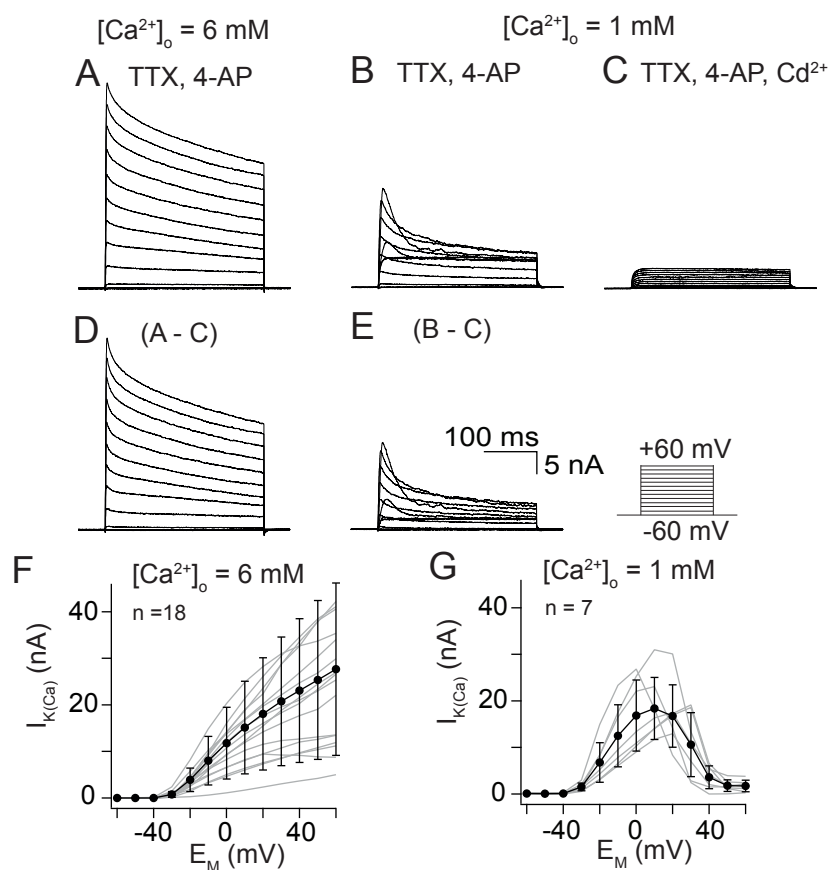
Figure 3.5. Steady-state activation of $I_{K(Ca)}$ from uPNs. (A – E) Current traces of steady-state activation elicited by 300 ms depolarizing voltage steps from -60 mV to 60 mV in 10 mV increments. (A) Current traces elicited by influx of 6 mM $[Ca^{2+}]_O$. (B) Current traces elicited by influx of 1 mM $[Ca^{2+}]_O$. (C) Current traces elicited by the same depolarizing voltage steps as A and B but during additional application of 5×10^{-4} M $CdCl_2$. (D – E) Digital subtraction of the $CdCl_2$ treated series from 'untreated' series yielded in $I_{K(Ca)}$ activated by 6mM $[Ca^{2+}]_O$ (D) and 1mM $[Ca^{2+}]_O$ (E). (F) *I/V* relation of steady-state activation with 6 mM $[Ca^{2+}]_O$. (G) *I/V* relation of steady-state activation with 1 mM $[Ca^{2+}]_O$.
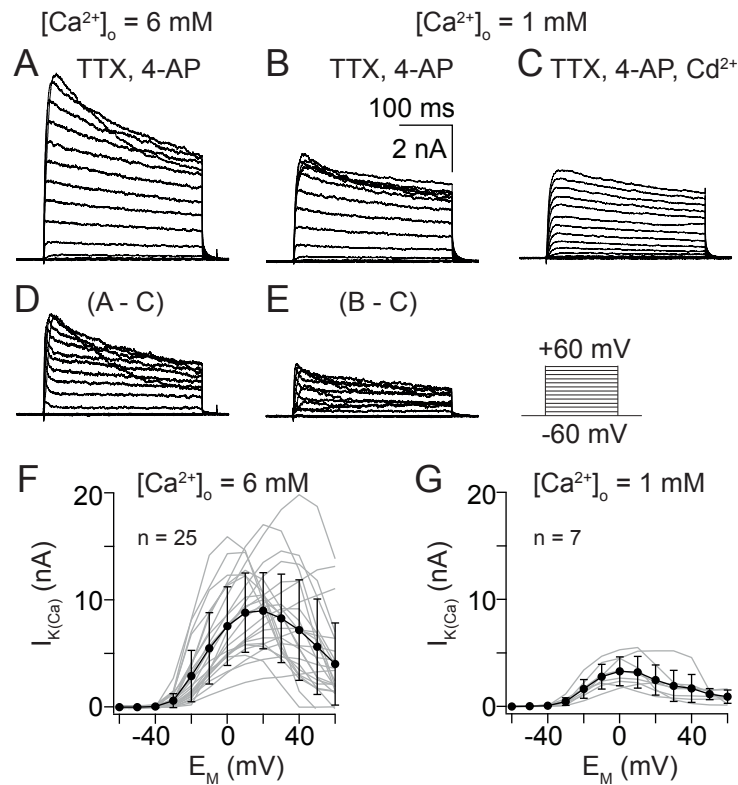
Figure 3.6. Steady-state activation of $I_{K(Ca)}$ from type I LNs. (A – E) Current traces for steady-state activation elicited by 300 ms depolarizing voltage steps from -60 mV to 60 mV in 10 mV increments. (A) Current traces elicited with 6 mM $[Ca^{2+}]_O$. (B) Current traces elicited with 1 mM $[Ca^{2+}]_O$. (C) Current traces elicited during additional application of 5×10^{-4} M $CdCl_2$. (D – E) Digital subtraction of the $CdCl_2$ treated series from 'untreated' series yielded in $I_{K(Ca)}$ activated by influx of 6mM $[Ca^{2+}]_O$ (D) and 1mM $[Ca^{2+}]_O$ (E). (F) *I/V* relation of steady-state activation with 6 mM $[Ca^{2+}]_O$. (G) *I/V* relation of steady-state activation with 1 mM $[Ca^{2+}]_O$.

Type I LNs

With 6 mM $[Ca^{2+}]_O$, decreasing $I_{K(Ca)}$ amplitudes were observed at progressively depolarizing voltage pulses (Fig. 3.6D and E). Type I LNs displayed the lowest current amplitudes compared to other AL interneurons. With 6 mM $[Ca^{2+}]_O$, a maximal $I_{K(Ca)}$ amplitude of 9 ± 4 nA was reached at 28 ± 17 mV and decreasing the $[Ca^{2+}]_O$ to 1 mM shifted the voltage of maximal current activation to more negative potentials (Fig. 3.6F and G). With 1 mM $[Ca^{2+}]_O$, a maximal current amplitude of 3 ± 1 nA was reached at 5 ± 11 mV.

Type II LNs

The most diverse current voltage relation was observed within the type IIa LN population. With 6 mM $[Ca^{2+}]_O$, $I_{K(Ca)}$ amplitude increased with progressively depolarizing voltage pulses (Fig. 3.7D) in the major part of neurons and a maximal current amplitude of 16 ± 8 nA was reached at 60 mV (n = 22, Fig. 3.7F). However, 12 out of 34 recorded type IIa LNs displayed decreasing current amplitude with progressively depolarizing voltage steps, maximal current amplitudes of 23 ± 18 nA were reached at 28 ± 10 mV (n = 12, Fig. 3.7F). When $[Ca^{2+}]_O$ was reduced to 1 mM, the major part of type IIa LNs displayed decreasing $I_{K(Ca)}$ amplitudes with progressively depolarizing voltage steps and a peak current of 7 ± 6 nA was reached at 13 ± 17 mV (n = 11, Fig. 3.7G). However, in five out of 16 investigated type IIa LNs, $I_{K(Ca)}$ amplitudes continued to increase with progressively depolarizing voltage pulses and reached a maximal amplitude of 15 ± 7 nA at 60 mV (n = 5, Fig. 3.7G).

By contrast, all type IIb LNs displayed increasing $I_{K(Ca)}$ amplitudes with progressively depolarizing voltage steps when activated by simultaneous influx of 6 mM $[Ca^{2+}]_O$. Maximal current amplitude of 16 ± 9 nA was reached at 60 mV (Fig. 3.8 F). Diluting the $[Ca^{2+}]_O$ to 1 mM shifted the voltage of peak current activation to more negative potentials, a maximal current amplitude of 7 ± 5 nA was reached at 23 ± 15 mV (n = 4, Fig. 3.8 G).

With 6 mM $[Ca^{2+}]_O$ uPNs, type IIb LNs and the major part of type IIa LNs display increasing $I_{K(Ca)}$ amplitudes with progressively depolarizing voltage pulses, reflected in a linearly increasing *I/V* relation. Decreasing the $[Ca^{2+}]_O$ to 1 mM altered the *I/V* relation in all uPNs as well as the major part of type IIa and type IIb LNs to an inverted U-shaped *I/V* relation. The inverted U-shaped *I/V* relation mirrored the *I/V* relation of I_{Ca} as the driving force for Ca^{2+} declined at higher voltages (Husch *et al.*, 2009a). In type I LNs, a bell-shaped *I/V* relation of $I_{K(Ca)}$ was observed with both applied $[Ca^{2+}]_O$. Assuming that influx of 6 mM $[Ca^{2+}]_O$ was high enough to uncouple $I_{K(Ca)}$ activation from I_{Ca}, 1 mM $[Ca^{2+}]_O$ constitute appropriate conditions to study the biophysical properties of $I_{K(Ca)}$.
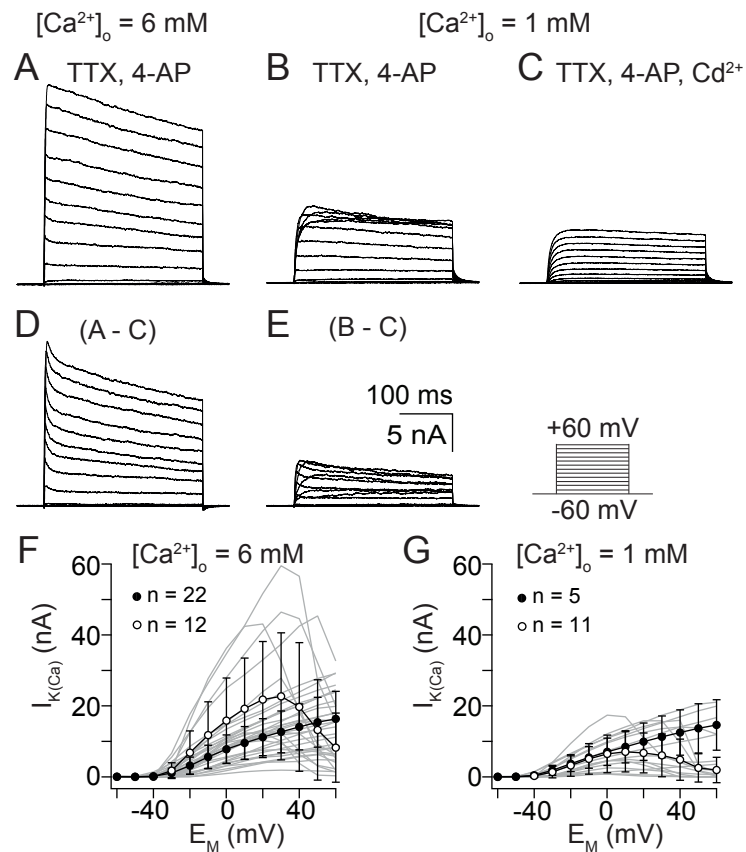
Figure 3.7. Steady-state activation of $I_{K(Ca)}$ from type IIa LNs. (A – E) Current traces for steady-state activation elicited by 300 ms depolarizing voltage steps from -60 mV to 60 mV in 10 mV increments. (A) Current traces elicited with 6 mM $[Ca^{2+}]_O$. (B) Current traces elicited with 1 mM $[Ca^{2+}]_O$. (C) Current traces elicited by the same depolarizing voltage steps as A and B but during additional application of 5×10^{-4} M $CdCl_2$. (D – E) Digital subtraction of the $CdCl_2$ treated series from 'untreated' series yielded in $I_{K(Ca)}$ activated by influx of 6mM $[Ca^{2+}]_O$ (D) or 1mM $[Ca^{2+}]_O$ (E). (F) *I/V* relation for steady-state activation with 6 mM $[Ca^{2+}]_O$. (G) *I/V* relation for steady-state activation with 1 mM $[Ca^{2+}]_O$. Open circles ○ indicate bell-shaped *I/V* relation, filled circles • indicate linear *I/V* relation.
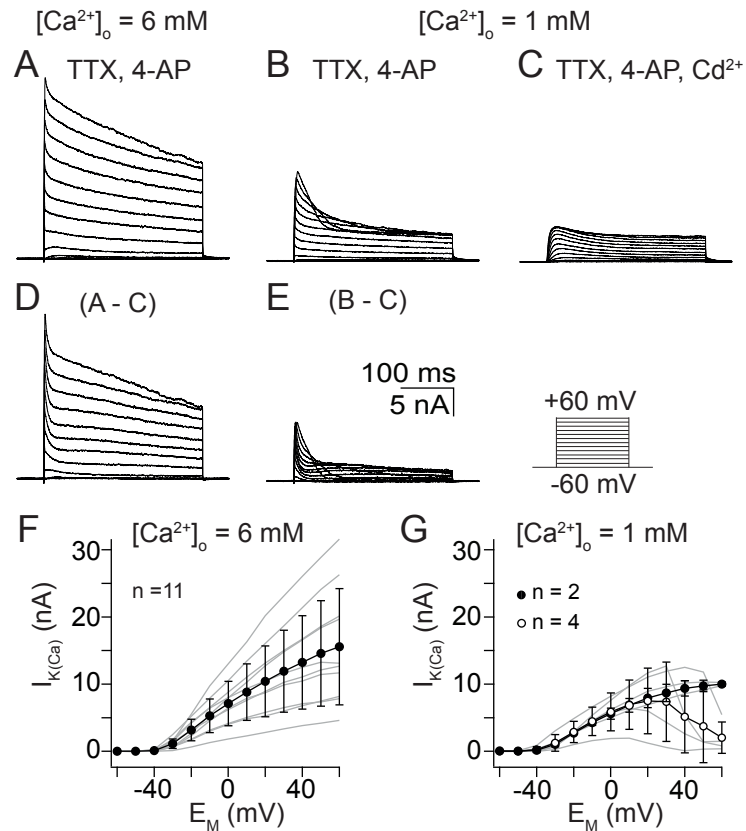
Figure 3.8. Steady-state activation of $I_{K(Ca)}$ from type IIb LNs. (A – E) Current traces for steady-state activation elicited by 300 ms depolarizing voltage steps from -60 mV to 60 mV in 10 mV increments. (A) Current traces elicited with 6 mM $[Ca^{2+}]_O$. (B) Current traces elicited with 1 mM $[Ca^{2+}]_O$. (C) Current traces elicited during additional application of 5×10^{-4} M $CdCl_2$. (D – E) Digital subtraction of the $CdCl_2$ treated series from 'untreated' series yielded in $I_{K(Ca)}$ activated by influx of 6mM $[Ca^{2+}]_O$ (D) or 1mM $[Ca^{2+}]_O$ (E). (F) *I/V* relation of steady-state activation with 6 mM $[Ca^{2+}]_O$. (G) *I/V* relation of steady-state activation with 1 mM $[Ca^{2+}]_O$. Open circles ∘ indicate bell-shaped *I/V* relation, filled circles • indicate linear *I/V* relation.

Table 3.2. Parameters of steady-state activation with influx of 1 and 6 mM [Ca^{2+}]$_O$.
Currents were evoked by 300 ms depolarizing voltage pulses from -60 to 60 mV in 10mV
increments. Values are expressed as mean ± SD.

	uPNs	type I LNs	type IIa LNs	type IIb LNs
	6 mM [Ca^{2+}]$_O$			
activation threshold (mV)	-40	-40	-50	-40
I_{max} (nA)	28 ± 18	9 ± 4	23 ± 18	16 ± 9
E$_{max}$ (mV)	60	28 ± 17	28 ± 10	60
	1 mM [Ca^{2+}]$_O$			
activation threshold (mV)	-40	-50	-50	-40
I_{max} (nA)	21 ± 6	3 ± 1	7 ± 6	7 ± 5
E$_{max}$ (mV)	17 ± 11	5 ± 11	13 ± 17	23 ± 15

3.2.3 Current-voltage relations of $I_{K(Ca)}$

Steady-state activation with simultaneously activated I_{Ca} was used to determine *I/V* relations. Whole-cell capacitance of respective measurment was used to calculate current density from current amplitude. All values are expressed as mean ± SD.

Uniglomerular Projection Neurons

In uPNs an average whole-cell capacitance of 17.9 ± 3.7 pF (n = 7) was given. This corresponds to a mean current density of 1.18 ± 0.45 nA/pF (n = 7, Fig. 3.9A1). Assuming that K^+ is the main charge carrier, this equals to a mean conductance density of 10.4 ± 4.8 nS/pF (n = 7). To compare potentials of maximal $I_{K(Ca)}$ activation, current amplitudes elicited by 1 mM and 6 mM $[Ca^{2+}]_O$ were normalized to its respective maximum (Fig. 3.9 A2 and A3). With both $[Ca^{2+}]_O$, $I_{K(Ca)}$ started to activate at potentials more depolarized than -40 mV and with 1 mM $[Ca^{2+}]_O$ maximal $I_{K(Ca)}$ amplitudes were reached at 17 ± 11 mV (Fig. 3.9A2).

Type I LNs

An average whole-cell capacitance of 25.5 ± 9.8 pF (n = 7) was measured in type I LNs. This corresponds to a mean current density of 117 ± 50 pA/pF (n = 7, Fig. 3.9 B1), and 1.2 ± 0.3 nS/pF mean conductance density (n = 7). $I_{K(Ca)}$ started to activate at -50 mV and maximal activation was reached at 5 ± 11 mV with 1 mM $[Ca^{2+}]_O$ (Fig. 3.9 B2). With 6 mM $[Ca^{2+}]_O$ voltage for activation and maximal activation was shifted to more depolarized potentials, $I_{K(Ca)}$ started to activate at potentials more depolarized than -40 mV and maximal current amplitude was reached at 28 ± 17 mV (Fig. 3.9 B3).

Type IIa LNs

Type IIa LNs exhibited an average whole-cell capacitance of 61.9 ± 38.2 pF. This corresponds to an average conductance density with a maximum of 182 ± 95 pA/pF (n = 11, Fig. 3.9C1) at 10 mV for type IIa LNs with decreasing $I_{K(Ca)}$ amplitude.

Type IIa LNs that displayed increasing $I_{K(Ca)}$ amplitude with progressively de-polarizing voltage pulses, reached a mean current density of 154 ± 47 pA/pF (n = 5, Fig. 3.9C1) at 60 mV. This resulted in a mean conductance density of 1.2 ± 0.2 nS/pF for type IIa LNs with decreasing $I_{K(Ca)}$ (n = 11) and 1.4 ± 0.6 nS/pF for type IIa LNs with increasing $I_{K(Ca)}$. In type IIa LNs, $I_{K(Ca)}$ activated at potentials more depolarized than -50 mV with both applied $[Ca^{2+}]_O$. In the case of neurons that display decreasing $I_{K(Ca)}$ amplitude with progressively depolariz-ing voltage pulses, potential for maximal activation was shifted from 13 ± 17 mV in 1 mM $[Ca^{2+}]_O$ (n = 11, Fig. 3.9 C2) to 28 ± 10 mV in 6 mM $[Ca^{2+}]_O$ (n = 12, Fig. 3.9 C3).

Type IIb LNs

Given a mean whole-cell capacitance of 75.0 ± 38.4 pF, resulted in an average conductance density of 137 ± 108 pA/pF with a maximum at 20 mV (n = 4, Fig. 3.9 D1). This corresponds to a mean conductance density of 945 ± 586 pS/pF for neurons with decreasing $I_{K(Ca)}$. Maximal current amplitudes were reached at 23 ± 15 mV (n = 4, Fig. 3.9D2). Type IIb LNs with $I_{K(Ca)}$ being maximal activated at 60 mV, displayed a mean current density of 241 ± 206 pA/pF resulting in a mean conductance density of 1.4 ± 1.2 nS/pF (n = 2, Fig. 3.9D1).

Clearly, the exact time course and amplitude of $I_{K(Ca)}$ are complex functions of membrane potential, voltage dependence of I_{Ca}, local intracellular Ca^{2+} concen-tration at the K_{Ca} channel and Ca^{2+}-, as well as voltage dependence of the un-derlying K_{Ca} channels. Accordingly, only limited conclusions about K_{Ca} channel intrinsic activation and inactivation properties can be made from the shape of whole-cell currents activated by simple voltage steps depolarizing the neuron for 300 ms (Prakriya *et al.*, 1996). Hence, elaborate voltage protocols were used to study the complex aspects of Ca^{2+} and voltage activation.
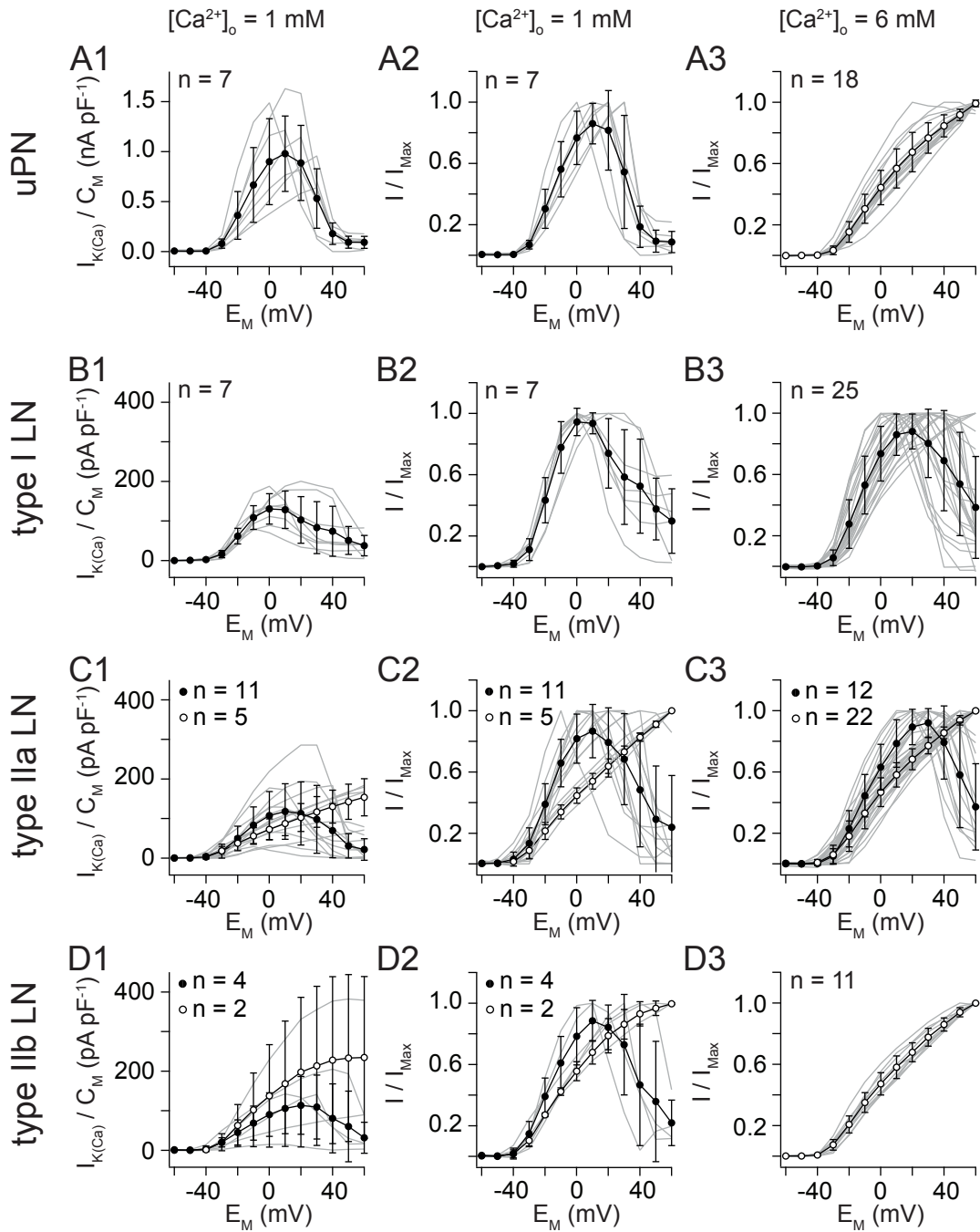
Figure 3.9. *I/V relation of $I_{K(Ca)}$ from uPNs (A), type I LNs (B), type IIa LNs (C), and type IIb LNs (D).* (A1 – D1) Current density of $I_{K(Ca)}$ with 1 mM $[Ca^{2+}]_O$. (A2 – D2) Normalized current voltage relation with 1 mM $[Ca^{2+}]_O$. (A3 – D3) Normalized current-voltage relation with 6 mM $[Ca^{2+}]_O$. Filled circles •indicate bell-shaped *I/V* relation, open circles ○ indicate linear *I/V* relation.

3.3 Calcium dependence of $I_{K(Ca)}$

To further study the dependence of $I_{K(Ca)}$ on I_{Ca}, two-step voltage protocols were executed. A test pulse depolarized the membrane to +60 mV, where voltage activated Ca^{2+} influx does not occure since the membrane is depolarized beyond the Ca^{2+} equilibrium potential. The test pulse was preceded by depolarizing voltage pulses (Ca^{2+} loading steps) of varying amplitude or duration, which modified the intracellular Ca^{2+} concentration. Thus, during the +60 mV test pulse, $I_{K(Ca)}$ is activated by depolarized membrane potential, the varying amount of Ca^{2+} delivered by the loading steps, and the Ca^{2+} resting level. Taking into account that I_{Ca} inactivates during a sustained voltage pulse, the instantaneous Ca^{2+} influx during the loading pulse is dependent a) from the potential of the loading pulse and b) how long I_{Ca} has been activated. Experiments were perfomed by Dr. Cathleen Bradler and myself.

In a first set of experiments 200 ms loading steps were used from -60 mV to +60 mV increased in 10 mV increments. This voltage range covers the complete voltage operating range of I_{Ca} (Husch *et al.*, 2009a). Figures 3.10 – 3.13 illustrate the Ca^{2+}-dependence of $I_{K(Ca)}$ in uPNs (Fig. 3.10), type I LNs (Fig. 3.11), type IIa LNs (Fig. 3.12), and type IIb LNs (Fig. 3.13). Panels A of Fig. 3.10 – 3.13 show recordings in which the test pulse is preceded by a loading step to +10 mV (large Ca^{2+} influx) and +60 mV (no Ca^{2+} influx). While Ca^{2+} influx of the +10 mV loading pulse is terminated by the +60 mV test pulse, $I_{K(Ca)}$ is activated by the amount of Ca^{2+} influx through voltage-gated Ca^{2+} channels (Ca_V channels) from preceeding loading potential and the depolarized test pulse potential of 60 mV. $I_{K(Ca)}$ displayed a solely transient current profile during the test pulse, consisting of a fast activation and complete inactivation within a few milliseconds.

The whole experiment with a complete set of loading pulses from different AL interneurons, respectively are shown in Fig. (3.10 – 3.13)B and magnification of $I_{K(Ca)}$ transients are depicted in Fig. (3.10 – 3.13)C. Plotting the normalized amplitudes of $I_{K(Ca)}$ transients during the test pulse over loading pulse potential revealed inverted U-shaped *I/V* relations (Fig. (3.10 – 3.13)D and 3.14A) with

maxima between -10 and 20 mV, the voltage range in which I_{Ca} diplay maximal activation (Husch *et al.*, 2009a). The mirrored *I/V* relations of $I_{K(Ca)}$ and I_{Ca} clearly demonstrate strong Ca^{2+} dependence of $I_{K(Ca)}$.

In a second set of experiments the 60 mV test pulse was preceded by loading steps with increasing duration (5, 10, 25, 50, 100, 200 and 400 ms), to determine the temporal dynamics of $I_{K(Ca)}$ transients. The loading step potential was induvidually chosen which elicited maximal $I_{K(Ca)}$ transients in previous loading potential experiments Fig. (3.10 – 3.13)E. Thus, the proportion of activated $I_{K(Ca)}$ is dependent on a) activation and inactivation kinetics of Ca_V and K_{Ca} channels and b) the proximity and concerted activity of Ca_V and K_{Ca} channels. Ca^{2+} entering the cytosol via Ca_V channels leads to local and large increases of intracellular Ca^{2+} concentration ($[Ca^{2+}]_i$) in immediate vicinity to the channel pore but rapidly equilibrates due to difussion and buffering (Augustine *et al.*, 2003; Fakler & Adelman, 2008; Pippow *et al.*, 2009). Therefore, inactivation of $I_{K(Ca)}$ during the test pulse should resemble intrinsic inactivation after ceasing Ca^{2+} influx of varying amount. Due to inactivation of I_{Ca} during a sustained depolarization the instantaneous Ca^{2+} influx at the end of each loading pulse is decreasing with increasing length of the loading pulse.

Uniglomerular Projection Neurons

$I_{K(Ca)}$ was activated by prepulse potentials between -40 and 50 mV, an average maximum was achieved at 10 mV prepulse potential (n = 6), Fig. 3.10D). Alteration of prepulse duration (Fig. 3.10E and F) yielded in slowest decay of $I_{K(Ca)}$ transients at 10 ms, which equaled 6.4 ± 3.9 ms. Prolonged prepulse duration of 400 ms expedited the decay to 3.3 ± 0.7 ms (n = 4, Fig. 3.10F). In 4 out of 5 uPNs, $I_{K(Ca)}$ maxima were elicited with 5 ms prepulses, peristing loading pulse duration led to decreasing $I_{K(Ca)}$ amplitudes, but even prepulse duration of 400 ms elicited 58% of $I_{K(Ca)}$ amplitude (n = 5, Fig. 3.10G).
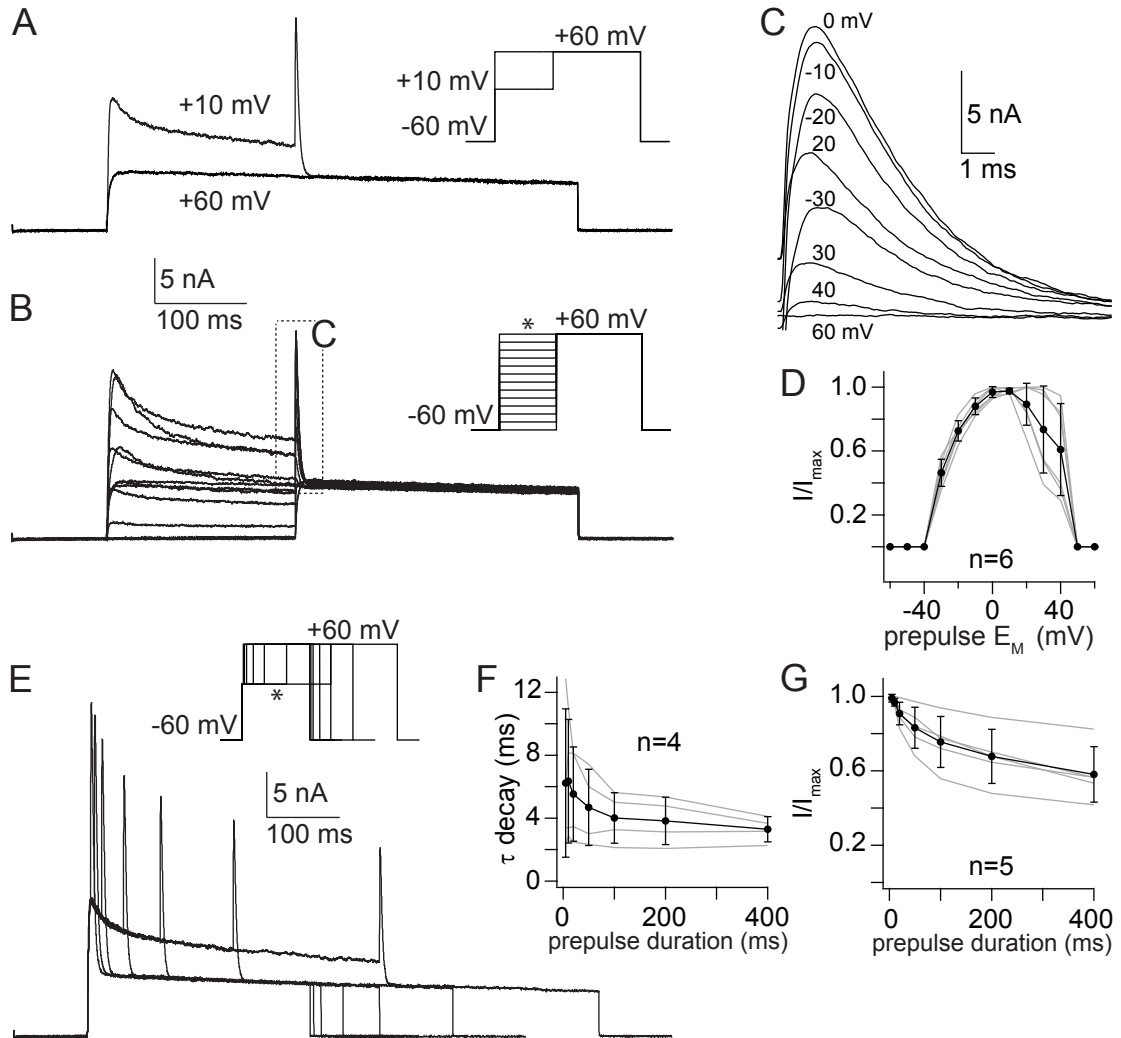
Figure 3.10. Ca²⁺ dependence of $I_{K(Ca)}$ from uPNs. (A) Current trace with a loading step to +10 mV (large Ca²⁺ influx) was followed by transient activation of $I_{K(Ca)}$ during the 60 mV test pulse, while prepulse potential of 60 mV (no Ca²⁺ influx) led to no $I_{K(Ca)}$ activation. (B) Whole experiment with a complete set of loading pulses. The 300 ms test pulse is preceded by 200 ms loading pulses between -60 and +60 mV, increased in 10 mV increments. (C) Magnification of $I_{K(Ca)}$ transients. (D) Fractional $I_{K(Ca)}$ amplitude plotted as a function of loading pulse potential. (E) $I_{K(Ca)}$ activation by loading steps of variable duration. The 300 ms test pulse was preceded by loading pulses of 5, 10, 25, 50, 100, 200 and 400 ms to that potential which elicited maximal $I_{K(Ca)}$ transients in B (∗). (F) Decay of $I_{K(Ca)}$ transients as a function of prepulse duration. (G) Fractional $I_{K(Ca)}$ amplitude as a function of loading pulse duration. This figure was kindly provided by Dr. Cathleen Bradler.

Type I LNs

In type I LNs, $I_{K(Ca)}$ was activated by prepulse potentials between -30 and 30 mV. Maximal $I_{K(Ca)}$ activation was achieved by 0 mV prepulse potential (n = 9, Fig. 3.11D). $I_{K(Ca)}$ transients displayed the slowest decay of 2.7 ± 0.3 ms after prepulses of 50 ms duration, shorter or longer prepulse duration both led to an decay within 1.9 ms (n = 8, Fig. 3.11F). Maximal $I_{K(Ca)}$ amplitudes were elicited after 50 ms prepulses too, 5 ms prepulses elicited 69%, and 400 ms prepulses elicited even 76% of $I_{K(Ca)}$ amplitude (n = 8, Fig. 3.11G).

Type IIa LNs

$I_{K(Ca)}$ was activated by prepulse potentials between -50 mV and 50 mV with maximal activation at 0 mV (n = 12, Fig. 3.12D). Transients displayed slowest decay of 4.4 ± 3.3 ms after 10 ms prepulses, but time constants were in the same range after 5 and 25 ms prepulses, respectively (n = 10, Fig. 3.12F). Maximal $I_{K(Ca)}$ amplitudes were elicited after 10 ms prepulses too, after 400 ms prepulses 54% of $I_{K(Ca)}$ amplitudes were reached (Fig. 3.12G).

Type IIb LNs

In type IIb LNs, $I_{K(Ca)}$ was activated by prepulse potentials between -50 and 50 mV with an average maximum at 0 mV (n = 5, Fig. 3.13D). Maximal $I_{K(Ca)}$ transients were reached with 5 ms prepulses and decayed within 3.4 ± 1.0 ms (n = 4, Fig. 3.13F). Persisting loading pulse duration led to further decreasing $I_{K(Ca)}$ amplitudes, and prepulses duration of 400 ms elicited only 41% of $I_{K(Ca)}$ amplitudes (n = 5, Fig. 3.13G).

All AL interneurons displayed maximal $I_{K(Ca)}$ activation with prepulse potentials between 0 and 10 mV according to potentials of maximal I_{Ca} activation (Husch *et al.*, 2009b,a). $I_{K(Ca)}$ in type I LNs was activated by the most limited range of prepulse potential, only prepulses between -30 and 30 mV elicited $I_{K(Ca)}$ transients (Fig. 3.14A). Plotting the fractional $I_{K(Ca)}$ amplitude during the test pulse over
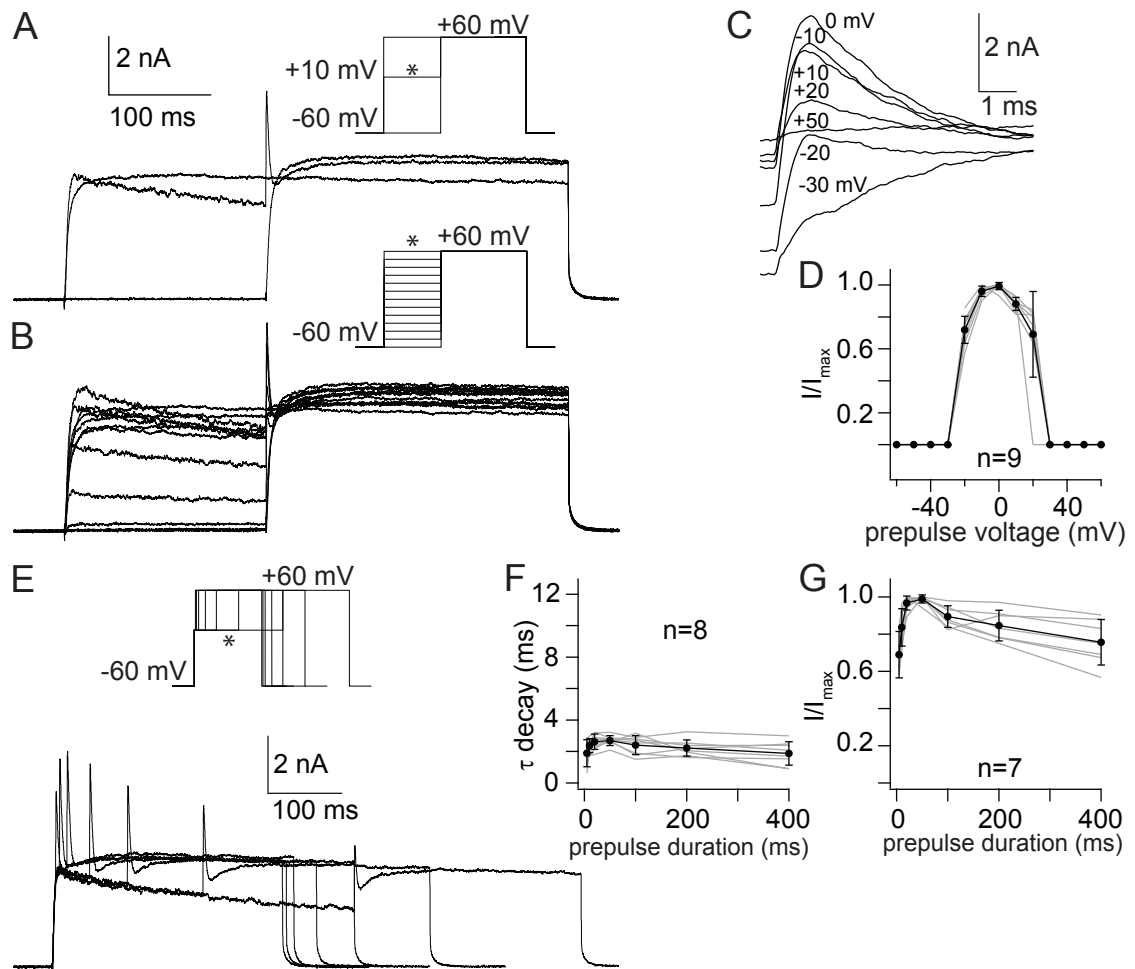
Figure 3.11. Ca^{2+} dependence of $I_{K(Ca)}$ from type I LNs. (A) Current traces with loading steps to -60, 10 and +60 mV. Prepulse potential of 10 mV (large Ca^{2+} influx) was followed by transient $I_{K(Ca)}$ during the 60 mV test pulse. With prepulse potential of -60 and 60 mV (no Ca^{2+} influx) no $I_{K(Ca)}$ activation was observed. (B) Whole experiment with a complete set of loading pulses. The 300 ms test pulse is preceded by 200 ms loading pulses between -60 and +60 mV, increased in 10 mV increments. (C) Magnification of $I_{K(Ca)}$ transient. (D) Fractional $I_{K(Ca)}$ amplitude as a function of loading pulse potential. (E) $I_{K(Ca)}$ activation by loading steps of variable duration. The test pulse was preceded by loading pulses of 5, 10, 25, 50, 100, 200 and 400 ms to that potential which elicited maximal $I_{K(Ca)}$ transients in B (*). (F) Decay of $I_{K(Ca)}$ transients as function of prepulse duration. (G) Fractional $I_{K(Ca)}$ amplitude as a function of loading pulse duration.

Figure 3.12. Ca²⁺ dependence of $I_{K(Ca)}$ from type IIa LNs. (A) Current traces with loading step to -60, 0 and +60 mV. Prepulse potential of 0 mV (large Ca²⁺ influx) was followed by transient $I_{K(Ca)}$ during the 60 mV test pulse. With prepulse potential of -60 and 60 mV (no Ca²⁺ influx) no $I_{K(Ca)}$ activation was observed. (B) Whole experiment with a complete set of loading pulses. The 300 ms test pulse is preceded by 200 ms loading pulses between -60 and +60 mV, increased in 10 mV increments. (C) Magnification of $I_{K(Ca)}$ transients. (D) Fractional $I_{K(Ca)}$ amplitude as a function of loading pulse potential. (E) $I_{K(Ca)}$ activation by loading steps of variable duration. The test pulse was preceded by loading pulses of 5, 10, 25, 50, 100, 200 and 400 ms to that potential which elicited maximal $I_{K(Ca)}$ transients in B (∗). (F) Decay of $I_{K(Ca)}$ transients as a function of prepulse duration. (G) Fractional $I_{K(Ca)}$ amplitude as a function of loading pulse duration. Panels A – C and E were kindly provided by Dr. Cathleen Bradler.

Figure 3.13. Ca^{2+} dependence of $I_{K(Ca)}$ from type IIb LNs. (A) Current traces with loading step to -60, 10 and +60 mV. Prepulse potential of 10 mV (large Ca^{2+} influx) was followed by transient $I_{K(Ca)}$ during the 60 mV test pulse. With prepulse potential of -60 and 60 mV (no Ca^{2+} influx) no $I_{K(Ca)}$ activation was observed. (B) Whole experiment with a complete set of loading pulses. The 300 ms test pulse is preceded by 200 ms loading pulses between -60 and +60 mV. (C) Magnification of $I_{K(Ca)}$ transient. (D) Fractional $I_{K(Ca)}$ amplitude as a function of loading pulse potential. (E) $I_{K(Ca)}$ activation by loading steps of variable duration. The test pulse was preceded by loading pulses of 5, 10, 25, 50, 100, 200 and 400 ms to that potential which elicited maximal $I_{K(Ca)}$ transients in B (∗). (F) Decay of $I_{K(Ca)}$ transients as a function of prepulse duration. (G) Fractional $I_{K(Ca)}$ amplitude as a function of loading pulse duration. Panels A –C and E were kindly provided by Dr. Cathleen Bradler.
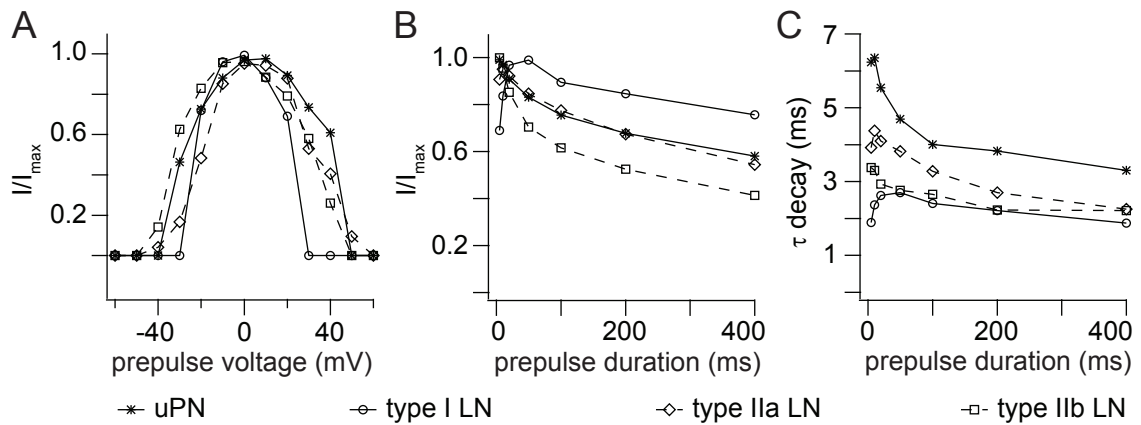
Figure 3.14. Dependence of $I_{K(Ca)}$ to I_{Ca} from different AL interneurons (A) Fractional $I_{K(Ca)}$ amplitude as a function of loading pulse potential. (B) Fractional $I_{K(Ca)}$ amplitude as a function of loading pulse duration. (C) Decay of $I_{K(Ca)}$ transients as function of prepulse duration.

loading pulse duration revealed differences between AL interneurons. Amplitude of $I_{K(Ca)}$ transients reached maxima with 5 ms prepulses in uPNs and type IIb LNs. In these neurons $I_{K(Ca)}$ amplitude decreased constantly with further elongated loading pulse duration to roughly 50% of maximal $I_{K(Ca)}$ amplitude. Type IIa LNs exhibit maximal $I_{K(Ca)}$ amplitudes with 5 to 25 ms prepulse duration, peak values were observed with 10 ms loading pulses. Type I LNs displayed the most complex relation between loading duration and $I_{K(Ca)}$ amplitude, 5 ms prepulses elicited only 69% of the peak current which was reached with 50 ms loading pulses. With further persisting prepulse duration current amplitude decreased, but even after 400 ms prepulses 76% of maximal $I_{K(Ca)}$ activation was achieved (Fig. 3.14B). $I_{K(Ca)}$ transients displayed slowest decay in the range from 6.4 to 2.7 ms with prepulse durations activating $I_{K(Ca)}$ maximally. With 50 ms loading pulses the decay τ equaled 4.7 ± 2.4 ms in uPNs, 2.7 ± 0.3 ms in type I LNs, 3.8 ± 2.3 ms in type IIa LNs and 2.8 ± 0.9 ms in type IIb LNs (Fig. 3.14C).

Table 3.3. Activation of $I_{K(Ca)}$ by previous Ca^{2+} influx. Two-step voltage protocols were used to study the Ca^{2+} dependence of $I_{K(Ca)}$. $I_{K(Ca)}$ was elicited by a test pulse, depolarizing the menbrane to 60 mV and preceeding Ca^{2+} loading steps of various potential or duration.

	uPNs	type I LNs	type IIa LNs	type IIb LNs
$I_{K(Ca)}$ activation by Ca^{2+} loading pulses of different potential				
prepulse potential E (mV)	-40 − +50	-30 − +30	-50 − +50	-50 − +50
prepulse potential E_{max} (mV)	+10	0	0	0
$I_{K(Ca)}$ activation by Ca^{2+} loading pulses of various duration				
I_{max} with prepulse duration (ms)	5	50	10	5
I/I_{max} after 400 ms prepulses	58%	76%	54%	41%
slowest decay τ_{max} (ms)	6.4 ± 3.9	2.7 ± 0.3	4.4 ± 3.3	3.4 ± 1.0
decay τ_{min} (ms)	3.3 ± 0.7	1.9 ± 0.7	2.3 ± 0.8	2.2 ± 0.9

3.4 Pharmacological properties of $I_{K(Ca)}$

$I_{K(Ca)}$ is mediated by SK, IK and BK channels, which can be distinguished by their sensitivity to toxins. Here, I examined the effect of apamin, charybdotoxin (ChTX), and iberiotoxin (IbTX) on $I_{K(Ca)}$ from different AL interneurons. An $[Ca^{2+}]_O$ of 6 mM was chosen to boost $I_{K(Ca)}$ amplitude, and currents were evoked by a depolarizing voltage step to 0 mV. Concentration-response relations were determined by application of one toxin in consecutive concentrations between 10 pM and 100 nM. Amplitudes were calculated as a fraction of $I_{K(Ca)}$ amplitude under control conditions (I_{max}) and fit to equation (2.2, see Methods). While application of 1 μM apamin had no effect on $I_{K(Ca)}$ from all AL interneurons, both ChTX and IbTX blocked $I_{K(Ca)}$ in a concentration dependent way, however IbTX had less potent effect on $I_{K(Ca)}$. Complete $I_{K(Ca)}$ inhibition was achieved by application of ChTX, while IbTX application even at the highest concentration resulted in only partial current block (Fig. 3.15).

ChTX started to block $I_{K(Ca)}$ from uPNs at concentrations around 1 nM, concentrations higher than 50 nM blocked $I_{K(Ca)}$ completely, yielding in an EC_{50} of 2.4 nM for ChTX. IbTX started to suppress $I_{K(Ca)}$ at concentrations around 10 pM, but only 59% of $I_{K(Ca)}$ were blocked during application of 100 nM IbTX (Fig. 3.15A). The concentration-response fit yielded in EC_{50} of 157 pM for IbTX.

ChTX started to block $I_{K(Ca)}$ from type I LNs at concentrations around 3 nM and

Figure 3.15 *(following page).* **Pharmacology of $I_{K(Ca)}$ from different AL interneurons.** (A) Concentration-response relation of ChTX (n = 12) and IbTX (n = 8) from uPNs. Fractional $I_{K(Ca)}$ amplitudes were fit to equation (2.2), yielding in an EC_{50} of 2.4 nM for ChTX and 157 pM for IbTX. (B) Current traces from two uPNs under control conditions and during application of different IbTX (upper part) or ChTX (lower part) concentrations. (C) Concentration-response relation of ChTX (n = 6) and IbTX (n = 6) from type I LNs. Fractional $I_{K(Ca)}$ amplitudes were fit to equation (2.2), yielding in an EC_{50} of 4.3 nM for ChTX and 277 pM for IbTX. (D) Current traces from two type I LNs under control conditions and during application of different IbTX (upper part) or ChTX (lower part) concentrations. (E) Concentration-response relation of ChTX (n = 7) and IbTX (n = 7) from type II LNs. Fractional $I_{K(Ca)}$ amplitudes were fit to equation (2.2), yielding in an EC_{50} of 4.2 nM for ChTX and 7.5 nM for IbTX. (F) Current traces of two type II LNs under control conditions and during application of different IbTX (upper part) or ChTX (lower part) concentrations.

uniglomerular Projection Neurons

Type I LNs
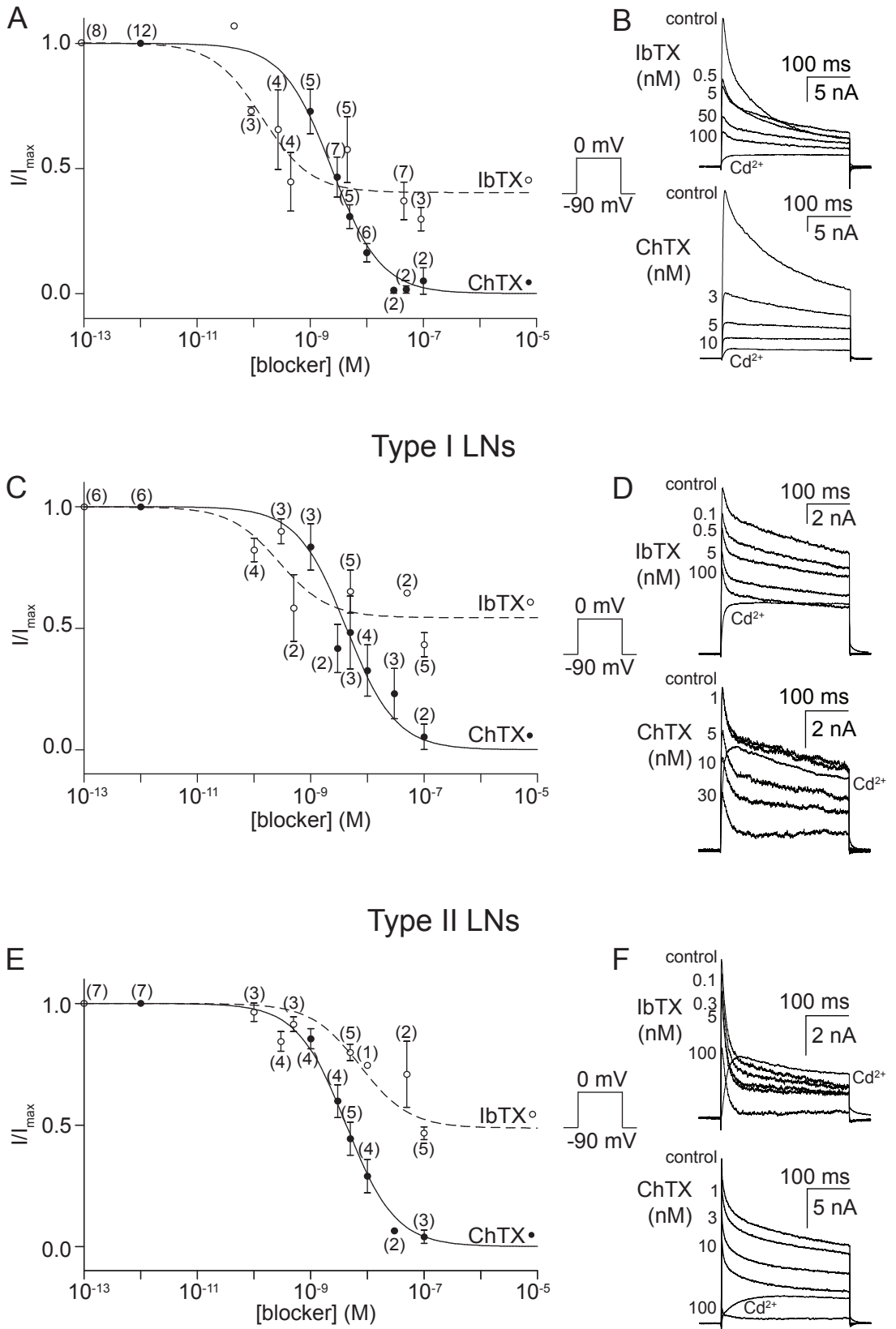
Type II LNs

Table 3.4. Pharmacology of $I_{K(Ca)}$ from different AL interneurons. Currents were calculated as a fraction of maximal current amplitude and fit to equation (2.2, see Methods).

		uPNs	type I LNs	type II LNs
ChTX	EC_{50} (nM)	2.4	4.3	4.2
	residual current (%) at 10 nM	20	30	30
IbTX	EC_{50} (nM)	0.18	0.28	7.5
	residual current (%) at 10 nM	41	56	71
	residual current (%) at 100 nM	40	55	52

application of 100 nM ChTX resulted in complete $I_{K(Ca)}$ inhibition, yielding in an EC_{50} of 4.3 nM. IbTX started to suppress $I_{K(Ca)}$ at concentrations around 10 pM but only 46% of $I_{K(Ca)}$ were blocked even at highest toxin concentration applied (Fig. 3.15C). The concentration-response fit yielded in an EC_{50} of 277 pM for IbTX. Type II LNs displayed similar sensitivity to ChTX as type I LNs, but they were less sensitive to IbTX compared to all other AL interneurons. As no difference of $I_{K(Ca)}$ sensitivity to ChTX and IbTX was observed between LNII subtypes, data for both subtypes were combined and analyzed. In type II LNs ChTX started to block $I_{K(Ca)}$ at concentrations around 1 nM and 50 nM ChTX blocked $I_{K(Ca)}$ completely, yielding in an EC_{50} of 4.2 nM. IbTX started to suppress $I_{K(Ca)}$ at concentrations around 10 pM, but only 51% of $I_{K(Ca)}$ could be blocked even when 100 nM IbTX were applied (Fig. 3.15E). The concentration-response fit according to equation (2.2, see Methods) yielded in an EC_{50} of 7.5 nM.

In an effort to test whether SK channels contribute to $I_{K(Ca)}$, 1 µM apamin, a known SK channel blocker, was applied to the preparations. To assure that changes in current amplitude were due to blocker treatment, currents were elicited three times in 5 min intervals under control conditions, blocker treatment, and during wash out (Fig. 3.16A and B). Figure 3.16 depicts a recording from a single type I LN. The average fractional amplitude out of three subsequent applications equaled 0.91 ± 0.07 under control conditions and 0.90 ± 0.09 upon apamin appli-

cation, which constitute no significant change in current applitude (Fig. 3.16C). $I_{K(Ca)}$ from other AL interneurons was not sensitive to apamin application as well (data not shown).
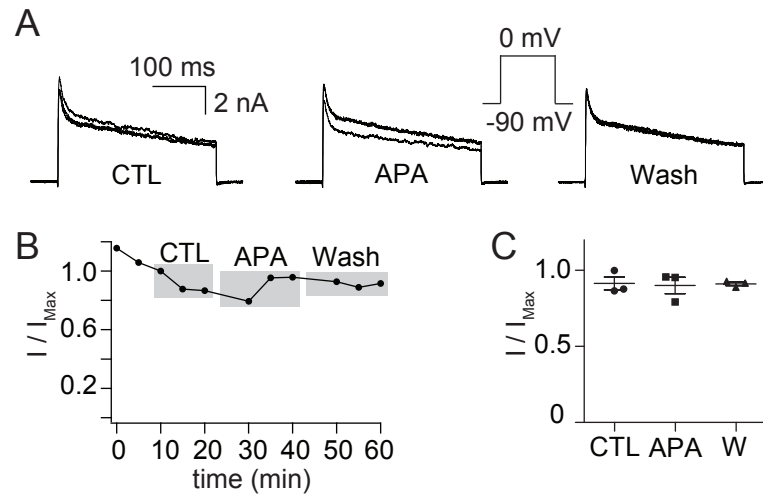
Figure 3.16. Application of the SK channel blocker apamin on type I LN. (A) $I_{K(Ca)}$ recorded under control conditions, after application of 1 μM apamin and subsequent wash out. Each row shows an overlay of three current traces recorded after 15 min of respective treatment. (B) Fractional $I_{K(Ca)}$ amplitude as a function of recording time, respective treatments are indicated by grey boxes. (C) Mean fractional $I_{K(Ca)}$ amplitude under control conditions, apamin application and wash out.

3.5 $I_{K(Ca)}$ and underlying currents

Charybdotoxin (ChTX) was the only toxin tested, which achieved complete inhibition of $I_{K(Ca)}$ from all AL interneurons. Therefore, I used 100 nM ChTX to accomplish comlete inhibition of $I_{K(Ca)}$ and demonstrate the pure amount of $I_{K(Ca)}$ and underlying currents. Recordings were performed according to isolation of $I_{K(Ca)}$ (see 3.2.2 Steady-state activation with calcium influx) with 1mM $[Ca^{2+}]_O$. Previous to Cd^{2+} application, ChTX was added to the extracellular solution and current traces consisting of I_{Ca} and $I_{K(V)}$ were elicited. Digital subtraction of consecutive treatments disclosed the pure amount of $I_{K(Ca)}$, I_{Ca} and $I_{K(V)}$ in different AL interneurons (Fig. 3.17).

Generally, uPNs displayed current profiles dominated by $I_{K(Ca)}$. $I_{K(V)}$ amplitude was remarkably smaller and, as a result of digital subtraction, I_{Ca} amplitudes appeared vanishingly small (Fig. 3.17A). *I/V* relation of $I_{K(Ca)}$ and current consisting of $I_{K(Ca)}$, I_{Ca}, and $I_{K(V)}$ were almost similar (Fig. 3.17B).

Application of TTX and 4-AP on a type I LN led to current profiles shaped by $I_{K(Ca)}$, I_{Ca} and $I_{K(V)}$ (Fig. 3.17C). Digital subtraction revealed a prominent I_{Ca}, and $I_{K(V)}$ reaching highest current amplitudes (Fig. 3.17D).

During 300 ms depolarizing voltage pulses $I_{K(Ca)}$ from type IIb LN displayed a prominent transient component. At progressively depolarizing potentials, current was superimposed by increasing $I_{K(V)}$ amplitude (Fig. 3.17E).

In all neurons, I_{Ca} displayed different current profiles and *I/V* relations than previously reported by Husch *et al.* (2009b). Subsequent application and required

Figure 3.17 *(following page).* **Steady-state activation of $I_{K(Ca)}$ and underlying currents from different AL interneurons.** Current traces were elicited by depolarizing voltage steps from -60 to 60 mV in 10 mV increments and cells were bathed in saline containing TTX and 4-AP. Additional application of 100 nM ChTX abolished $I_{K(Ca)}$ completely. Subsequent application of Cd^{2+} blocked I_{Ca} as well and only $I_{K(V)}$ was recorded. Digital subtraction revealed the amount of $I_{K(Ca)}$ and I_{Ca} within the investigated voltage range. (A) Steady-state activation from a single uPN. (B) *I/V* relation of recorded and digitally subtracted currents from this uPN. (C) Steady-state activation from a single type I LN. (D) *I/V* relation of recorded and digitally subtracted currents from this type I LN. (E) Steady-state activation from one type IIb LN. (F) *I/V* relation of recorded and digitally subtracted currents from this type IIb LN.

uniglomerular Projection Neuron
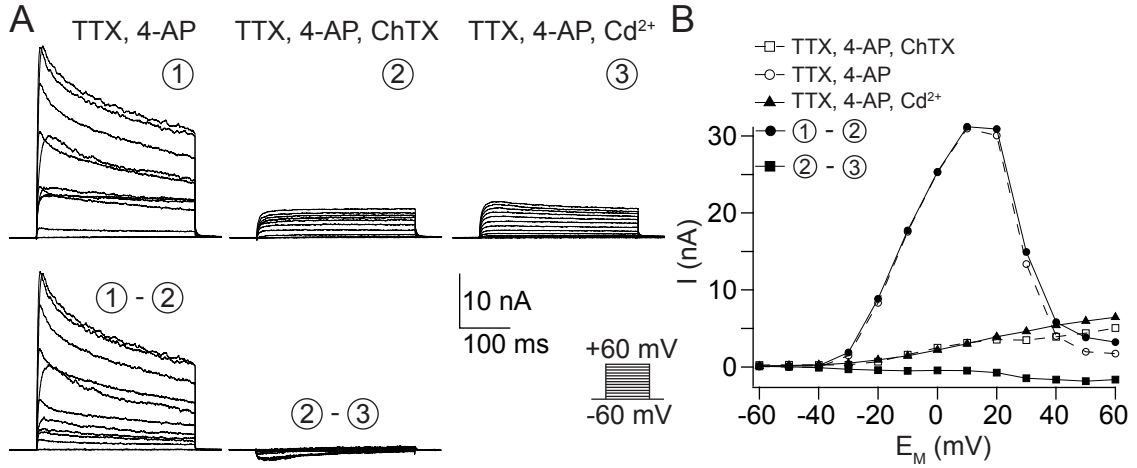
Type I LN
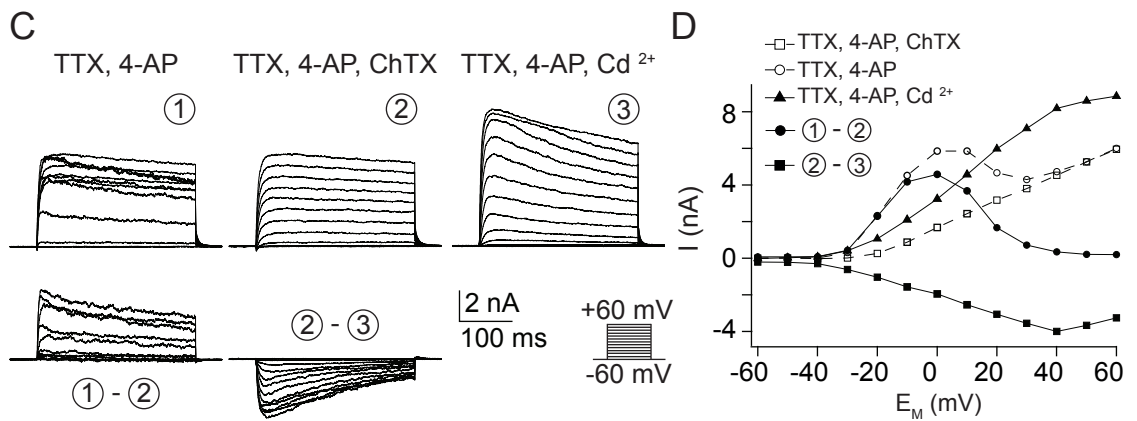
Type IIb LN
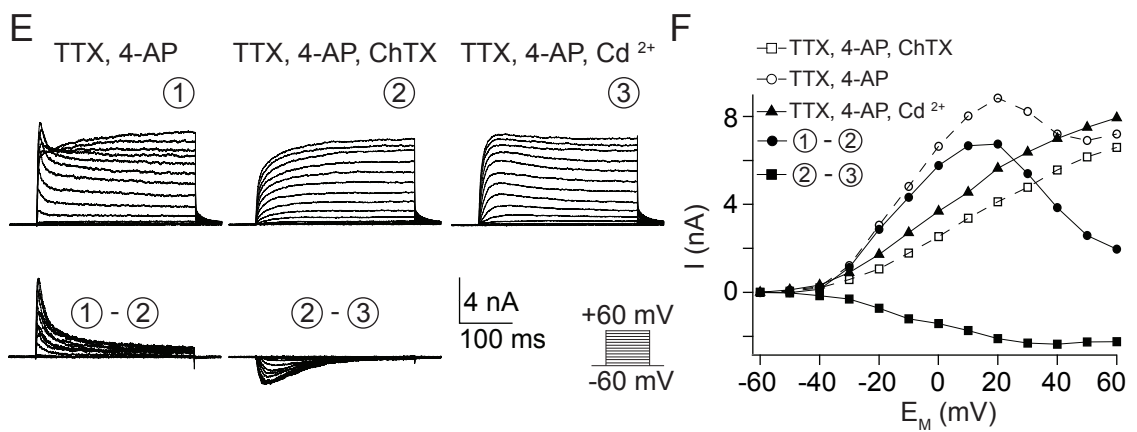
incubation time might cause inaccuracies in the *I/V* relationship, thus digital subtraction is less reliable than pharmacological isolation to evaluate current profiles and *I/V* relations. I_{Ca} amplitudes of were in the same range as previously described (Husch *et al.*, 2009a,b). Comparison of defined $I_{K(Ca)}$ with underlying I_{Ca} (○ Fig. 3.17) and pure $I_{K(Ca)}$ (● Fig. 3.17) demonstrate that current profiles and *I/V* relation were clearly dominated by $I_{K(Ca)}$.

4 Discussion

Within the AL network, distinct neurons perform different tasks to accomplish olfactory processing (Olsen *et al.*, 2007; Olsen & Wilson, 2008; Assisi *et al.*, 2012; Wilson, 2013). Distinct electrophysiological properties arise from neuron intrinsic ion channels and cell specific mechanisms (Husch *et al.*, 2009a,b; Pippow *et al.*, 2009; Demmer & Kloppenburg, 2009). Only uPNs and type I LNs generate Na^+ action potentials because they express voltage-dependent Na^+ channels. Type II LNs do not possess voltage-dependent Na^+ channels and accordingly do not fire action potentials but presumably implement graded transmitter release. Furthermore, non-spiking type II LNs can be subdivided into IIa and IIb subtypes by their active membrane properties and characteristics of voltage activated Ca^{2+} currents. To enhance our knowledge how distinct electrophysiological properties are produced by intrinsic ion channels, detailed studies of ionic currents from different AL interneurons are indispensable.

The aim of this study was to investigate pharmacological and biophysical properties of $I_{K(Ca)}$ from different AL interneurons which will help to understand how $I_{K(Ca)}$ contributes to the electrophysiological properties of these specific neurons. Parameters from steady-state activation of $I_{K(Ca)}$ was analyzed at fixed $[Ca^{2+}]_i$ and with low and high concentrated Ca^{2+} influx. To further study the Ca^{2+} dependence of $I_{K(Ca)}$ two-step voltage protocols were executed. In the second part, toxin peptides of high selectivity were used to assign K_{Ca} channels mediating $I_{K(Ca)}$. Additionally, concentration-response relations were established and complete inhibition of $I_{K(Ca)}$ was accomplished to unveile the pure amount of $I_{K(Ca)}$ and underlying I_{Ca}. Based on pharmacological experiments, exclusion experi-

ments will be performed in which $I_{K(Ca)}$ is partially blocked to reveal the functional impact of $I_{K(Ca)}$ in spiking uPNs and type I LNs.

All recordings in this study were performed in an intact brain preparation. Given that complex arborizations were still intact, perfect voltage control across the entire neuron can not be assumed. However, current waveforms did not indicate significant voltage control problems suggesting that they originated from well voltage-clamped regions. Given the long, thin primary neurite, it is assumed that the major part of measured currents originate from the cell bodies.

4.1 Biophysical properties of $I_{K(Ca)}$

Steady-state activation of $I_{K(Ca)}$ was determined with Ca^{2+} influx of 1 and 6 mM $[Ca^{2+}]_O$ and with defined $[Ca^{2+}]_i$. With simultaneous Ca^{2+} influx of 1 and 6 mM, the current profile consisted of a sustained, noninactivating component and a more or less prominent, transient component, inactivating at diverse time scales. In studies from rat chromaffin cells inactivating and noninactivating BK currents have been identified (Solaro *et al.*, 1995). Inactivating BK currents are sensitive to cytosolic trypsin, which slowed till removed inactivation (Solaro & Lingle, 1992; Solaro *et al.*, 1997; Li *et al.*, 1999). Although the structural component of BK channels that confers inactivation has not been identified, two alternative splice variants of *Slo* are found in chromaffin cells which are able to form heteromultimers leading to inactivation rates of diverse time course (Saito *et al.*, 1997; Ding *et al.*, 1998; Lovell *et al.*, 2000). A biphasic current profile of $I_{K(Ca)}$ is also consistent with studies from insect DUM neurons (Derst *et al.*, 2003; Heidel & Pflüger, 2006) or Kenyon cells (Schäfer *et al.*, 1994; Demmer & Kloppenburg, 2009).

When defined $[Ca^{2+}]_i$ were applied via the recording pipette, $I_{K(Ca)}$ displayed a sustained non-inactivating current profile, like pSlo currents measured in HEK 293 cells after heterologous expression (Derst *et al.*, 2003). Hence, inactivation of $I_{K(Ca)}$ during a sustained voltage pulse seems to be caused by I_{Ca} inactivation and reduction of Ca^{2+} concentration at the K_{Ca} channels.

4.1.1 Calcium sensitivity and voltage dependent activation

When constant $[Ca^{2+}]_i$ were applied, $I_{K(Ca)}$ from all AL interneurons displayed clear voltage dependence. *In situ* recordings of AL interneurons showed that voltages of half-maximal activation $V_{0.5(act)}$ were shifted to more positive potentials compared to pSlo currents from heterologous expression (Derst *et al.*, 2003). Additionally, steady-state activation at defined $[Ca^{2+}]_i$ from unequivocally identified AL interneurons revealed differential Ca^{2+} sensitivity of $I_{K(Ca)}$ among cell types. Within the population of AL interneurons, $I_{K(Ca)}$ from type I LNs was activated with lowest $[Ca^{2+}]_i$ accounting to highest Ca^{2+} sensitivity, while uPNs require 10 fold higher $[Ca^{2+}]_i$ to activate at comparable membrane potential (see table 3.1). Physiological membrane potential of non-spiking type II LNs is more hyperpolorized than in spiking neurons, but an $[Ca^{2+}]_i$ of 1.8 mM lead to half-maximal $I_{K(Ca)}$ activation at 87 and 62 mV, indicating that type II LNs need even higher $[Ca^{2+}]_i$ to activate $I_{K(Ca)}$ within the range of their physiological membrane potential.

Elevation of $[Ca^{2+}]_i$ in this extent occure only in very local spatiotemporal domains close to Ca_V channels which are linked to K_{Ca} channel (Augustine *et al.*, 2003; Berkefeld *et al.*, 2006; Fakler & Adelman, 2008). Although both channel types are directly linked by channel-channel interaction, diverse coupling of Ca_V- and K_{Ca} channels has been reported (Berkefeld *et al.*, 2006). P-type calcium channels couple to the activation of BK channels or SK channels in cerebellar Purkinje cells (Edgerton & Reinhart, 2003). L-type Ca_V channels have been reported to activate BK channels in chromaffin cells (Marcantoni *et al.*, 2010), whereas in CA1 hippocampal neurons L-type channels specifically activate SK channels and BK channels are activated by N-type Ca_V channels (Marrion & Tavalin, 1998). A given cell can link differential Ca_V channels to the same K_{Ca} channel for selective activation or that K_{Ca} channels respond to the domains of intracellular calcium increase produced by several different Ca_V channel subtypes (Davies *et al.*, 1996; Turner *et al.*, 2011). Additionally, modulatory binding partners and scaffold proteins increase the potential for subtle modulation (Levitan, 2006), for example

the *slowpoke*-binding protein (Slob) has been proven to alter voltage dependent activation (Zeng *et al.*, 2005).

4.1.2 Parameters of steady-state activation

Steady-state activation of $I_{K(Ca)}$ with simultaneous Ca^{2+} influx, revealed current amplitudes in the same range as reported from cockroach DUM neurons (Grolleau & Lapied, 1995; Derst *et al.*, 2003; Gautier *et al.*, 2008). However, comparison of activation by influx of 1 and 6 mM $[Ca^{2+}]_O$ unveiled disparate *I/V* relations. Activated by influx of 6 mM $[Ca^{2+}]_O$, $I_{K(Ca)}$ from uPNs, type IIb LNs, and the major part of type IIa LNs displayed increasing current amplitudes with progressively depolarizing voltage steps. Linear *I/V* relations of $I_{K(Ca)}$ have been also reported from studies in cockroach and locust DUM neurons which used 5 mM $[Ca^{2+}]_O$ (Grolleau & Lapied, 1995; Derst *et al.*, 2003; Heidel & Pflüger, 2006). Although N- or bell-shaped *I/V* relations were refered to be characteristic of $I_{K(Ca)}$ (Thomas, 1984; Nightingale & Pitman, 1989; Solaro *et al.*, 1995).

Reducing the $[Ca^{2+}]_O$ to 1 mM resulted in smaller current amplitudes, decreasing with progressively depolarizing voltage pulses. This resulted in characteristic bell-shaped *I/V* relations of $I_{K(Ca)}$, which have also been described from insect Kenyon cells (Schäfer *et al.*, 1994; Demmer & Kloppenburg, 2009). Linear *I/V* relation might be produced by robust elevations of $[Ca^{2+}]_i$ which presumably saturate cytoplasmatic Ca^{2+} clearance mechanisms (Pippow *et al.*, 2009). Reducing the $[Ca^{2+}]_O$ shifted voltage of maximal activation to more hyperpolarized potentials too. With 1 mM $[Ca^{2+}]_O$, $I_{K(Ca)}$ started to activate at membrane potentials like I_{Ca} in the corresponding neuron type (table 4.1), but maximum $I_{K(Ca)}$ amplitudes were reached at more depolarized potential than I_{Ca} (Husch *et al.*, 2009a,b).

This indicates strong Ca^{2+} dependence and suggests that $I_{K(Ca)}$ is active at subthreshold membrane potential, reducing the excitability of respective neuron by counteracting I_{Ca}. Current-clamp recordings of uPNs and type I LNs displayed unstable membrane potential leading to spontaneous high frequency spike trains when $I_{K(Ca)}$ was completely blocked by application of 100 nM ChTX (see 5 Appendix). In contrast, 80% or at least 44% inhibition of $I_{K(Ca)}$ had no effect on

Table 4.1. Comparison of $I_{K(Ca)}$ and I_{Ca}.

		uPNs	type I LNs	type IIa LNs	type IIb LNs
$I_{K(Ca)}$	threshold (mV)	-40	-50	-50	-40
	E_{max} (mV)	17 ± 11	5 ± 11	13 ± 17	23 ± 15
I_{Ca}	threshold (mV)	-35	-50	-55	-45
	E_{max} (mV)	5.8 ± 4.9	9.0 ± 6.1	-8 ± 8	-7 ± 7
(Husch *et al.*, 2009a,b)					

average membrane potential in both types of spiking AL interneurons (see 5 Appendix).

Additionally, a remarkable high mean current density of $I_{K(Ca)}$ was observed in uPNs, which was 10 fold higher compared to LN types (among which current density was in the same range) or DUM neurons from *P. americana* (Heidel & Pflüger, 2006), and 2 fold higher than Kenyon cells (Demmer & Kloppenburg, 2009). Current density of I_{Ca} from uPNs was also significantly higher compared to all LN types (Husch *et al.*, 2009a). In Kenyon cells, where remarkable high current density of both I_{Ca} and $I_{K(Ca)}$ has been reported too, both currents support Kenyon cell intrinsic firing properties including spike frequency adaptation (SFA) during depolarizing current injection (Demmer & Kloppenburg, 2009).

In synaptically isolated uPNs depolarizing current injections induced trains of action potentials with relatively regular firing patterns. Typically spike frequency increased slightly during prolonged depolarization, spike frequency- or spike wave form adaptations could never be observed (see Appendix Fig. 5.1). Instead, functional parameters of $I_{K(Ca)}$ and I_{Ca} are subtle tuned to ensure concerted activation which sharpen excitatory potentials, contributing to spike broadening and afterhyperpolarization in spiking AL interneurons (see Appendix Fig. 5.1 and 5.2). In contrast, type I LNs displayed two modes of repetetive firing: One population displayed sustained firing with weak spike frequency adaptation, whereas the second population showed likewise phasic firing pattern with strong spike frequency adaptation. In both cases, application of ChTX or IbTX did not abol-

ish spike frequency adaptation (see Appendix Fig. 5.2). Different mechanism are known which contribute SFA , including Ca^{2+}-activated potassium und chlorid conductance (Faber & Sah, 2003; Peron & Gabbiani, 2009) or Na^+-activated potassium conductance, as well as inactivation of I_{Na} (Miles *et al.*, 2005; Bhattacharjee & Kaczmarek, 2005). Mechanisms controlling SFA seem cell specific, whereby in lateral amygdala pyramidal neurons sAHP current and voltage activated K^+ current act together with I_A determining the initial firing frequency (Faber & Sah, 2005).

4.1.3 Calcium dependent activation

To further study the calcium dependence of $I_{K(Ca)}$, double-pulse experiments were performed in which Ca^{2+} influx was modified by potential and duration. Maximal $I_{K(Ca)}$ amplitudes were achieved with prepulse potentials activating maximal I_{Ca} amplitudes, which leads to almost perfectly mirrored I/V relations, again demonstrating strong Ca^{2+} dependence of $I_{K(Ca)}$ (Solaro *et al.*, 1995; Husch *et al.*, 2009a).

During the test pulse, $I_{K(Ca)}$ displayed pure transient current profiles with fast activation and complete inactivation. The time course of inactivation was fit by a monoexponential function, resulting in τ (time constant of decay) between 3 and 6 ms, which is consistent with inactivating $I_{K(Ca)}$ from frog saccular hair cells (Armstrong & Roberts, 2001). While inactivation of $I_{K(Ca)}$ from chromaffin cells occured within $25 - 100$ ms (Ding *et al.*, 1998; Lovell *et al.*, 2000).

With Ca^{2+} loading steps of various duration, the time course of $I_{K(Ca)}$ transients should reflect, at least in part, the time course of Ca^{2+} dependent activation and intrinsic inactivation since Ca^{2+} influx is stopped at test pulse potential. Variation of prepulse duration revealed that short periods of Ca^{2+} entry were sufficient to activate maximal $I_{K(Ca)}$ transients in uPNs and type IIb LNs. In type I LNs, maximal $I_{K(Ca)}$ activation was reached after 50 ms of Ca^{2+} influx, shorter loading pulses activated only 69% of $I_{K(Ca)}$, but $I_{K(Ca)}$ following prolonged loading pulses $I_{K(Ca)}$ displayed less attenuation in amplitude. In rat chromaffin cells the existence of two K_{Ca} channel populations has been proposed (Prakriya *et al.*,

Table 4.2. Biophysiological parameters of $I_{K(Ca)}$ from different AL interneurons.

	uPNs	type I LNs	type IIa LNs	type IIb LNs
			$V_{0.5(act)}$ (mV) at defined $[Ca^{2+}]_i$	
143 µM $[Ca^{2+}]_i$	100 ± 11	58 ± 2	215 ± 1	113 ± 3
1800 µM $[Ca^{2+}]_i$	50 ± 2	–	87 ± 1	62 ± 2
	$I_{K(Ca)}$ activation by simultaneous influx of 6 mM $[Ca^{2+}]_O$			
I_{max} (nA)	28 ± 18	9 ± 4	23 ± 18	16 ± 9
E_{max} (mV)	60	28 ± 17	28 ± 10	60
	$I_{K(Ca)}$ activation by simultaneous influx of 1 mM $[Ca^{2+}]_O$			
I_{max} (nA)	21 ± 6	3 ± 1	7 ± 6	7 ± 5
E_{max} (mV)	17 ± 11	5 ± 11	13 ± 17	23 ± 15
current density I_{max}/C_M (pA/pF)	1181 ± 447	117 ± 50	182 ± 95	137 ± 108
	$I_{K(Ca)}$ activation by previous Ca^{2+} influx at different potential			
prepulse potential E (mV)	-40 – +50	-30 – +30	-50 – +50	-50 – +50
prepulse potential E_{max} (mV)	+10	0	0	0
	$I_{K(Ca)}$ activation by previous Ca^{2+} influx of various duration			
I_{max} with prepulse duration (ms)	5	50	10	5
I/I_{max} after 400 ms prepulses	58%	76%	54%	41%
slowest decay τ_{max} (ms)	6.4 ± 3.9	2.7 ± 0.3	4.4 ± 3.3	3.4 ± 1.0
decay τ_{min} (ms)	3.3 ± 0.7	1.9 ± 0.7	2.3 ± 0.8	2.2 ± 0.9

1996). One population is activated during brief Ca^{2+} influx and closely associated to Ca_V channels (Prakriya & Lingle, 1999; Berkefeld *et al.*, 2006). Whereas the second population require longer Ca^{2+} influx and are activated by Ca^{2+} that diffuses some distance from open Ca_V channels (Braun *et al.*, 2000; Prakriya & Lingle, 2000). Despite $I_{K(Ca)}$ from type I LNs exhibit high Ca^{2+} sensitivity, slow Ca^{2+} mediated activation suggests that coassembly of K_{Ca} and Ca_V channels is less dense compared to uPNs and type II LNs.

4.2 Pharmacology of $I_{K(Ca)}$ from AL interneurons

$I_{K(Ca)}$ is mediated by BK, IK, and SK channels which can be distinguished by their sensitivity to toxins (Dreyer, 1990; Wei *et al.*, 2005). In this study, I used apamin, iberiotoxin, and charybdotoxin to identify K_{Ca} channel subtypes that mediate $I_{K(Ca)}$ in AL interneurons and established concentration-response relations for ChTX and IbTX.

4.2.1 $I_{K(Ca)}$ from AL interneurons is apamin-insensitive

SK channels are characterized by their high sensitivity to the bee venom toxin apamin. Consequently the peptide toxin has been used extensively to reveal the role of SK channels on neuronal firing properties (Bond *et al.*, 2005; Pedarzani & Stocker, 2008; Faber, 2009; Adelman *et al.*, 2012). SK channels contribute to AHP that control the pattern and frequency of action potential discharge in many cell types (Pineda *et al.*, 1992; Bennett *et al.*, 2000; Abel *et al.*, 2004). In this study, 1 µM apamin were used to test whether $I_{K(Ca)}$ or at least a portion of $I_{K(Ca)}$ are mediated by SK channels and if apamin-sensitive currents contribute to uPN intrinsic friring properties. $I_{K(Ca)}$ was not altered upon apamin application and uPNs displayed no change in firing frequency, AHP or any other parameter describing cellular firing characteristics at all (see Appendix Fig. 5.1). Consequently, no apamin-sensitive SK channel contribute to $I_{K(Ca)}$ from AL interneurons. Despite numerous studies from vertebrate SK channels exist, studies from invertebrate species are rare. The *Drosophila* genome contains one SK channel gene (Littleton

& Ganetzky, 2000), which encodes a slow $I_{K(Ca)}$ in photoreceptors from ommatidia (Hardie, 1995; Gu *et al.*, 2005). The reported channel from insects ommatidia shows high similarity with its mammalian homologs but differs in two amino acid residues that are contiguous in space and have been shown to be important for apamin binding (Abou Tayoun *et al.*, 2011). Additionally, a SK-like K$^+$ conductance which mediates SFA in visual interneurons of the locust, has been proven insensitive to even 10 µM apamin (Peron & Gabbiani, 2009).

4.2.2 Sensitivity of $I_{K(Ca)}$ to ChTX and IbTX

Application of 100 nM ChTX completely blocked $I_{K(Ca)}$ from all AL interneurons, yielding in EC$_{50}$ values of 2.4 nM for uPNs and 4.3 nM for both, type I and type II LNs. While pSlo currents have been proven sensitive to ChTX (EC$_{50}$ of 158 nM), dSlo currents were insensitive to ChTX at nanomolar concentration (Derst *et al.*, 2003). Unfortunatelly, ChTX is not a selective inhibitor of BK channels, it is also a potent inhibitor of IK channels (Kaczorowski *et al.*, 1996; Vandorpe *et al.*, 1998; Fioretti *et al.*, 2004). ChTX is also known to block other types of K$^+$ channels, including *Shaker* K$^+$ channels cloned from *Drosophila* and expressed in *Xenopus* oocytes or mammalian cells but not the corresponding current I_A in *Drosophila* (Zagotta *et al.*, 1989).

IbTX is a second peptide toxin which has been extensively studied for its specific inhibition of BK channel (Galvez *et al.*, 1990; Giangiacomo *et al.*, 1992). Although IbTX blocked $I_{K(Ca)}$ from Al interneurons in a concentration dependent way, a fraction of $I_{K(Ca)}$ remained even when 100 nM IbTX were applied. $I_{K(Ca)}$ from spiking AL interneurons, was more sensitive to IbTX than to ChTX, yielding in EC$_{50}$ values of 157 pM (uPNs) and 277 pM (type I LNs). However, only 59% of $I_{K(Ca)}$ from uPNs and 46% of $I_{K(Ca)}$ from type I LNs was suppressed even at the highest IbTX concentration. In type II LNs a similar fraction, namely 53% of $I_{K(Ca)}$ was suppressed by 100 nM IbTX. However, $I_{K(Ca)}$ of type II LNs was also less sensitive to IbTX than $I_{K(Ca)}$ from spiking AL interneurons, a 10 fold higher EC$_{50}$ of 7.5 nM was achieved. Generally, IbTX had similar but less potent effects

on $I_{K(Ca)}$ from AL interneurons than ChTX, which has also been reported of $I_{K(Ca)}$ from DUM neurons (Heidel & Pflüger, 2006).

Although a portion of $I_{K(Ca)}$ was not blocked by IbTX but by application of ChTX, it is doubtful that IK channels contribute to $I_{K(Ca)}$ in AL interneurons, since to date no insect SK4 gene has been reported (Littleton & Ganetzky, 2000; Wicher *et al.*, 2001; Berkefeld *et al.*, 2010). Confirmation may be achieved by application of other neurotoxins with high specificity for either BK or IK channels. Limbat-ustoxin from venom of the scorpion *Centruroides limbatus* and slotoxin from *Centruriodes noxius* Hoffmann scorpion venom are highly selective blockers of BK channels (Garcia *et al.*, 1997; Garcia-Valdes *et al.*, 2001). Maurotoxin was found to produce specific inhibition of IK channels without effects on SK or BK channels (Castle *et al.*, 2003; Kharrat *et al.*, 1996). However, evenmore neurotoxins specifically targeting insect BK channels were identified (Gunning *et al.*, 2008; Windley *et al.*, 2011).

Structural determinants of ChTX and IbTX sensitivity

ChTX or α-KTx1.1 belongs to the subfamily 1 of scorpion venom peptides, as iberiotoxin (IbTX or α-KTx1.2) and limbatustoxin (LbTX or α-KTx1.4) which inhibit BK channels with high affinity (Miller, 1995). IbTX and ChTX contain 37 amino acids resulting in nearly superimposable structures of the α-carbon backbone, consequently differences in specificity must arise from differences in the amino acid side chains (Giangiacomo *et al.*, 2007, 2008). Molecular cloning and recombinant expression of ChTX and IbTX, helped to identify amino acid residues directly involved in the interaction with the $K_{(Ca)}$ channel (Mullmann *et al.*, 1999; Giangiacomo *et al.*, 2007). Both peptide toxins have a globular structure and the interaction surface is formed from 8 of the 37 residues that cover about 25% of the peptide's molecular surface (Park & Miller, 1992; Stampe *et al.*, 1994). Ser10, Trp14, Arg25, Lys27, Met29, Asn30, Arg34, and Tyr36 were classified as crucial for channel-blocking function (Stampe *et al.*, 1994). The positively charged Lys27 is positioned at the center of the peptide-channel complex to form a hydrogen bonding with Tyr290 in the selectivity filter of the BK channel (Gao & Garcia,

2003). Two important aromatic residues in the BK channel vestibule, Tyr294 and Phe266 form aromatic π-π interaction groups with Trp14 and Tyr36 of ChTX and IbTX (Gao & Garcia, 2003). Additionally, Met29 could form favorable contacts with Phe299 and Tyr294, contributing to the hydrophobic core (Gao & Garcia, 2003). Whereas Asn30 in ChTX and Gly30 in IbTX are important determinants of specificity for BK channels over K_V channels (Giangiacomo *et al.*, 2007). However, these toxins should not be considered as pharmacological tools that reliably dissect the numerous K^+ currents found in neurons (Miller, 1995). Many examples exsist of K channels with similar functional behavior but huge differences in sensitivities to toxin homologs, or conversively, with functional differences but similar toxin affinities. The molecular basis underlying these varied toxin susceptibilities could be slight sequence variation in the toxin receptor domain of the channel (Miller, 1995). Nevertheless, much of the knowledge how K_{Ca} channels regulate cellular processes depends on the specificity of inhibition with peptide neurotoxins (Gu *et al.*, 2007; Haghdoost-Yazdi *et al.*, 2008).

4.3 Summary

At defined $[Ca^{2+}]_i$ amplitudes of $I_{K(Ca)}$ from all AL interneurons increased with progressively depolarizing voltage pulses, showing clear voltage dependence of steady-state activation. Increasing $[Ca^{2+}]_i$ lowered the voltage threshold for activation and the voltage for half-maximal activation ($V_{0.5(act)}$). Since BK channels are equipped with a voltage-sensing segment (S2–4) they display clear voltage dependence, whereas SK and IK channel currents are voltage-insensitive (Köhler *et al.*, 1996; Horrigan & Aldrich, 2002; Latorre *et al.*, 2010; Adelman *et al.*, 2012). Furthermore, $I_{K(Ca)}$ from all AL interneurons were sensitive to nanomolar concentrations of the BK channel blocker ChTX. Classification of vertebrate K_{Ca} channels is difficult to transfer to insect $I_{K(Ca)}$, but $I_{K(Ca)}$ from AL interneurons exhibit characterisics typical for BK channels. Despite conformities in voltage dependent activation and pharmacological properties, $I_{K(Ca)}$ from different AL interneurons exhibit individual qualities.

Uniglomerular Projection Neurons

At an $[Ca^{2+}]_i$ of 1.8 mM, $I_{K(Ca)}$ was half-maximal activated at 50 mV membrane potential, ascribing $I_{K(Ca)}$ from uPNs comparable Ca^{2+} sensitivity to $I_{K(Ca)}$ from type IIb LNs. Activated by simultaneous influx of 1 mM $[Ca^{2+}]_O$, maximal $I_{K(Ca)}$ activation was achieved at 17 mV suggesting a beneficial effect by activation through underlying I_{Ca}. Influx of 6 mM $[Ca^{2+}]_O$ presumably saturated cytoplasmatic clearance mechanisms and uncoupled $I_{K(Ca)}$ from I_{Ca}, resulting in a linear *I/V* relation. $I_{K(Ca)}$ displayed peak amplitudes after preceding Ca^{2+} influx of 5 – 10 ms and inactivation within 3 – 6 ms.

Although $I_{K(Ca)}$ is active at subthreshold potential, recordings in current-clamp mode showed no effect on average resting potential, even when 80% of $I_{K(Ca)}$ were blocked (see 5 Appendix). Inhibition of $I_{K(Ca)}$ reduced action potential repolarization rate and afterhyperpolarization, whereby spike width was prolonged and spike frequency increased (see Appendix Fig. 5.1). Beside the impact of $I_{K(Ca)}$ on reducing the excitability of uPN, high current density of both $I_{K(Ca)}$ and I_{Ca}, together with biophysical properties hint to cooperative activation of $I_{K(Ca)}$ and I_{Ca} to ensure concerted activation with temporal precision.

Type I LNs

At an $[Ca^{2+}]_i$ of 143 µM, $I_{K(Ca)}$ was half-maximal activated at 58 mV membrane potential, ascribing highest Ca^{2+} sensitivity to $I_{K(Ca)}$ from type I LNs. Activated by Ca^{2+} influx, $I_{K(Ca)}$ displayed bell-shaped *I/V* relation at both applied $[Ca^{2+}]_O$, contrary to the major part of AL interneurons. Despite its Ca^{2+} sensitivity, $I_{K(Ca)}$ from type I LNs was activated by the most limited range of prepulse potential, maximal $I_{K(Ca)}$ activation was achieved only after 25 – 50 ms preceeding Ca^{2+} influx whereas inactivation occured within 2 – 3 ms.

Despite current clamp recordings of type I LNs asign $I_{K(Ca)}$ same impact on spike width, repolarization, and afterhyperpolarization like in uPNs (see 5 Appendix), biophysical properties hint to a less dense coupling of K_{Ca} and Ca_V channels in type I LNs. Instead $I_{K(Ca)}$ act as highly sensitive Ca^{2+} sensors in distance from the

Ca^{2+} source and exhibit rigid activation following Ca^{2+} influx. Generally, type I LNs display less spiking activity than uPNs and the impact of $I_{K(Ca)}$ is more important on buffering the membrane potential after excitation than on signal precision. Although type I LNs displayed SFA, even 70% inhibition of $I_{K(Ca)}$ had no effect on SFA but increased spiking activity in response to depolarizing current injection (see Appendix Fig. 5.2).

Type IIb LNs

At an $[Ca^{2+}]_i$ of 1.8 mM, half-maximal activation occured at 62 mV membrane potential which ascribes type IIb LNs less Ca^{2+} sensitivity than uPNs. Activated by influx of 1 mM $[Ca^{2+}]_O$, $I_{K(Ca)}$ started to activate with voltage steps more depolarized than -40 mV suggesting a beneficial effect of $I_{K(Ca)}$ activation and I_{Ca} at physiological membrane potential. Linear *I/V* relation of $I_{K(Ca)}$ was observed with influx of 6 mM $[Ca^{2+}]_O$. $I_{K(Ca)}$ from type IIb LNs displayed peak amplitudes after preceding Ca^{2+} influx of 5 ms, prolonged loading pulses led to a robust decrease in amplitude, whereby inactivation occured within 2 – 3 ms.

Current-clamp recordings have to prove whether $I_{K(Ca)}$ contributes to resting potential of type IIb LNs since high Ca^{2+} concentration are prerequisite for $I_{K(Ca)}$ activation. Elevation of $[Ca^{2+}]_i$ in this extent occur only in close proximity of a calcium source which can also be e.g. nicotinic acetylcholine receptors or intracellular calcium stores. However, Ca^{2+} dependence and time course of $I_{K(Ca)}$ suggest precise temporal signaling. Type IIb LNs are broadly tuned and respond to odorants of many chemical classes with sustained, relatively smooth depolarizations, implementing graded transmitter release. (Husch *et al.*, 2009b). Calcium dependence and activation of $I_{K(Ca)}$ are tuned to immediately respond on I_{Ca}, which might smoothen and repolarize calcium driven depolarization.

Type IIa LNs

Highest $[Ca^{2+}]_i$ were required to activate $I_{K(Ca)}$, at an $[Ca^{2+}]_i$ of 1.8 mM, half-maximal activation occured at 87 mV membrane potential. Activation by influx of 1 mM $[Ca^{2+}]_O$ hint to a beneficial effect of $I_{K(Ca)}$ activation and I_{Ca}, like in uPNs

and type IIb LNs. With 1 mM $[Ca^{2+}]_O$, the major part of type IIa LNs exhibit bell-shaped *I/V* relations, while 6 mM $[Ca^{2+}]_O$ led to linear a *I/V* relation in the major part of neurons. Although current density was comparable to type I LNs time course of activation and inactivation displayed similarity to $I_{K(Ca)}$ from uPNs, while individual values from different type IIa LNs varied within the complete range bounded by uPNs and type I LNs. $I_{K(Ca)}$ from type IIa LNs displayed peak amplitudes after 5 – 25 ms preceding Ca^{2+} influx and an inactivation within 2 – 4 ms after ceasing Ca^{2+} influx.

In type IIa LN population greatest variability of data was observed which might arise from different subtypes of LNs. Type IIa LN population can be further subdivided by their response to odor stimulation, transmitter content, and fine morphological patterns. Nonspiking type IIa1 LNs express ChAT-like immunoreactivity and response to odor stimulation with elaborate patterns of excitation sometimes culminating in Ca^{2+}-driven transients (Husch *et al.*, 2009b; Fusca *et al.*, 2013). While the transmitter content of type IIa2 LNs is unknown yet, their response to odor stimulation consist either of hyperpolarization or gradual depolarization, but never included Ca^{2+}-driven spikelets (Husch *et al.*, 2009b; Fusca *et al.*, 2013). Furthermore, type IIa LNs display strong active membrane properties which correlate to biophysical properties of I_{Ca}. Concerted activation of $I_{K(Ca)}$ and I_{Ca} together with fast inactivation might generate Ca^{2+} transients.

This study provides a detailed analysis of calcium and voltage interplay activating $I_{K(Ca)}$ from a large number of experiments in unequivocally identified Al interneurons, allowing comparision among neuron types with disinct electrophysiological properties. Biophysical properties of $I_{K(Ca)}$ delineate distinct qualities in calcium sensitivity and calcium dependent as well as voltage dependent activation, even though $I_{K(Ca)}$ seems to be mediated by BK channels in all types of AL interneurons.

5 Appendix

The impact of $I_{K(Ca)}$ on spike waveform and firing properties

Odor responses and tuning profiles of AL interneurons are determined by their synaptic input on the one hand, and by their intrinsic electrophysiological properties on the other. To define the role of $I_{K(Ca)}$ for the intrinsic electrophysiological properties of AL interneurons, exclusion experiments were performed. Spiking AL interneurons were recorded in current-clamp mode and $I_{K(Ca)}$ was partially blocked by ChTX or IbTX. Additionally, cells were pharmacologically isolated from all detectable synaptic input by application of CNQX, picrotoxin and D-AP5. Before, during and after application of $I_{K(Ca)}$ blocker, a set of current injection protocols were applied to analyze specific intrinsic elecrophysiological properties including: resting membrane potential, cell input resistance, afterhyperpolarization (AHP), spike width, repolarization rate, latency to firing upon current injection, firing threshold and postinhibitory rebound (Fig. 5.1 and 5.2).

Uniglomerular Projection Neurons

In synaptically isolated uPNs depolarizing current injections induced trains of action potentials with relatively regular firing patterns. Typically spike frequency increased slightly during prolonged depolarization, spike frequency- or spike wave form adaptations could never be observed. Application of 100 nM ChTX which blocked 100% of $I_{K(Ca)}$ caused the resting potential to become very unstable and led to spontaneous high frequency spike trains, which made controlled

recordings impossible. Accordingly ChTX concentration was reduced to 10 nM which blocked ~ 80% of $I_{K(Ca)}$ (see table 3.4). Upon application of 10 nM ChTX there was no effect on the resting potential, cell input resitance or firing threshold (n = 10, data not shown). Spike waveform was noticeably effected with a significant decrease in AHP from -72.4 ± 4.6 mV to -66.7 ± 5.1 mV, as well as repolarization rate from -174 ± 16 to -119 ± 10 mV/ms, and an increase in spike width from 505 ± 60 μs to 668 ± 40 μs (n = 10; p < 0.0001 for all parameters) (Fig. 5.1 A – D). The frequency of spike trains elicited by a depolarizing current pulse increased significantly upon ChTX application from 12.9 ± 5.9 Hz to 27.7 ± 7.3 Hz (n = 10; p = 0.0005) with a significant decrease in the latency to the first spike from 252 ± 106 ms to 123 ± 46.8 ms (n = 10; p = 0.0041). After wash out of ChTX spike width, repolarization rate, and AHP returned significantly to control values. Although the wash out of ChTX was not significant for spike latency and firing frequency, these parameters showed a tendency to return to control values. Application of 10 nM IbTX, which blocked ~59% of $I_{K(Ca)}$ (see table 3.4), had similar effects as 10 nM ChTX but resulted in a more unstable resting potential. However, there was no significant change in resting membrane potential, input resistance or firing threshold (n = 6, data not shown). IbTX reduced AHP from -76.2 ± 5.9 mV to 64.0 ± 4.8 mV, increased spike width from 417 ± 64 μs to 468 ± 53 μs, and decreased repolarization rate from 205 ± 31 to 151 ± 29 mVs^{-1} (n = 6; Fig 3.5 E – G). All these effects were reversible upon wash out. Despite these intense effects of IbTX on spike waveform, effects on spike latency and spike frequency were not significant (n = 6; Fig. 3.5 O – Q). The wash out of IbTX

Figure 5.1 *(following page)*. **Effect of ChTX, IbTX and apamin on uPN firing properties.** (A) Alterations in a single spike upon application of 10 and 50 nM ChTX and subsequent wash out. Mean changes (B – J) in spike width (B, E and H), repolarization rate (C, F and I) and AHP (D, G and J) upon application of 10 nM ChTX (A – D), 100 nM IbTX (E – G) and 1 μM apamin (H – I). (K) Change of firing frequency upon application of 10 nM ChTX and subsequent wash out. Mean changes (L – T) of latency to firing (L, O and R), firing frequency (M, P and S) and firing threshold (N, Q and T) upon application of 10 nM ChTX (K – N), 100 nM IbTX (O – Q) and 1 μM apamin (R – T). This figure was kindly provided by Dr. Ben Warren.

Charybdotoxin (ChTX)

Iberiotoxin (IbTX)

Apamin (APA)

Charybdotoxin (ChTX)

Iberiotoxin (IbTX)

Apamin (APA)
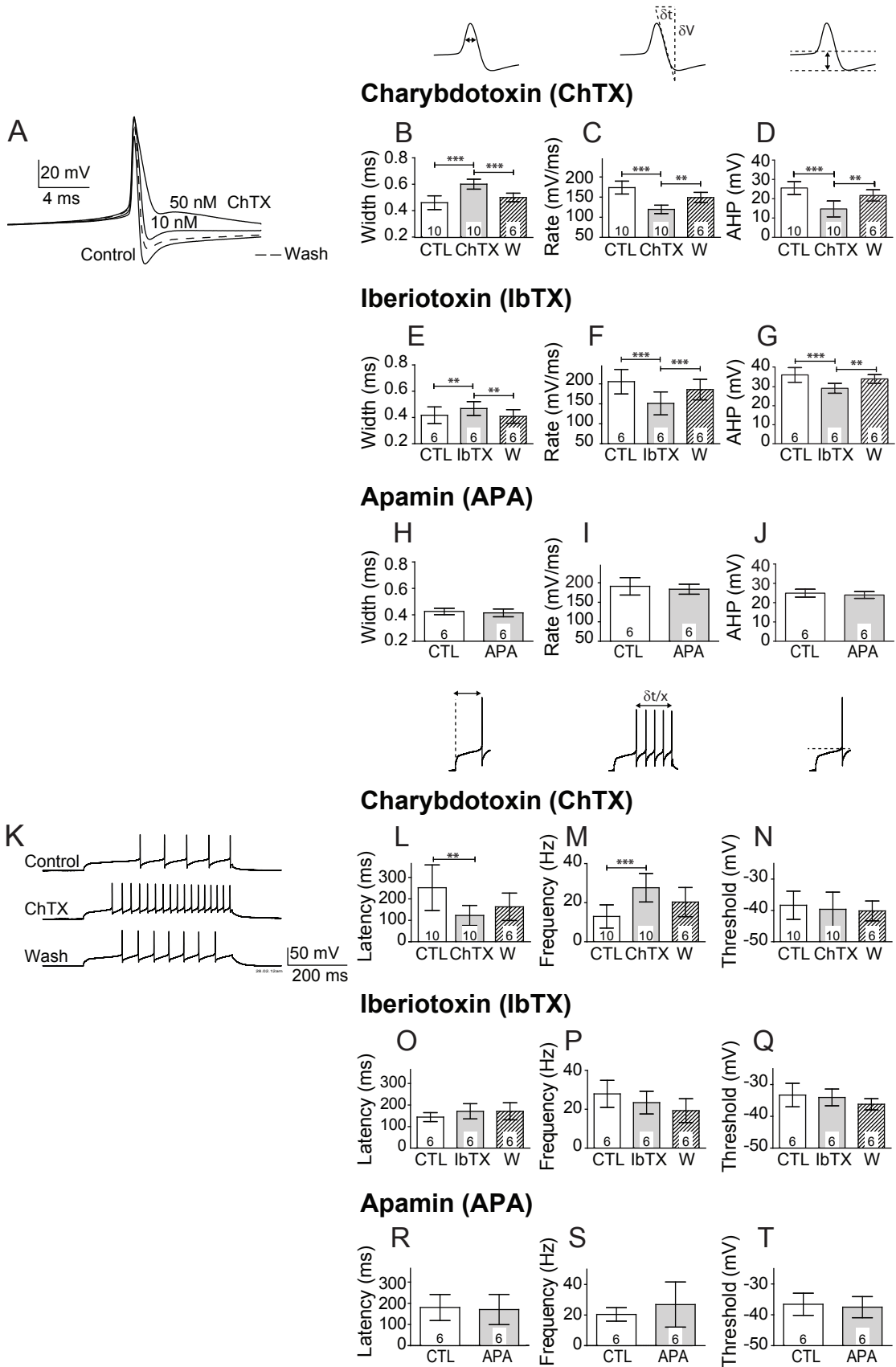
was significant for only some parameters as spike width, repolarization rate and AHP.

In an effort to block SK channels which could contribute to $I_{K(Ca)}$, 1 µM apamin was applied to the preparation. Application of apamin had no significant effect on any parameter concerning spike waveform or spike frequency (Fig. 3.5 H – I and R – T). Current-clamp recordings of uPNs were performed by Ben Warren and Viktor Bardos. Analysis and figures were kindly provided by Ben Warren.

Type I LNs

In synaptically isolated type I LNs depolarizing current injections induced trains of action potentials with irregular firing patterns. One portion of type I LNs displayed sustained firing during current pulses with weak spike frequency adaptation (SFA)(Fig. 5.2H$_i$) whereas the second proportion of type I LNs showed likewise phasic firing pattern with strong SFA (Fig. 5.2H$_{ii}$). In both cases, application of ChTX did not abolish spike frequency adaptation. However, analysis of other electrophysiological properties such as membrane potential, spike amplitude, spike width, repolarization rate or amplitude of AHP revealed no significant differences of these parameters therefore data were pooled for further analysis. Recordings were performed by Sandra Wendler. Analysis and figures were kindly provided by Dr. Cathleen Bradler.

Upon application of 10 nM ChTX which blocked ~ 70% of $I_{K(Ca)}$ (see table 3.4, no effect on resting potential, cell input resistance or firing threshold could be observed (n = 9). Spike waveform was noticeably effected with a significant decrease in the AHP from -22.3 ± 4.6 mV to -18.9 ± 4.2 mV (n = 9; p = 0.0009), Fig. 5.2B) and a significant reduction in repolarization rate from 123.3 ± 24.7 mV/ms to 95.9 ± 19.9 mV/ms (n = 9; p < 0.0001; Fig. 5.2D). Spike width was extended from 677 ± 99 µs to 732 ± 109 µs (n = 9; p < 0.0001; Fig. 5.2C). The frequency of spike trains elicited by a depolarizing current pulse increased significantly upon ChTX application from 5.9 ± 4.7 Hz to 12.0 ± 7.2 Hz(n = 8; p < 0.0184; Fig. 5.2K) with a significant increase in the threshold for firing from -39.3 ± 4.6 mV to -37.5 ± 4.4 mV (n = 9; p < 0.0001; Fig. 5.2J). Although the wash out of ChTX was
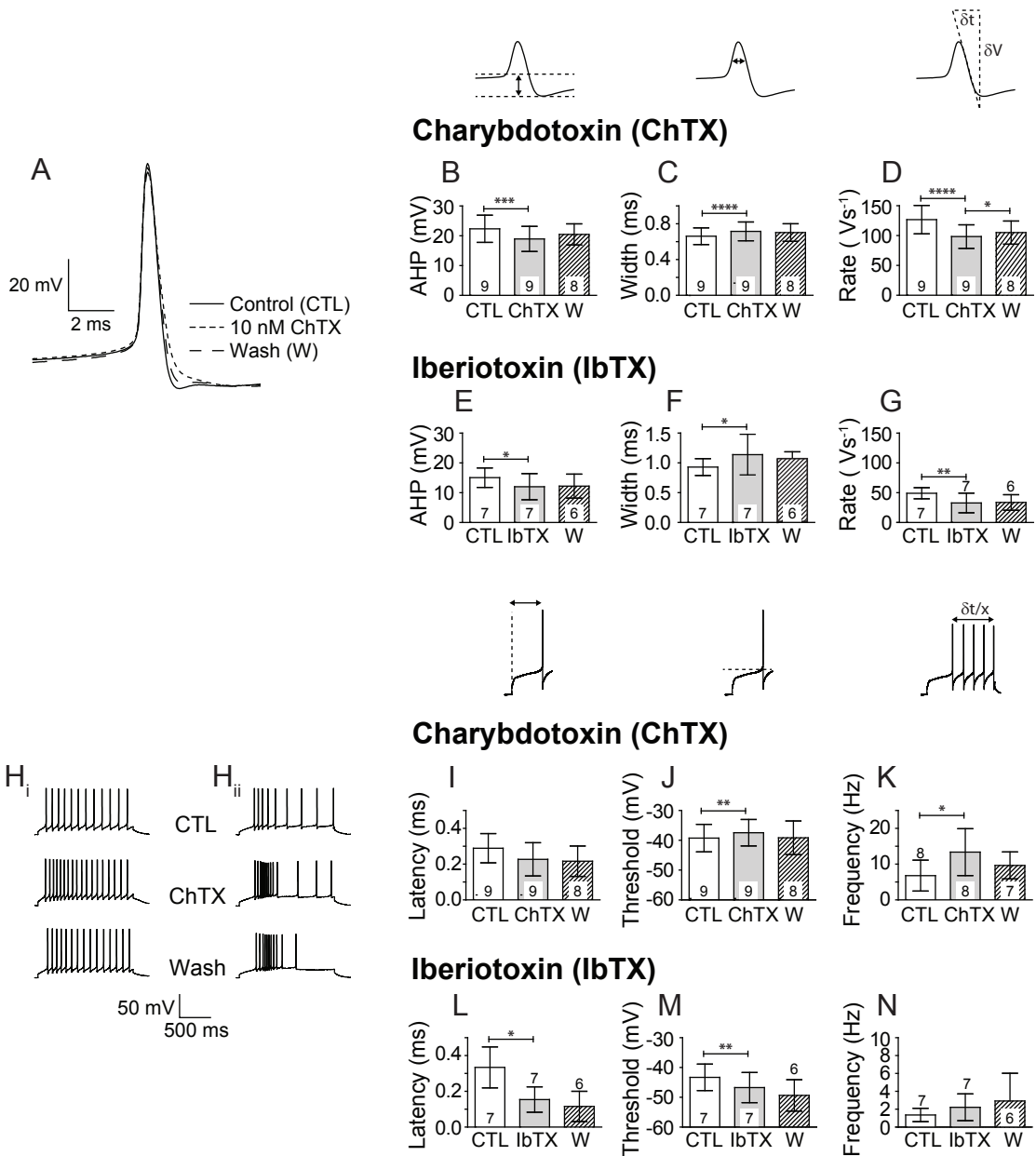
Figure 5.2. Effect of ChTX and IbTX on type I LN firing properties. (A) Alterations in a single spike upon application of 10 nM ChTX and subsequent wash out. Mean changes (B – G) in spike width (B and E), repolarization rate (C and F) and AHP (D and G) upon application of 10 nM ChTX (B – D) and 10 nM IbTX (E – G). (H_i and H_ii) Change of firing frequency upon application of 10 nM ChTX and subsequent wash out. Mean changes (I – N) of latency to firing (I and L), firing threshold (J and M) and firing frequency (K and N) upon application of 10 nM ChTX (I – K) and 10 nM IbTX (L – N). This figure was kindly provided by Dr. Cathleen Bradler.

Table 5.1. Impact of $I_{K(Ca)}$ on action potential wave form and repetitive firing.

	uPN		type I LN	
	ChTX	IbTX	ChTX	IbTX
spike width	*** ↑	** ↑	**** ↑	* ↑
repolarization rate	*** ↓	*** ↓	**** ↓	** ↓
AHP	*** ↓	*** ↓	*** ↓	* ↓
frequency	*** ↑	n.s.	* ↑	n.s.
latency to the first spike	** ↓	n.s.	n.s.	** ↓
threshold	n.s.	n.s.	** ↑	** ↓

significant for the repolorization rate only, all parameter showed a tendency to return to control values.

Current-clamp recordings of type I LNs upon IbTX application, were performed by Merit Klemann. Analysis and figures were kindly provided by Dr. Cathleen Bradler. Application of 10 nM IbTX which blocked ~ 44% of $I_{K(Ca)}$ (see table 3.4, caused no significant change in resting membrane potential, cell input resistance or firing frequency (n = 7). IbTX reduced AHP from -15.1. ± 3.3 mV to -12.0 ± 4.4 mV (n = 7; p = 0.0170), Fig. 5.2E) and slowed the repolarization rate from 49.1 ± 9.3 mV/ms to 32.8 ± 16.5 mV/ms (n = 7; p < 0.0072; Fig. 5.2G). Spike width was extended from 930 ± 140 μs to 1140 ± 340 μs (n = 7; p < 0.0001; Fig. 5.2F). Latency to the first spike was significantly reduced upon IbTX application from 330 ± 110 ms to 150 ± 70 ms (n = 7; p < 0.0112; Fig. 5.2L) with a significant decrease in firing threshold from -43.3 ± 4.4 mV to -46.7 ± 5.0 mV (n = 7; p < 0.0072; Fig. 5.2M).

List of Figures

List of Tables

References

ABEL, H. J., LEE, J C F., CALLAWAY, J. C., & FOEHRING, R. C. 2004. Relationships between intracellular calcium and afterhyperpolarizations in neocortical pyramidal neurons. *J Neurophysiol*, **91**(1), 324–335.

ABOU TAYOUN, AHMAD N., LI, XIAOFENG, CHU, BRIAN, HARDIE, ROGER C., JUUSOLA, MIKKO, & DOLPH, PATRICK J. 2011. The Drosophila SK channel (dSK) contributes to photoreceptor performance by mediating sensitivity control at the first visual network. *J Neurosci*, **31**(39), 13897–13910.

ADELMAN, J. P., SHEN, K. Z., KAVANAUGH, M. P., WARREN, R. A., WU, Y. N., LAGRUTTA, A., BOND, C. T., & NORTH, R. A. 1992. Calcium-activated potassium channels expressed from cloned complementary DNAs. *Neuron*, **9**(2), 209–216.

ADELMAN, JOHN P., MAYLIE, JAMES, & SAH, PANKAJ. 2012. Small-conductance Ca2+-activated K+ channels: form and function. *Annu Rev Physiol*, **74**, 245–269.

ARMSTRONG, C. E., & ROBERTS, W. M. 2001. Rapidly inactivating and non-inactivating calcium-activated potassium currents in frog saccular hair cells. *J Physiol*, **536**(Pt 1), 49–65.

ASSISI, COLLINS, STOPFER, MARK, & BAZHENOV, MAXIM. 2012. Excitatory local interneurons enhance tuning of sensory information. *PLoS Comput Biol*, **8**(7), e1002563.

ATKINSON, N. S., ROBERTSON, G. A., & GANETZKY, B. 1991. A component of calcium-activated potassium channels encoded by the Drosophila slo locus. *Science*, **253**(5019), 551–555.

ATKINSON, N. S., BRENNER, R., BOHM, R. A., YU, J. Y., & WILBUR, J. L. 1998. Behavioral and electrophysiological analysis of Ca-activated K-channel transgenes in Drosophila. *Ann N Y Acad Sci*, **860**(Nov), 296–305.

AUGUSTE, P., HUGUES, M., GRAVÉ, B., GESQUIERE, J. C., MAES, P., TARTAR, A., ROMEY, G., SCHWEITZ, H., & LAZDUNSKI, M. 1990. Leiurotoxin I (scyllatoxin), a peptide ligand for Ca2(+)-activated K+ channels. Chemical synthesis, radiolabeling, and receptor characterization. *J Biol Chem*, **265**(8), 4753–4759.

AUGUSTE, P., HUGUES, M., MOURRE, C., MOINIER, D., TARTAR, A., & LAZDUNSKI, M. 1992. Scyllatoxin, a blocker of Ca(2+)-activated K+ channels: structure-function relationships and brain localization of the binding sites. *Biochemistry*, **31**(3), 648–654.

AUGUSTINE, GEORGE J., SANTAMARIA, FIDEL, & TANAKA, KEIKO. 2003. Local calcium signaling in neurons. *Neuron*, **40**(2), 331–346.

BAO, LIN, & COX, DANIEL H. 2005. Gating and ionic currents reveal how the BKCa channel's Ca2+ sensitivity is enhanced by its beta1 subunit. *J Gen Physiol*, **126**(4), 393–412.

BAZHENOV, M., STOPFER, M., RABINOVICH, M., ABARBANEL, H. D., SEJNOWSKI, T. J., & LAURENT, G. 2001. Model of cellular and network mechanisms for odor-evoked temporal patterning in the locust antennal lobe. *Neuron*, **30**(2), 569–581.

BENNETT, B. D., CALLAWAY, J. C., & WILSON, C. J. 2000. Intrinsic membrane properties underlying spontaneous tonic firing in neostriatal cholinergic interneurons. *J Neurosci*, **20**(22), 8493–8503.

BERKEFELD, HENRIKE, SAILER, CLAUDIA A., BILDL, WOLFGANG, ROHDE, VOLKER, THUMFART, JÖRG-OLIVER, EBLE, SILKE, KLUGBAUER, NORBERT, REISINGER, ELLEN, BISCHOFBERGER, JOSEF, OLIVER, DOMINIK, KNAUS, HANS-GÜNTHER, SCHULTE, UWE, & FAKLER, BERND. 2006. BKCa-Cav chan-

nel complexes mediate rapid and localized Ca2+-activated K+ signaling. *Science*, **314**(5799), 615–620.

BERKEFELD, HENRIKE, FAKLER, BERND, & SCHULTE, UWE. 2010. Ca2+-activated K+ channels: from protein complexes to function. *Physiol Rev*, **90**(4), 1437–1459.

BHATTACHARJEE, ARIN, & KACZMAREK, LEONARD K. 2005. For K+ channels, Na+ is the new Ca2+. *Trends Neurosci*, **28**(8), 422–428.

BICKER, G. 1999. Histochemistry of classical neurotransmitters in antennal lobes and mushroom bodies of the honeybee. *Microsc Res Tech*, **45**(3), 174–183.

BLATZ, A. L., & MAGLEBY, K. L. 1986. Single apamin-blocked Ca-activated K+ channels of small conductance in cultured rat skeletal muscle. *Nature*, **323**(6090), 718–720.

BOECKH, J., & TOLBERT, L. P. 1993. Synaptic organization and development of the antennal lobe in insects. *Microsc Res Tech*, **24**(3), 260–280.

BOECKH, J, ERNST, KD, SASS, H, & WALDOW, U. 1984. Anatomical and physiological characteristics of individual neurones in the central antennal pathway of insects. *Journal of insect physiology*, **30**(1), 15–26.

BOND, CHRIS T., MAYLIE, JAMES, & ADELMAN, JOHN P. 2005. SK channels in excitability, pacemaking and synaptic integration. *Curr Opin Neurobiol*, **15**(3), 305–311.

BRAUN, A. P., HEIST, E. K., & SCHULMAN, H. 2000. Inhibition of a mammalian large conductance, calcium-sensitive K+ channel by calmodulin-binding peptides. *J Physiol*, **527 Pt 3**(Sep), 479–492.

BRENNER, R., THOMAS, T. O., BECKER, M. N., & ATKINSON, N. S. 1996. Tissue-specific expression of a Ca(2+)-activated K+ channel is controlled by multiple upstream regulatory elements. *J Neurosci*, **16**(5), 1827–1835.

BYCHKOV, ROSTISLAV, BURNHAM, MATTHEW P., RICHARDS, GILLIAN R., EDWARDS, GILLIAN, WESTON, ARTHUR H., FÉLÉTOU, MICHEL, & VANHOUTTE,

PAUL M. 2002. Characterization of a charybdotoxin-sensitive intermediate conductance Ca2+-activated K+ channel in porcine coronary endothelium: relevance to EDHF. *Br J Pharmacol*, **137**(8), 1346–1354.

CASTLE, N. A., LONDON, D. O., CREECH, C., FAJLOUN, Z., STOCKER, J. W., & SABATIER, J-M. 2003. Maurotoxin: a potent inhibitor of intermediate conductance Ca2+-activated potassium channels. *Mol Pharmacol*, **63**(2), 409–418.

CHRISTENSEN, TA, WALDROP, BR, HARROW, ID, & HILDEBRAND, JG. 1993. Local interneurons and information processing in the olfactory glomeruli of the moth Manduca sexta. *Journal of Comparative Physiology A*, **173**(4), 385–399.

CHRISTENSEN, THOMAS A, WALDROP, BRIAN R, & HILDEBRAND, JOHN G. 1998. Multitasking in the olfactory system: context-dependent responses to odors reveal dual GABA-regulated coding mechanisms in single olfactory projection neurons. *The Journal of neuroscience*, **18**(15), 5999–6008.

CLELAND, THOMAS A, & LINSTER, CHRISTIANE. 2002. How synchronization properties among second-order sensory neurons can mediate stimulus salience. *Behav Neurosci*, **116**(2), 212–221.

DACKS, ANDREW M., REISENMAN, CAROLINA E., PAULK, ANGELIQUE C., & NIGHORN, ALAN J. 2010. Histamine-immunoreactive local neurons in the antennal lobes of the hymenoptera. *J Comp Neurol*, **518**(15), 2917–2933.

DANIELS, RICHARD W, GELFAND, MARIA V, COLLINS, CATHERINE A, & DIANTONIO, AARON. 2008. Visualizing glutamatergic cell bodies and synapses in Drosophila larval and adult CNS. *Journal of Comparative Neurology*, **508**(1), 131–152.

DAVIES, P. J., IRELAND, D. R., & MCLACHLAN, E. M. 1996. Sources of Ca2+ for different Ca(2+)-activated K+ conductances in neurones of the rat superior cervical ganglion. *J Physiol*, **495 (Pt 2)**(Sep), 353–366.

DEMMER, HEIKE, & KLOPPENBURG, PETER. 2009. Intrinsic membrane properties and inhibitory synaptic input of kenyon cells as mechanisms for sparse coding? *J Neurophysiol*, **102**(3), 1538–1550.

DERST, C., MESSUTAT, S., WALTHER, C., ECKERT, M., HEINEMANN, S. H., & WICHER, D. 2003. The large conductance Ca2+-activated potassium channel (pSlo) of the cockroach Periplaneta americana: structure, localization in neurons and electrophysiology. *Eur J Neurosci*, **17**(6), 1197–1212.

D'HOEDT, DIETER, HIRZEL, KLAUS, PEDARZANI, PAOLA, & STOCKER, MARTIN. 2004. Domain analysis of the calcium-activated potassium channel SK1 from rat brain. Functional expression and toxin sensitivity. *J Biol Chem*, **279**(13), 12088–12092.

DING, J. P., LI, Z. W., & LINGLE, C. J. 1998. Inactivating BK channels in rat chromaffin cells may arise from heteromultimeric assembly of distinct inactivation-competent and noninactivating subunits. *Biophys J*, **74**(1), 268–289.

DISTLER, P. 1989. Histochemical demonstration of GABA-like immunoreactivity in cobalt labeled neuron individuals in the insect olfactory pathway. *Histochemistry*, **91**(3), 245–249.

DISTLER, P. G., & BOECKH, J. 1998. An improved model of the synaptic organization of insect olfactory glomeruli. *Ann N Y Acad Sci*, **855**(Nov), 508–510.

DISTLER, PAUL G, GRUBER, CLAUDIA, & BOECKH, JÜRGEN. 1998. Synaptic connections between GABA-immunoreactive neurons and uniglomerular projection neurons within the antennal lobe of the cockroach, Periplaneta americana. *Synapse*, **29**(1), 1–13.

DREYER, F. 1990. Peptide toxins and potassium channels. *Rev Physiol Biochem Pharmacol*, **115**, 93–136.

EDGERTON, JEREMY R., & REINHART, PETER H. 2003. Distinct contributions of small and large conductance Ca2+-activated K+ channels to rat Purkinje neuron function. *J Physiol*, **548**(Pt 1), 53–69.

EISTHEN, HEATHER L. 2002. Why are olfactory systems of different animals so similar? *Brain Behav Evol*, **59**(5-6), 273–293.

ERNST, K. D., & BOECKH, J. 1983. A neuroanatomical study on the organization of the central antennal pathways in insects. III. Neuroanatomical characterization of physiologically defined response types of deutocerebral neurons in Periplaneta americana. *Cell Tissue Res*, **229**(1), 1–22.

FABER, E S LOUISE. 2009. Functions and modulation of neuronal SK channels. *Cell Biochem Biophys*, **55**(3), 127–139.

FABER, E S LOUISE, & SAH, PANKAJ. 2003. Calcium-activated potassium channels: multiple contributions to neuronal function. *Neuroscientist*, **9**(3), 181–194.

FABER, E S LOUISE, & SAH, PANKAJ. 2005. Independent roles of calcium and voltage-dependent potassium currents in controlling spike frequency adaptation in lateral amygdala pyramidal neurons. *Eur J Neurosci*, **22**(7), 1627–1635.

FAKLER, BERND, & ADELMAN, JOHN P. 2008. Control of K(Ca) channels by calcium nano/microdomains. *Neuron*, **59**(6), 873–881.

FIALA, ANDRÉ. 2007. Olfaction and olfactory learning in Drosophila: recent progress. *Current opinion in neurobiology*, **17**(6), 720–726.

FIORETTI, BERNARD, CASTIGLI, EMILIA, CALZUOLA, ISABELLA, HARPER, ALEXANDER A., FRANCIOLINI, FABIO, & CATACUZZENO, LUIGI. 2004. NPPB block of the intermediate-conductance Ca2+-activated K+ channel. *Eur J Pharmacol*, **497**(1), 1–6.

FUSCA, DEBORA, HUSCH, ANDREAS, BAUMANN, ARND, & KLOPPENBURG, PETER. 2013. Choline acetyltransferase-like immunoreactivity in a physiologically distinct subtype of olfactory nonspiking local interneurons in the cockroach (periplaneta americana). *J Comp Neurol*, **521**(15), 3556–3569.

GALIZIA, C. G., SACHSE, S., RAPPERT, A., & MENZEL, R. 1999. The glomerular code for odor representation is species specific in the honeybee Apis mellifera. *Nat Neurosci*, **2**(5), 473–478.

GALIZIA, C GIOVANNI, & ROESSLER, WOLFGANG. 2010. Parallel olfactory systems in insects: anatomy and function. *Annual review of entomology*, **55**, 399–420.

GALVEZ, A., GIMENEZ-GALLEGO, G., REUBEN, J. P., ROY-CONTANCIN, L., FEIGENBAUM, P., KACZOROWSKI, G. J., & GARCIA, M. L. 1990. Purification and characterization of a unique, potent, peptidyl probe for the high conductance calcium-activated potassium channel from venom of the scorpion Buthus tamulus. *J Biol Chem*, **265**(19), 11083–11090.

GAO, YING-DUO, & GARCIA, MARIA L. 2003. Interaction of agitoxin2, charybdotoxin, and iberiotoxin with potassium channels: selectivity between voltage-gated and Maxi-K channels. *Proteins*, **52**(2), 146–154.

GARCIA, M. L., HANNER, M., KNAUS, H. G., KOCH, R., SCHMALHOFER, W., SLAUGHTER, R. S., & KACZOROWSKI, G. J. 1997. Pharmacology of potassium channels. *Adv Pharmacol*, **39**, 425–471.

GARCIA-VALDES, J., ZAMUDIO, F. Z., TORO, L., POSSANI, L. D., & POSSAN, L. D. 2001. Slotoxin, alphaKTx1.11, a new scorpion peptide blocker of MaxiK channels that differentiates between alpha and alpha+beta (beta1 or beta4) complexes. *FEBS Lett*, **505**(3), 369–373.

GARDOS, G. 1958. The function of calcium in the potassium permeability of human erythrocytes. *Biochim Biophys Acta*, **30**(3), 653–654.

GAUTIER, HÉLÈNE, AUGER, JACQUES, LEGROS, CHRISTIAN, & LAPIED, BRUNO. 2008. Calcium-activated potassium channels in insect pacemaker neurons as unexpected target site for the novel fumigant dimethyl disulfide. *J Pharmacol Exp Ther*, **324**(1), 149–159.

GHATTA, SRINIVAS, NIMMAGADDA, DEEPTHI, XU, XIAOPING, & O'ROURKE, STEPHEN T. 2006. Large-conductance, calcium-activated potassium channels: structural and functional implications. *Pharmacol Ther*, **110**(1), 103–116.

GIANGIACOMO, K. M., GARCIA, M. L., & MCMANUS, O. B. 1992. Mechanism of iberiotoxin block of the large-conductance calcium-activated potassium channel from bovine aortic smooth muscle. *Biochemistry*, **31**(29), 6719–6727.

GIANGIACOMO, KATHLEEN M., BECKER, JENNIFER, GARSKY, CHRISTOPHER, FELIX, JOHN P., PRIEST, BIRGIT T., SCHMALHOFER, WILLIAM, GARCIA, MARIA L., & MULLMANN, THEODORE J. 2007. Revealing the molecular determinants of neurotoxin specificity for calcium-activated versus voltage-dependent potassium channels. *Biochemistry*, **46**(18), 5358–5364.

GIANGIACOMO, KATHLEEN M., BECKER, JENNIFER, GARSKY, CHRISTOPHER, SCHMALHOFER, WILLIAM, GARCIA, MARIA L., & MULLMANN, THEODORE J. 2008. Novel alpha-KTx sites in the BK channel and comparative sequence analysis reveal distinguishing features of the BK and KV channel outer pore. *Cell Biochem Biophys*, **52**(1), 47–58.

GROLLEAU, F., & LAPIED, B. 1995. Separation and identification of multiple potassium currents regulating the pacemaker activity of insect neurosecretory cells (DUM neurons). *J Neurophysiol*, **73**(1), 160–171.

GU, NING, VERVAEKE, KOEN, & STORM, JOHAN F. 2007. BK potassium channels facilitate high-frequency firing and cause early spike frequency adaptation in rat CA1 hippocampal pyramidal cells. *J Physiol*, **580**(Pt.3), 859–882.

GU, YUCHUN, OBERWINKLER, JOHANNES, POSTMA, MARTEN, & HARDIE, ROGER C. 2005. Mechanisms of light adaptation in Drosophila photoreceptors. *Curr Biol*, **15**(13), 1228–1234.

GUNNING, SIMON J., MAGGIO, FRANCESCO, WINDLEY, MONIQUE J., VALENZUELA, STELLA M., KING, GLENN F., & NICHOLSON, GRAHAM M. 2008. The Janus-faced atracotoxins are specific blockers of invertebrate K(Ca) channels. *FEBS J*, **275**(16), 4045–4059.

HAGHDOOST-YAZDI, HASHEM, JANAHMADI, MAHYAR, & BEHZADI, GILA. 2008. Iberiotoxin-sensitive large conductance Ca2+ -dependent K+ (BK) chan-

nels regulate the spike configuration in the burst firing of cerebellar Purkinje neurons. *Brain Res*, **1212**(May), 1–8.

HAMILL, OP, MARTY, A, NEHER, E, SAKMANN, BERT, & SIGWORTH, FJ. 1981. Improved patch-clamp techniques for high-resolution current recording from cells and cell-free membrane patches. *Pflügers Archiv*, **391**(2), 85–100.

HARDIE, R. C. 1995. Effects of intracellular Ca2+ chelation on the light response in Drosophila photoreceptors. *J Comp Physiol A*, **177**(6), 707–721.

HEIDEL, E., & PFLÜGER, H-J. 2006. Ion currents and spiking properties of identified subtypes of locust octopaminergic dorsal unpaired median neurons. *Eur J Neurosci*, **23**(5), 1189–1206.

HILDEBRAND, J. G., & SHEPHERD, G. M. 1997. Mechanisms of olfactory discrimination: converging evidence for common principles across phyla. *Annu Rev Neurosci*, **20**, 595–631.

HIRSCHBERG, B., MAYLIE, J., ADELMAN, J. P., & MARRION, N. V. 1999. Gating properties of single SK channels in hippocampal CA1 pyramidal neurons. *Biophys J*, **77**(4), 1905–1913.

HOMBERG, UWE. 2002. Neurotransmitters and neuropeptides in the brain of the locust. *Microsc Res Tech*, **56**(3), 189–209.

HORRIGAN, FRANK T., & ALDRICH, RICHARD W. 2002. Coupling between voltage sensor activation, Ca2+ binding and channel opening in large conductance (BK) potassium channels. *J Gen Physiol*, **120**(3), 267–305.

HOSKINS, SALLY G, HOMBERG, UWE, KINGAN, TIMOTHY G, CHRISTENSEN, THOMAS A, & HILDEBRAND, JOHN G. 1986. Immunocytochemistry of GABA in the antennal lobes of the sphinx moth Manduca sexta. *Cell and tissue research*, **244**(2), 243–252.

HUSCH, ANDREAS, PAEHLER, MORITZ, FUSCA, DEBORA, PAEGER, LARS, & KLOPPENBURG, PETER. 2009a. Calcium current diversity in physiologically different local interneuron types of the antennal lobe. *J Neurosci*, **29**(3), 716–726.

HUSCH, ANDREAS, PAEHLER, MORITZ, FUSCA, DEBORA, PAEGER, LARS, & KLOPPENBURG, PETER. 2009b. Distinct electrophysiological properties in subtypes of nonspiking olfactory local interneurons correlate with their cell type-specific Ca2+ current profiles. *J Neurophysiol*, **102**(5), 2834–2845.

IGNELL, R. 2001. Monoamines and neuropeptides in antennal lobe interneurons of the desert locust, Schistocerca gregana: an immunocytochemical study. *Cell Tissue Res*, **306**(1), 143–156.

ISHII, T. M., MAYLIE, J., & ADELMAN, J. P. 1997a. Determinants of apamin and d-tubocurarine block in SK potassium channels. *J Biol Chem*, **272**(37), 23195–23200.

ISHII, T. M., SILVIA, C., HIRSCHBERG, B., BOND, C. T., ADELMAN, J. P., & MAYLIE, J. 1997b. A human intermediate conductance calcium-activated potassium channel. *Proc Natl Acad Sci U S A*, **94**(21), 11651–11656.

ITO, IORI, ONG, ROSE CHIK-YING, RAMAN, BARANIDHARAN, & STOPFER, MARK. 2008. Sparse odor representation and olfactory learning. *Nat Neurosci*, **11**(10), 1177–1184.

JENSEN, B. S., STRØBAEK, D., OLESEN, S. P., & CHRISTOPHERSEN, P. 2001. The Ca2+-activated K+ channel of intermediate conductance: a molecular target for novel treatments? *Curr Drug Targets*, **2**(4), 401–422.

JENSEN, B. S., HERTZ, M., CHRISTOPHERSEN, P., & MADSEN, L. S. 2002. The Ca2+-activated K+ channel of intermediate conductance: a possible target for immune suppression. *Expert Opin Ther Targets*, **6**(6), 623–636.

JOINER, W. J., WANG, L. Y., TANG, M. D., & KACZMAREK, L. K. 1997. hSK4, a member of a novel subfamily of calcium-activated potassium channels. *Proc Natl Acad Sci U S A*, **94**(20), 11013–11018.

JOINER, W. J., TANG, M. D., WANG, L. Y., DWORETZKY, S. I., BOISSARD, C. G., GAN, L., GRIBKOFF, V. K., & KACZMAREK, L. K. 1998. Formation

of intermediate-conductance calcium-activated potassium channels by interaction of Slack and Slo subunits. *Nat Neurosci*, **1**(6), 462–469.

KACZOROWSKI, G. J., KNAUS, H. G., LEONARD, R. J., MCMANUS, O. B., & GARCIA, M. L. 1996. High-conductance calcium-activated potassium channels; structure, pharmacology, and function. *J Bioenerg Biomembr*, **28**(3), 255–267.

KHANNA, R., CHANG, M. C., JOINER, W. J., KACZMAREK, L. K., & SCHLICHTER, L. C. 1999. hSK4/hIK1, a calmodulin-binding KCa channel in human T lymphocytes. Roles in proliferation and volume regulation. *J Biol Chem*, **274**(21), 14838–14849.

KHARRAT, R., MABROUK, K., CREST, M., DARBON, H., OUGHIDENI, R., MARTIN-EAUCLAIRE, M. F., JACQUET, G., EL AYEB, M., VAN RIETSCHOTEN, J., ROCHAT, H., & SABATIER, J. M. 1996. Chemical synthesis and characterization of maurotoxin, a short scorpion toxin with four disulfide bridges that acts on K+ channels. *Eur J Biochem*, **242**(3), 491–498.

KÖHLER, M., HIRSCHBERG, B., BOND, C. T., KINZIE, J. M., MARRION, N. V., MAYLIE, J., & ADELMAN, J. P. 1996. Small-conductance, calcium-activated potassium channels from mammalian brain. *Science*, **273**(5282), 1709–1714.

LATORRE, RAMON, MORERA, FRANCISCO J., & ZAELZER, CRISTIAN. 2010. Allosteric interactions and the modular nature of the voltage- and Ca2+-activated (BK) channel. *J Physiol*, **588**(Pt 17), 3141–3148.

LAURENT, G. 1999. A systems perspective on early olfactory coding. *Science*, **286**(5440), 723–728.

LAURENT, G., WEHR, M., & DAVIDOWITZ, H. 1996. Temporal representations of odors in an olfactory network. *J Neurosci*, **16**(12), 3837–3847.

LEI, HONG, REISENMAN, CAROLINA E., WILSON, CAROLINE H., GABBUR, PRASAD, & HILDEBRAND, JOHN G. 2011. Spiking patterns and their functional implications in the antennal lobe of the tobacco hornworm Manduca sexta. *PLoS One*, **6**(8), e23382.

LEMONA, WILLIAM C, & GETZ, WAYNE M. 1998. Responses of cockroach antennal lobe projection neurons to pulsatile olfactory stimuli. *Annals of the New York Academy of Sciences*, **855**(1), 517–520.

LEVITAN, IRWIN B. 2006. Signaling protein complexes associated with neuronal ion channels. *Nat Neurosci*, **9**(3), 305–310.

LI, Z. W., DING, J. P., KALYANARAMAN, V., & LINGLE, C. J. 1999. RINm5f cells express inactivating BK channels whereas HIT cells express noninactivating BK channels. *J Neurophysiol*, **81**(2), 611–624.

LITTLETON, J. T., & GANETZKY, B. 2000. Ion channels and synaptic organization: analysis of the Drosophila genome. *Neuron*, **26**(1), 35–43.

LOVELL, P. V., JAMES, D. G., & MCCOBB, D. P. 2000. Bovine versus rat adrenal chromaffin cells: big differences in BK potassium channel properties. *J Neurophysiol*, **83**(6), 3277–3286.

MALUN, D. 1991a. Inventory and distribution of synapses of identified uniglomerular projection neurons in the antennal lobe of Periplaneta americana. *J Comp Neurol*, **305**(2), 348–360.

MALUN, D. 1991b. Synaptic relationships between GABA-immunoreactive neurons and an identified uniglomerular projection neuron in the antennal lobe of Periplaneta americana: a double-labeling electron microscopic study. *Histochemistry*, **96**(3), 197–207.

MARCANTONI, ANDREA, VANDAEL, DAVID H F., MAHAPATRA, SATYAJIT, CARABELLI, VALENTINA, SINNEGGER-BRAUNS, MARTINA J., STRIESSNIG, JOERG, & CARBONE, EMILIO. 2010. Loss of Cav1.3 channels reveals the critical role of L-type and BK channel coupling in pacemaking mouse adrenal chromaffin cells. *J Neurosci*, **30**(2), 491–504.

MARRION, N. V., & TAVALIN, S. J. 1998. Selective activation of Ca2+-activated K+ channels by co-localized Ca2+ channels in hippocampal neurons. *Nature*, **395**(6705), 900–905.

MARTY, A. 1981. Ca-dependent K channels with large unitary conductance in chromaffin cell membranes. *Nature*, **291**(5815), 497–500.

MCMANUS, O. B. 1991. Calcium-activated potassium channels: regulation by calcium. *J Bioenerg Biomembr*, **23**(4), 537–560.

MEERA, P., WALLNER, M., SONG, M., & TORO, L. 1997. Large conductance voltage- and calcium-dependent K+ channel, a distinct member of voltage-dependent ion channels with seven N-terminal transmembrane segments (S0-S6), an extracellular N terminus, and an intracellular (S9-S10) C terminus. *Proc Natl Acad Sci U S A*, **94**(25), 14066–14071.

MILES, G. B., DAI, Y., & BROWNSTONE, R. M. 2005. Mechanisms underlying the early phase of spike frequency adaptation in mouse spinal motoneurones. *J Physiol*, **566**(Pt 2), 519–532.

MILLER, C. 1995. The charybdotoxin family of K+ channel-blocking peptides. *Neuron*, **15**(1), 5–10.

MILLER, C., MOCZYDLOWSKI, E., LATORRE, R., & PHILLIPS, M. 1985. Charybdotoxin, a protein inhibitor of single Ca2+-activated K+ channels from mammalian skeletal muscle. *Nature*, **313**(6000), 316–318.

MULLMANN, T. J., MUNUJOS, P., GARCIA, M. L., & GIANGIACOMO, K. M. 1999. Electrostatic mutations in iberiotoxin as a unique tool for probing the electrostatic structure of the maxi-K channel outer vestibule. *Biochemistry*, **38**(8), 2395–2402.

NÄSSEL, DICK R, & HOMBERG, UWE. 2006. Neuropeptides in interneurons of the insect brain. *Cell and tissue research*, **326**(1), 1–24.

NEUPERT, SUSANNE, FUSCA, DEBORA, SCHACHTNER, JOACHIM, KLOPPENBURG, PETER, & PREDEL, REINHARD. 2012. Toward a single-cell-based analysis of neuropeptide expression in Periplaneta americana antennal lobe neurons. *The Journal of Comparative Neurology*, **520**(4), 694–716.

NIGHTINGALE, W. D., & PITMAN, R. M. 1989. Ionic currents in the soma of an identified cockroach motoneurone recorded under voltage-clamp. *Comp Biochem Physiol A Comp Physiol*, **93**(1), 85–93.

OLSEN, SHAWN R, & WILSON, RACHEL I. 2008. Lateral presynaptic inhibition mediates gain control in an olfactory circuit. *Nature*, **452**(7190), 956–960.

OLSEN, SHAWN R, BHANDAWAT, VIKAS, & WILSON, RACHEL I. 2007. Excitatory Interactions between Olfactory Processing Channels in the Drosophila Antennal Lobe. *Neuron*, **54**(1), 89–103.

ORIO, PATRICIO, ROJAS, PATRICIO, FERREIRA, GONZALO, & LATORRE, RAMON. 2002. New disguises for an old channel: MaxiK channel beta-subunits. *News Physiol Sci*, **17**(Aug), 156–161.

PARK, C. S., & MILLER, C. 1992. Interaction of charybdotoxin with permeant ions inside the pore of a K+ channel. *Neuron*, **9**(2), 307–313.

PEDARZANI, P., & STOCKER, M. 2008. Molecular and cellular basis of small– and intermediate-conductance, calcium-activated potassium channel function in the brain. *Cell Mol Life Sci*, **65**(20), 3196–3217.

PERON, SIMON, & GABBIANI, FABRIZIO. 2009. Spike frequency adaptation mediates looming stimulus selectivity in a collision-detecting neuron. *Nat Neurosci*, **12**(3), 318–326.

PETERSEN, O. H., & MARUYAMA, Y. 1984. Calcium-activated potassium channels and their role in secretion. *Nature*, **307**(5953), 693–696.

PINEDA, J. C., GALARRAGA, E., BARGAS, J., CRISTANCHO, M., & ACEVES, J. 1992. Charybdotoxin and apamin sensitivity of the calcium-dependent repolarization and the afterhyperpolarization in neostriatal neurons. *J Neurophysiol*, **68**(1), 287–294.

PIPPOW, ANDREAS, HUSCH, ANDREAS, POUZAT, CHRISTOPHE, & KLOPPENBURG, PETER. 2009. Differences of Ca2+ handling properties in identified central olfactory neurons of the antennal lobe. *Cell Calcium*, **46**(2), 87–98.

PRAKRIYA, M., & LINGLE, C. J. 1999. BK channel activation by brief depolarizations requires Ca2+ influx through L- and Q-type Ca2+ channels in rat chromaffin cells. *J Neurophysiol*, **81**(5), 2267–2278.

PRAKRIYA, M., & LINGLE, C. J. 2000. Activation of BK channels in rat chromaffin cells requires summation of Ca(2+) influx from multiple Ca(2+) channels. *J Neurophysiol*, **84**(3), 1123–1135.

PRAKRIYA, M., SOLARO, C. R., & LINGLE, C. J. 1996. [Ca2+]i elevations detected by BK channels during Ca2+ influx and muscarine-mediated release of Ca2+ from intracellular stores in rat chromaffin cells. *J Neurosci*, **16**(14), 4344–4359.

QIU, SU, YI, HONG, LIU, HUI, CAO, ZHIJIAN, WU, YINGLIANG, & LI, WENXIN. 2009. Molecular Information of charybdotoxin blockade in the large conductance calcium-activated potassium channel. *J Chem Inf Model*, **49**(7), 1831–1838.

REISENMAN, CAROLINA E., DACKS, ANDREW M., & HILDEBRAND, JOHN G. 2011. Local interneuron diversity in the primary olfactory center of the moth Manduca sexta. *J Comp Physiol A Neuroethol Sens Neural Behav Physiol*, **197**(6), 653–665.

ROBITAILLE, R., GARCIA, M. L., KACZOROWSKI, G. J., & CHARLTON, M. P. 1993. Functional colocalization of calcium and calcium-gated potassium channels in control of transmitter release. *Neuron*, **11**(4), 645–655.

SACHSE, SILKE, & GALIZIA, C. GIOVANNI. 2003. The coding of odour-intensity in the honeybee antennal lobe: local computation optimizes odour representation. *Eur J Neurosci*, **18**(8), 2119–2132.

SAH, P. 1996. Ca(2+)-activated K+ currents in neurones: types, physiological roles and modulation. *Trends Neurosci*, **19**(4), 150–154.

SAITO, M., NELSON, C., SALKOFF, L., & LINGLE, C. J. 1997. A cysteine-rich domain defined by a novel exon in a slo variant in rat adrenal chromaffin cells and PC12 cells. *J Biol Chem*, **272**(18), 11710–11717.

SCHÄFER, S., ROSENBOOM, H., & MENZEL, R. 1994. Ionic currents of Kenyon cells from the mushroom body of the honeybee. *J Neurosci*, **14**(8), 4600–4612.

SCHUMACHER, M. A., RIVARD, A. F., BÄCHINGER, H. P., & ADELMAN, J. P. 2001. Structure of the gating domain of a Ca2+-activated K+ channel complexed with Ca2+/calmodulin. *Nature*, **410**(6832), 1120–1124.

SEKI, YOICHI, & KANZAKI, RYOHEI. 2008. Comprehensive morphological identification and GABA immunocytochemistry of antennal lobe local interneurons in Bombyx mori. *Journal of Comparative Neurology*, **506**(1), 93–107.

SEUTIN, V., & JOHNSON, S. W. 1999. Recent advances in the pharmacology of quaternary salts of bicuculline. *Trends Pharmacol Sci*, **20**(7), 268–270.

SHANG, YUHUA, CLARIDGE-CHANG, ADAM, SJULSON, LUCAS, PYPAERT, MARC, & MIESENBÖCK, GERO. 2007. Excitatory local circuits and their implications for olfactory processing in the fly antennal lobe. *Cell*, **128**(3), 601–612.

SHAO, L. R., HALVORSRUD, R., BORG-GRAHAM, L., & STORM, J. F. 1999. The role of BK-type Ca2+-dependent K+ channels in spike broadening during repetitive firing in rat hippocampal pyramidal cells. *J Physiol*, **521 Pt 1**(Nov), 135–146.

SILBERING, ANA F., OKADA, RYUICHI, ITO, KEI, & GALIZIA, C GIOVANNI. 2008. Olfactory information processing in the Drosophila antennal lobe: anything goes? *J Neurosci*, **28**(49), 13075–13087.

SOLARO, C. R., & LINGLE, C. J. 1992. Trypsin-sensitive, rapid inactivation of a calcium-activated potassium channel. *Science*, **257**(5077), 1694–1698.

SOLARO, C. R., PRAKRIYA, M., DING, J. P., & LINGLE, C. J. 1995. Inactivating and noninactivating Ca(2+)- and voltage-dependent K+ current in rat adrenal chromaffin cells. *J Neurosci*, **15**(9), 6110–6123.

SOLARO, C. R., DING, J. P., LI, Z. W., & LINGLE, C. J. 1997. The cytosolic inactivation domains of BKi channels in rat chromaffin cells do not behave like simple, open-channel blockers. *Biophys J*, **73**(2), 819–830.

STAMPE, P., KOLMAKOVA-PARTENSKY, L., & MILLER, C. 1994. Intimations of K+ channel structure from a complete functional map of the molecular surface of charybdotoxin. *Biochemistry*, **33**(2), 443–450.

STOCKER, MARTIN, HIRZEL, KLAUS, D'HOEDT, DIETER, & PEDARZANI, PAOLA. 2004. Matching molecules to function: neuronal Ca2+-activated K+ channels and afterhyperpolarizations. *Toxicon*, **43**(8), 933–949.

STOPFER, MARK. 2005. Olfactory coding: inhibition reshapes odor responses. *Curr Biol*, **15**(24), R996–R998.

STRAUSFELD, NICHOLAS J, & HILDEBRAND, JOHN G. 1999. Olfactory systems: common design, uncommon origins? *Current opinion in neurobiology*, **9**(5), 634–639.

THOMAS, M. V. 1984. Voltage-clamp analysis of a calcium-mediated potassium conductance in cockroach (Periplaneta americana) central neurones. *J Physiol*, **350**(May), 159–178.

TURNER, RAY W., ANDERSON, DUSTIN, & ZAMPONI, GERALD W. 2011. Signaling complexes of voltage-gated calcium channels. *Channels (Austin)*, **5**(5), 440–448.

VANDAEL, DAVID H F., ZUCCOTTI, ANNALISA, STRIESSNIG, JOERG, & CARBONE, EMILIO. 2012. Ca(V)1.3-driven SK channel activation regulates pacemaking and spike frequency adaptation in mouse chromaffin cells. *J Neurosci*, **32**(46), 16345–16359.

VANDORPE, D. H., SHMUKLER, B. E., JIANG, L., LIM, B., MAYLIE, J., ADELMAN, J. P., DE FRANCESCHI, L., CAPPELLINI, M. D., BRUGNARA, C., & ALPER, S. L. 1998. cDNA cloning and functional characterization of the mouse Ca2+-gated K+ channel, mIK1. Roles in regulatory volume decrease and erythroid differentiation. *J Biol Chem*, **273**(34), 21542–21553.

VERGARA, C., LATORRE, R., MARRION, N. V., & ADELMAN, J. P. 1998. Calcium-activated potassium channels. *Curr Opin Neurobiol*, **8**(3), 321–329.

VOSSHALL, LESLIE B, & STOCKER, REINHARD F. 2007. Molecular architecture of smell and taste in Drosophila. *Annu. Rev. Neurosci.*, **30**, 505–533.

WALDROP, BRIAN, CHRISTENSEN, THOMAS A, & HILDEBRAND, JOHN G. 1987. GABA-mediated synaptic inhibition of projection neurons in the antennal lobes of the sphinx moth, Manduca sexta. *Journal of Comparative Physiology A*, **161**(1), 23–32.

WANG, LIGUO, & SIGWORTH, FRED J. 2009. Structure of the BK potassium channel in a lipid membrane from electron cryomicroscopy. *Nature*, **461**(7261), 292–295.

WATANABE, HIDEHIRO, AI, HIROYUKI, & YOKOHARI, FUMIO. 2012. Spatio-temporal activity patterns of odor-induced synchronized potentials revealed by voltage-sensitive dye imaging and intracellular recording in the antennal lobe of the cockroach. *Front Syst Neurosci*, **6**, 55.

WEI, A., SOLARO, C., LINGLE, C., & SALKOFF, L. 1994. Calcium sensitivity of BK-type KCa channels determined by a separable domain. *Neuron*, **13**(3), 671–681.

WEI, AGUAN D., GUTMAN, GEORGE A., ALDRICH, RICHARD, CHANDY, K GEORGE, GRISSMER, STEPHAN, & WULFF, HEIKE. 2005. International Union of Pharmacology. LII. Nomenclature and molecular relationships of calcium-activated potassium channels. *Pharmacol Rev*, **57**(4), 463–472.

WICHER, D., WALTHER, C., & WICHER, C. 2001. Non-synaptic ion channels in insects–basic properties of currents and their modulation in neurons and skeletal muscles. *Prog Neurobiol*, **64**(5), 431–525.

WILSON, RACHEL I. 2013. Early olfactory processing in Drosophila: mechanisms and principles. *Annu Rev Neurosci*, **36**(Jul), 217–241.

WILSON, RACHEL I, & MAINEN, ZACHARY F. 2006. Early events in olfactory processing. *Annu. Rev. Neurosci.*, **29**, 163–201.

WINDLEY, MONIQUE J., ESCOUBAS, PIERRE, VALENZUELA, STELLA M., & NICHOLSON, GRAHAM M. 2011. A novel family of insect-selective peptide neurotoxins targeting insect large-conductance calcium-activated K+ channels isolated from the venom of the theraphosid spider Eucratoscelus constrictus. *Mol Pharmacol*, **80**(1), 1–13.

WU, YUNKUN, YANG, YI, YE, SHENG, & JIANG, YOUXING. 2010. Structure of the gating ring from the human large-conductance Ca(2+)-gated K(+) channel. *Nature*, **466**(7304), 393–397.

XIA, X.-M., FAKLER, B., RIVARD, A., WAYMAN, G., JOHNSON-PAIS, T., KEEN, J. E., ISHII, T., HIRSCHBERG, B., BOND, C. T., LUTSENKO, S., MAYLIE, J., & ADELMAN, J. P. 1998. Mechanism of calcium gating in small-conductance calcium-activated potassium channels. *Nature*, **395**(6701), 503–507.

ZAGOTTA, W. N., HOSHI, T., & ALDRICH, R. W. 1989. Gating of single Shaker potassium channels in Drosophila muscle and in Xenopus oocytes injected with Shaker mRNA. *Proc Natl Acad Sci U S A*, **86**(18), 7243–7247.

ZENG, HAOYU, WEIGER, THOMAS M., FEI, HONG, JARAMILLO, ANGELA M., & LEVITAN, IRWIN B. 2005. The amino terminus of Slob, Slowpoke channel binding protein, critically influences its modulation of the channel. *J Gen Physiol*, **125**(6), 631–640.

Erklärung

Ich versichere, dass ich die von mir vorgelegte Dissertation selbständig angefertigt, die benutzten Quellen und Hilfsmittel vollständig angegeben und die Stellen der Arbeit – einschließlich Tabellen, Karten und Abbildungen –, die anderen Werken im Wortlaut oder dem Sinn nach entnommen sind, in jedem Einzelfall als Entlehnung kenntlich gemacht habe; dass diese Dissertation noch keiner anderen Fakultät oder Universität zur Prüfung vorgelegen hat; dass sie – abgesehen von unten angegebenen Teilpublikationen – noch nicht veröffentlicht worden ist sowie, dass ich eine solche Veröffentlichung vor Abschluss des Promotionsverfahrens nicht vornehmen werde.

Die Bestimmungen der Promotionsordnung sind mir bekannt. Die von mir vorgelegte Dissertation ist von Prof. Dr. Peter Kloppenburg betreut worden.

_____

(Sabine Schleicher)

Köln, den 05.05.2014

Teilpublikationen

Artikel

OLIVEIRA, EE., <u>SCHLEICHER, S.</u>, BÜSCHGES, A., SCHMIDT, J., KLOPPENBURG, P., SALGADO, VL. 2011. Desensitization of nicotinic acetylcholine receptors in central nervous system neurons of the stick insect (*Carausius morosus*) by imidacloprid and sulfoximine insecticides. *Insect Biochem Mol Biol*, **41**(11), 872–80.

BRADLER, C., <u>SCHLEICHER, S.</u>, WARREN, B., KLEIN, A., BARDOS V., KLOPPENBURG, P. 2014. Ca^{2+}-dependent K^+ currents in uniglomerular projection neurons of the antennal lobe. (in preparation)

Poster

<u>SCHLEICHER, S.</u>, PAEGER, L., ROTTE, C., KLOPPENBURG, P. 2011. Transient Potassium Currents in Olfactory Interneurons of the cockroach *Periplaneta americana*. *Proceedings of the 33th Göttingen Neurobiology Conference and the 9th Meeting of the German Neuroscience Society.*

<u>SCHLEICHER, S.</u>, PAEGER, L., ROTTE, C., KLOPPENBURG, P. 2011. Transient Potassium Currents in Olfactory Interneurons of the cockroach *Periplaneta americana*. *22nd NeuroDoWo (Annual Neurobiology Doctoral Student Workshop) Bonn, Germany.*

SCHLEICHER, S., ROTTE, C., WARREN, B., KLEIN, A., BARDOS, V., KLOPPEN-BURG, P. 2012. Characterization and Role of Ca^{2+}-dependent Outwards Currents in Uniglomerular Projection Neurons in the Antennal lobe of *Periplaneta americana*. *105th Annual Meeting of the German Zoological Society, Konstanz, Germany.*

SCHLEICHER, S., ROTTE, C., WARREN, B., KLEIN, A., BARDOS, V., KLOPPEN-BURG, P. 2013. Characterization and Role of Ca^{2+}-dependent Outwards Currents in Uniglomerular Projection Neurons in the Antennal lobe of *Periplaneta americana*. *Proceedings of the 34th Göttingen Neurobiology Conference and the 10th Meeting of the German Neuroscience Society.*

Vorträge

SCHLEICHER, S., ROTTE, C., WARREN, B., KLEIN, A., BARDOS, V., KLOPPEN-BURG, P. 2012. Characterization and Role of Ca^{2+}-dependent Outwards Currents in Uniglomerular Projection Neurons in the Antennal lobe of *Periplaneta americana*. *23rd NeuroDoWo (Annual Neurobiology Doctoral Student Workshop) Marburg, Germany.*